THE DELAMINATION THEORY OF WEAR-II

Nam P. Suh, et al

Massachusetts Institute of Technology

Prepared for:

Office of Naval Research

September 1975

THE DELAMINATION THEORY OF WEAR-II

Second Progress Report

to

The Advanced Research Project Agency, DOD
Contract No. N00014-67-A-0204-0080
NR 229-011

NAM P. SUH
SAID JAHANMIR
JONATHAN FLEMING
ERNEST P. ABRAHAMSON, II
NANNAJI SAKA
JORGE P. TEIXEIRA

MATERIALS PROCESSING LABORATORY
DEPARTMENT OF MECHANICAL ENGINEERING
MASSACHUSETTS INSTITUTE OF TECHNOLOGY
CAMBRIDGE, MASSACHUSETTS 02139

September 1975

THE DELAMINATION THEORY OF WEAR-II

Second Progress Report

to

The Advanced Research Project Agency, DOD
Contract No. N00014-67-A-0204-0080
NR 229-011

Nam P. Suh

Said Jahanmir

Jonathan Fleming

Ernest P. Abrahamson, II

Nannaji Saka

Jorge P. Teixeira

Materials Processing Laboratory
Department of Mechanical Engineering
Massachusetts Institute of Technology
Cambridge, Massachusetts 02139

September 1975

UNCLASSIFIED

SECURITY CLASSIFICATION OF THIS PAGE (When Data Entered)

REPORT DOCUMENTATION PAGE		READ INSTRUCTIONS BEFORE COMPLETING FORM
1. REPORT NUMBER —	2. GOVT ACCESSION NO. —	3. RECIPIENT'S CATALOG NUMBER —
4. TITLE (and Subtitle) The Delamination Theory of Wear-II Second Progress Report		5. TYPE OF REPORT & PERIOD COVERED Annual - May 1974-June 1975 6. PERFORMING ORG. REPORT NUMBER —
7. AUTHOR(s) Nam P. Suh, Said Jahanmir, Jonathan Fleming, Ernest P. Abrahamson, II Nannaji Saka, Jorge P. Teixeira		8. CONTRACT OR GRANT NUMBER(s) N00014-67-A-0204-0080 NR 229-011
9. PERFORMING ORGANIZATION NAME AND ADDRESS Materials Processing Laboratory Department of Mechanical Engineering Massachusetts Institute of Technology		10. PROGRAM ELEMENT, PROJECT, TASK AREA & WORK UNIT NUMBERS 000000#4D10
11. CONTROLLING OFFICE NAME AND ADDRESS Department of the Navy Office of Naval Research Arlington Virginia 22217 N00014		12. REPORT DATE September 1975 13. NUMBER OF PAGES 161
14. MONITORING AGENCY NAME & ADDRESS(if different from Controlling Office) Office of Naval Research MIT Resid. Repres. - 77 Massachusetts Ave., Bldg. E19-62B Cambridge, Mass. 02139 (N66017)		15. SECURITY CLASS. (of this report) Unclassified 15a. DECLASSIFICATION/DOWNGRADING SCHEDULE —

16. DISTRIBUTION STATEMENT (of this Report)

The distribution of this document is unlimited.

17. DISTRIBUTION STATEMENT (of the abstract entered in Block 20, if different from Report)

—

18. SUPPLEMENTARY NOTES

—

19. KEY WORDS (Continue on reverse side if necessary and identify by block number)

delamination, sliding wear, subsurface deformation, void formation, crack propagation, soft metallic coating, surface roughness, surface integrity, wear reduction, mechanics of delamination, steel, copper alloy, internally oxidized copper alloy

20. ABSTRACT (Continue on reverse side if necessary and identify by block number)

This second progress report describes the work done by the MIT-Wear Research Group on fundamentals of wear by delamination. Such topics as the mechanics of surface deformation, the relationship between friction and wear, the effect of microstructure on wear, the effect of surface roughness and integrity on wear, wear resistant soft metallic coatings and delamination in other types of wear are examined.

DD FORM 1 JAN 73 1473 EDITION OF 1 NOV 65 IS OBSOLETE
S/N 0102-014-6601

UNCLASSIFIED

SECURITY CLASSIFICATION OF THIS PAGE (When Data Entered)

The mechanisms of surface and subsurface deformation are investigated using a finite element computer program. It is shown that in sliding interaction, the material below the surface experiences a tension-compression cyclic state of loading. The compression region exists right under the contact, while the tension region is located right behind the moving contact. If it is hypothesized that subsurface crack propagation occures at the position of maximum tensile stress perpendicular to the surface, a correlation between observed and predicted crack depth as a function of friction coefficient can be found. Wear rate and friction coefficient are also shown to be related by an approximate energy analysis, yielding theoretical predictions that are surprisingly close to the experimental results.

Studies carried out on microstructural effects in sliding wear substantiate the predictions of the delamination theory that the wear rate is controlled by both the hardness and the number of void nucleation and crack propagation sites. The wear rate is decreased by increasing the hardness and decreasing the number of void nucleation and crack propagation sites.

Preliminary investigations in other modes of wear show that the delamination process may occur under any conditions where both normal and tangential forces exist at the contact. Evidence of sub-surface crack nucleation and propagation is found in fretting, abrasive and erosive wear. It is proposed that the measures which can be taken to reduce sliding wear can also be used to reduce fretting and catastrophic failure by fretting fatigue.

Studies on the effect of surface roughness on wear indicate that the original surface roughness of machined parts controls the initial wear behavior and not the steady state delamination wear rate. The influence of surface roughness on wear is shown to depend on the normal load. Under low contact loads, rough surfaces wear less than smoother ones, while at higher contact loads, the wear of rough surfaces is larger than smoother ones. The quality and the degree of subsurface damage generated during surface preparation has detrimental effects on the initial wear rate. This preliminary result indicates a strong need for quality control measures for surfaces machined for sliding applications.

The delamination theory of wear is used to develop wear-resistant metallic surfaces by application of a thin soft metallic plate. The wear rate of the combination can be reduced by three orders of magnitude if the coating is softer than the substrate, has an optimum thickness ($\simeq 0.1\ \mu m$), and is bonded strongly to the substrate. This phenomenon is demonstrated experimentally for cadmium, silver, gold and nickel-plated steel specimens.

Abstract

This second progress report describes the work done by the MIT-Wear Research Group on fundamentals of wear by delamination. Such topics as the mechanics of surface deformation, the relationship between friction and wear, the effect of microstructure on wear, the effect of surface roughness and integrity on wear, wear resistant soft metallic coatings and delamination in other types of wear are examined.

The mechanisms of surface and subsurface deformation are investigated using a finite element computer program. It is shown that in sliding interaction, the material below the surface experiences a tension-compression cyclic state of loading. The compression region exists right under the contact, while the tension region is located right behind the moving contact. If it is hypothesized that subsurface crack propagation occures at the position of maximum tensile stress perpendicular to the surface, a correlation between observed and predicted crack depth as a function of friction coefficient can be found. Wear rate and friction coefficient are also shown to be related by an approximate energy analysis, yielding theoretical predictions that are surprisingly close to the experimental results.

Studies carried out on microstructural effects in sliding wear substantiate the predictions of the delamination theory that the wear rate is controlled by both the hardness and the number of void nucleation and crack propagation sites. The wear rate is decreased by increasing the hardness and decreasing the number of void nucleation and crack propagation sites.

Preliminary investigations in other modes of wear show that the delamination process may occur under any conditions where both normal and tangential forces exist at the contact. Evidence of sub-surface crack nucleation and propagation is found in fretting, abrasive and erosive wear. It is proposed that the measures which can be taken to reduce sliding wear can also be used to reduce fretting and catastrophic failure by fretting fatigue.

Studies on the effect of surface roughness on wear indicate that the original surface roughness of machined parts controls the initial wear behavior and not the steady state delamination wear rate. The influence of surface roughness on wear is shown to depend on the normal load. Under low contact loads, rough surfaces wear less than smoother ones, while at

higher contact loads, the wear of rough surfaces is larger than smoother ones. The quality and the degree of subsurface damage generated during surface preparation has detrimental effects on the initial wear rate. This preliminary result indicates a strong need for quality control measures for surfaces machined for sliding applications.

The delamination theory of wear is used to develop wear-resistant metallic surfaces by application of a thin soft metallic plate. The wear rate of the combination can be reduced by three orders of magnitude if the coating is softer than the substrate, has an optimum thickness (≈ 0.1 μm), and is bonded strongly to the substrate. This phenomenon is demonstrated experimentally for cadmium, silver, gold and nickel-plated steel specimens.

ACKNOWLEDGEMENTS

The work reported in this report was sponsored by the Defense Advanced Research Projects Agency through the Office of Naval Research under contract N00014-67-A-0204-0080. We are grateful to Dr. Edward van Reuth and Lt. Richard S. Miller for their personal support and guidance of our work.

Table of Contents

LIST OF FIGURES

List of Tables

Chapter I

INTRODUCTION

Until recently the wear of materials and other surface-related phenomena have not received much attention from materials scientists and engineers, in spite of the fact that the durability of machines and structures is often controlled by surface-related phenomena such as wear and corrosion. The economic impact of a basic understanding of wear phenomena cannot be overemphasized. According to Jost, the U.S. could save as much as 16 billion dollars per annum by proper utilization of the existing knowledge in tribology alone[1].

The purpose of the MIT wear research program is to control friction and wear of materials through proper design of sliding surfaces. Innovative and rational design of surfaces from both the metallurgical and the mechanistic points of view can only be achieved if a basic theoretical description of the wear phenomenon exists. Therefore, we have chosen first to analyze the friction and wear behavior of materials in terms of both mechanical and microstructural aspects, and secondly to apply this understanding to the design of sliding surfaces. When these design criteria are established, the next task is to insure that the surfaces can be prepared as designed. To achieve this we are planning to develop quality control methods which can be used to check the acceptance or rejection of surfaces manufactured for various sliding applications. For instance, premature failure of machines frequently occurs owing to the lack of sufficient specification and control of those variables which directly affect surface behavior. On the other hand, manufacturing costs may sometimes be higher than necessary mainly due to the overspecification of surface finish requirements.

During the first year of the program, the hypotheses of the delamination theory were examined and proven experimentally[2]. In the second year of our effort advances have been made in understanding the mechanics of surface deformation, and the possible influences on wear behavior of various mechanical and microstructural properties of metals. Mechanistic effects in sliding wear that have been studied include the mechanics of energy dissipation, the relationship between wear and the coefficient of friction, and the effect of topography on wear as a function of normal load. Studies have been carried out on microstructural effects in sliding wear, concentrating on methods of selective hardening by dispersion, precipitation and solution hardening. Further work

on coated metal surfaces has indicated that when used properly they indeed show promise as a method for eliminating fretting wear, fretting fatigue, and sliding wear.

Scientific inquiry often leads to new questions with exciting consequences. In this sense, the results of our effort have been very gratifying. We have discovered new possibilities and implications in the delamination theory, and we have formulated many questions which must be answered before the delamination theory can be fully quantified. We hope to be able to answer all the questions we have raised, and to explore new possibilities in the reduction of wear and the prevention of failure.

Chapter II

DESCRIPTION OF THE DELAMINATION THEORY OF WEAR

II 1) Introduction

The delamination theory of wear was proposed to provide basic understanding of sliding wear mechanisms so that sliding surfaces could be designed rationally[3]. This theory, unlike previous theories of wear, emphasizes the controlling effect of the microstructure of metals on the mechanical behavior of the surface and the subsurface.

Metals wear by different mechanisms depending on the environment and the loading conditions. Wear can be caused by such mechanisms as diffusion, abrasion, and chemical reaction, as well as by the delamination mechanism. In a given situation, more than one mechanism may be operating simultaneously, but often the wear rate is controlled by a single dominant mechanism. In this report only those wear processes which are controlled by the deformation of the subsurface and crack nucleation and propagation are examined. The delamination theory of wear is reviewed in this chapter. It will be shown in a later chapter that a similar mechanism may be operative in such wear processes as fretting, abrasive, and erosive wear.

II 2) Adhesion Theories of Wear and Their Shortcomings

The important features of the delamination theory of wear can best be understood by contrasting it with the adhesion theories of wear which have dominated the thinking of tribologists.

Adhesion theories are based on the postulate that wear under sliding conditions is a consequence of asperity-asperity interactions between two opposing surfaces[4-7]. In particular, it is commonly assumed that the asperity junctions adhere to each other and the weaker asperities are subsequently sheared off by the tangential force at the contact. Therefore, much attention has been devoted in the past to the mechanism of adhesion between different materials and to the determination of the actual area of contact at the interface. The adhesion theories often cited are those of Archard for wear[4] and Green for friction[5]. Existing experimental evidence is sufficient to support the idea that the adhesion does indeed occur, though perhaps not to the extent assumed by the proponents of the adhesion theories.

The disputable point is the role of adhesion in sliding wear. The delamination theory of wear has postulated that the primary role of adhesion is to increase the surface traction which in turn causes greater deformation which leads to increased crack nucleation and propagation rates in the subsurface. These postulates were later confirmed by experimental results.(2)

There are some gross friction and wear phenomena which have been known to deviate from the postulates of the adhesion theories, e.g.,

a) The work required to create a given volume of wear particles by the adhesion mechanism, as given by the upper bound solutions of plasticity, is much less than the external work done. The difference is about two to three orders of magnitude.

b) The aspect ratio of wear particles is much larger than one, although the adhesion models imply an equiaxial wear particle.

c) Microstructural effects on wear cannot be accounted for by the adhesion theories.

d) The coefficient of friction tends to be much larger than that predicted by the adhesion theories.

II 3) The Wear Process According to the Delamination Theory of Wear

The above known deviations of the experimental results from the predictions of the adhesion theories motivated the examination of the basic hypothesis of these theories. As a consequence, the delamination theory of wear was conceived and formulated. The delamination theory explained previously unknown or misunderstood phenomena such as the existence of subsurface cracks, a "soft non-workhardening" surface layer, the role of hard particles, the primary role of hardness in wear of metals, and the shape of wear particles. These predictions have subsequently been verified by experiments.(2)

The delamination theory of wear refers to the following particular set of mechanisms which cause wear of metals under sliding conditions:

a) When two sliding surfaces come in contact, normal and tangential loads are transmitted through the contact points. Asperities of the softer surface are easily deformed and fractured by the repeated loading action, forming small wear particles and eventually creating a relatively smooth surface. At the same time the surface layer is deformed by the surface traction.

b) The plastic deformation occurs by generation and movement of dislocations. However, the dislocations very near the surface are subjected to a sufficient image force to be pulled out of the surface as the coherent oxide layer which may be present on the surface is broken by the moving asperities of the other sliding surface. The dislocations below a critical depth, where the image force is not strong enough, are stable and can accumulate and work-harden the subsurface. Consequently, the deformed material exhibits a flow stress gradient near the surface: as the distance from the surface increases the hardness initially increases, reaches a maximum value, and then decreases.*

c) A consequence of the flow stress gradient is that the hard asperities more easily "penetrate" the surface of the softer metal, displacing and spreading the softer metal at the surface. Therefore, the surface traction is caused by the plowing of the softer surface by hard asperities as well as by the adhesive force. Furthermore, once the major asperities are removed, the contact is not just asperity-to-asperity contact but rather the same loading history is repeated all along the softer surface as the asperities of the harder surface plow the softer surface.

d) As the subsurface deformation continues, cracks are nucleated away from the surface. Crack nucleation very near the surface is not favored for two reasons: a triaxial state of compressive stress just below the contact points, and the "soft" metal layer near the surface. In materials which contain hard particles (e.g. second phase or inclusions) crack nucleation is preferentially initiated at the particle-matrix interface.

e) Upon further deformation, cracks extend and propagate, joining the neighboring ones. The cracks tend to run parallel to the surface since the loading condition is the same all along the surface. The location of a long crack is likely to be controlled by the tensile state of loading existing below the surface in a region behind each asperity.

f) When these cracks finally propagate to the surface, thin wear sheets delaminate. The thickness of the wear sheet is controlled by the magnitude of the normal and the tangential loads at the surface, the minimum possible sheet thickness being that of the "soft" layer.

---

*The existance of a flow stress gradient is as yet controversial. The flow stress gradient contributes to, but is not necessary for, the following mechanisms (except for mechanism c).

II 4) Flow Stress Gradient at the Surface

Adhesion theorists had assumed that the flow stress at the very surface is either the same as or larger than the bulk. The delamination theory postulated that the very surface layer of metals may be softer and non-workhardening due to the instability of dislocations very near the surface, and that there is a flow stress gradient near the surface.

Two different kinds of experiments have been done to verify these postulates. Direct evidence for the flow stress gradient is obtained by microhardness measurements of the surface. Less explicit evidence, which shows that the very surface layer does not work-harden appreciably, is obtained through the application of this idea to the minimization of the wear rate of metals.

Direct microhardness tests have been made on worn surfaces of metals by Koba/Cook[8] and Kirk/Swanson[9] to verify the delamination theory. Later it was found that Savitskii[10] had published similar results earlier. Similar flow stress gradient near the surface of copper single crystals which have undergone bulk deformation was reported by Fourie[11]. Figure 2.1 shows the results obtained by Savitskii and Kirk. Savitskii obtained the hardness variation in aluminum by varying the indentation load, while Kirk et al. obtained their results by indenting the subsurface below the wear track after sectioning a copper specimen. The flow stress is indeed low at the very surface and increases to a maximum value before it decreases again. The experimental results of Savitskii show that the peak hardness in aluminum occurs at about 10-15 μm, while Kirk et al. found the peak hardness in copper at about 80 μm. Similar hardness variations in steel cannot be measured using this type of experimental technique, probably because the flow stress varies over an extremely shallow depth. The normal hardness variation in steel reported in the literature is not due to the dislocation mechanism but rather to phase transformation associated with thermal softening or quenching during the wear test. The hardness variation of unworn well annealed metals is different. Whitehouse[12] measured the hardness variation using a very fine indenter with a very light load (≈100 μN) on well annealed copper, which indicated that the hardness increases continuously all the way to the surface.

According to dislocation theory, the image force on a dislocation varies inversely as a function of depth from the surface. The depth at which the image

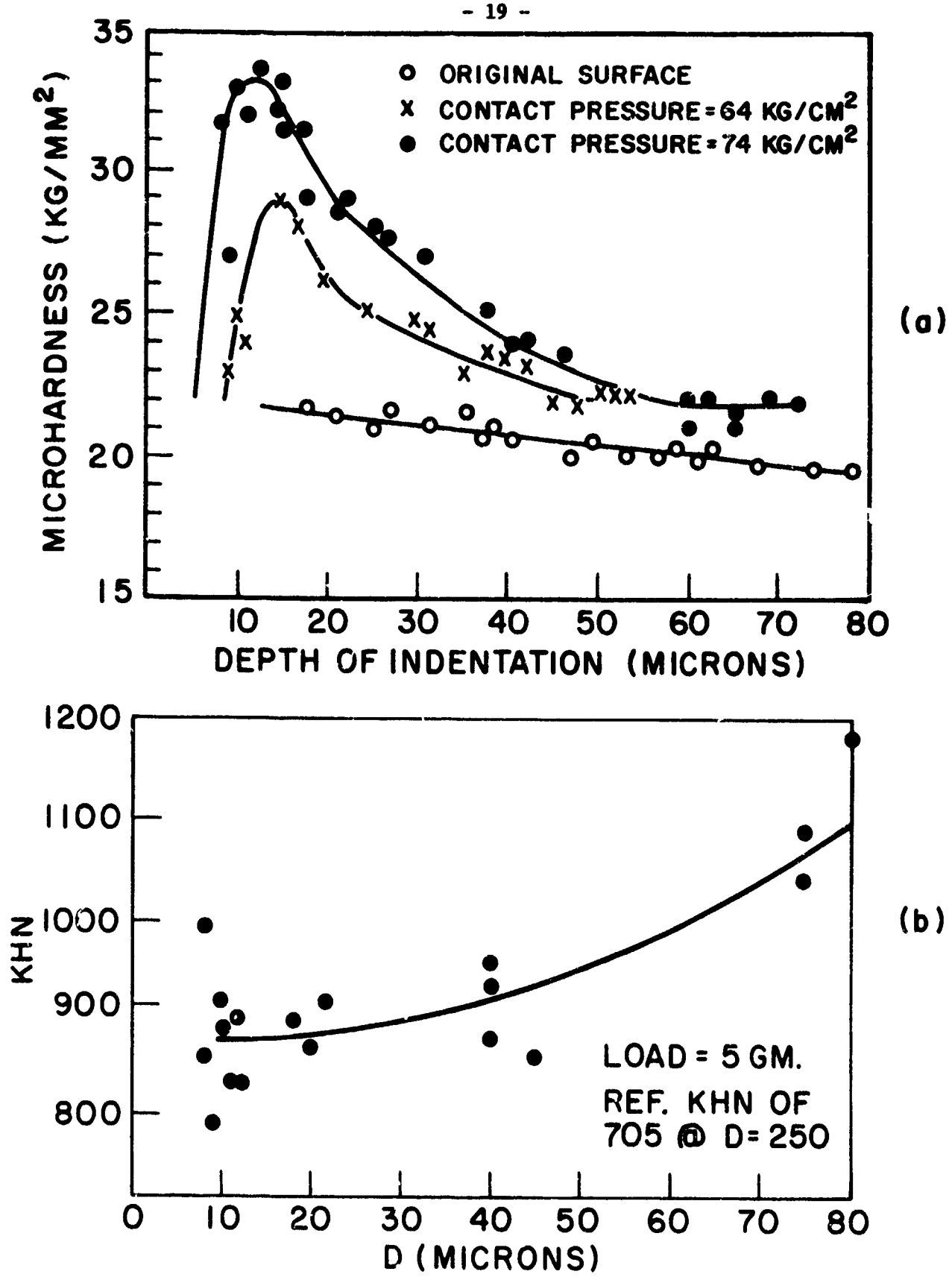

Figure 2.1

Subsurface hardness variation: (a) indentation hardness of the wear surface, varying the indentation load, aluminum specimen wear tested under normal stresses of 64 and 74 Kg/cm^2 (Ref.10); (b) indentation hardness of sectioned worn surface, constant indentation load, copper specimen wear tested under a normal load of 0.682 Kg (Ref. 9).

stress is equal to the friction stress acting on dislocations is inversely proportional to the dislocation friction stress. This depth is of the order of 0.1 μm for silicon-iron and 10 to 20 μm for well annealed copper[3] with a dislocation density of only 50 cm^{-2}. This depth seems to be smaller than the depth at which the subsurface hardness reaches a peak value. It is difficult to draw any definitive conclusions on the thickness of the "soft" layer, since the friction stress acting on dislocations and the dislocation dynamics during wear tests are not known for these particular specimens. It is reasonable to expect that other factors will also influence the flow stress variation, such as the formation of microcracks in the highly deformed surface layer.

Starting from the postulate that there is a "non-workhardening soft layer" near the surface due to the instability of dislocations, a method of minimizing sliding wear has been devised by plating a metal substrate with a very thin layer of a softer metal[13]. It was reasoned that when the thickness of the plated layer is less than a critical value, the accumulation of dislocations within the plated layer can be prevented and the resulting "soft" plated layer will deform continuously without work-hardening. Thus this minimizes the plastic deformation of the substrate and forestalls wear by delamination. If the thickness of the plated layer is thicker than its critical value, the delamination mechanism will function within the plated layer, generating wear sheets of the plated metal. This reasoning was subsequently verified by experiments[14].

II 5) Surface Traction

The delamination theory and the adhesion theory differ as to the role of surface traction. The adhesion model of Archard implies that wear is affected by the magnitude of the normal load but not by the magnitude of the tangential load. The delamination theory predicts that the magnitudes of both normal and tangential loads affect the wear particle size and the wear rate. Experimental evidence for the importance of both components of the load will be presented in a later section. Here, the mechanisms by which a tangential load arises will be discussed.

In the past, three mechanisms for the generation of frictional force between two sliding surfaces have been considered: adhesion between asperities,

deformation of the softer asperities by harder asperities, and the plowing of the softer surface by hard asperities. Much attention has been given to the first two mechanisms in determining the tangential load using the adhesion theory[5,6,15-17]. While it is generally accepted that adhesion plays an important role in friction and wear, there is serious doubt that the contribution of plowing to the frictional force, especially in the case of f.c.c. metals, can be neglected.

Plowing is a possible mechanism since the flow stress gradient existing near a worn surface favors the penetration of the softer surface by hard asperities and spreading of the softer material at the surface. Experimental results such as the topography of a worn surface shown in Fig. 2.2 support the existence of this mechanism. In order to check this possibility theoretically, the displacement field of an elasto-plastic solid in plane strain under the action of a much harder asperity is being investigated[18] by a finite element method using the computer program ADINA developed by Bathe[19]. The results show that the hard asperities can penetrate into and spread the softer metal. Since the asperities have a gradual slope of the order of 10^{-3}, the area of contact should increase as the asperities penetrate. When there is tangential motion of the penetrated asperities, the softer metal must flow around the asperities. This plowing action increases the frictional force over that due to adhesion alone.

II 6) Deformation of the Subsurface by Surface Traction

An important consequence of the surface traction all along the surface is uniform plastic deformation at each depth underneath the surface. This is shown to be the case experimentally as seen in Fig.2.3. The micrographs show cross-sectional views underneath the wear tracks of an AISI 1020 specimen and an AISI 1095 specimen. It should be noted that even the carbides in the pearlite region of the 1095 specimen deformed with the matrix. Figure 2.4 is a plot of the equivalent strain as a function of the distance away from the surface[20]. It should be noted that the maximum equivalent strain shown in the figure is several orders of magnitude greater than that observed in bulk fracture of tensile specimens. Such a large strain is due to the combined effect of the high compressive state of triaxial loading under asperities, the "soft" nature of the deformed metal surface, and the strain accumulation due to cyclic softening of the metal under constant stress cyclic loading.

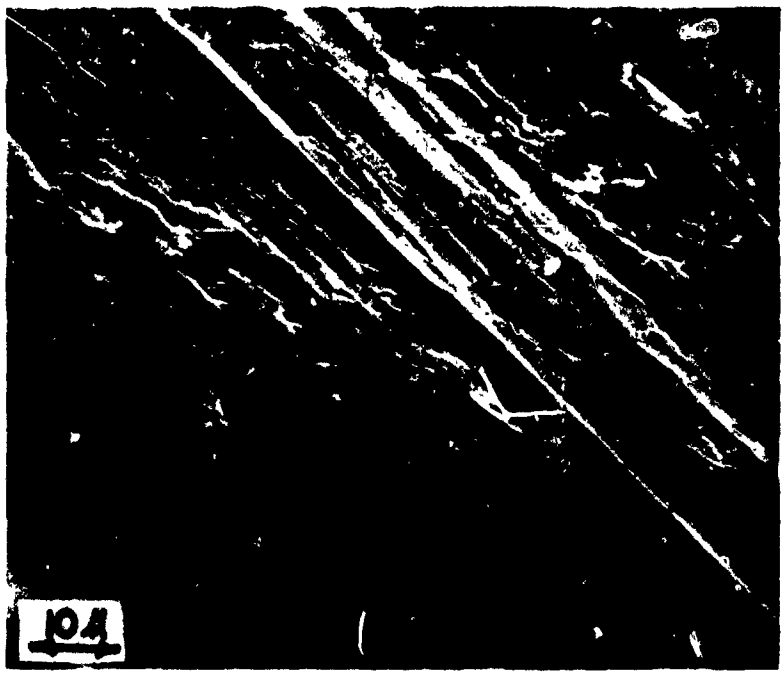

Figure 2.2

Evidence of plowing on the wear track of AISI 1020 steel tested under a normal load of 2.25 Kg for 10 minutes, lubricated.

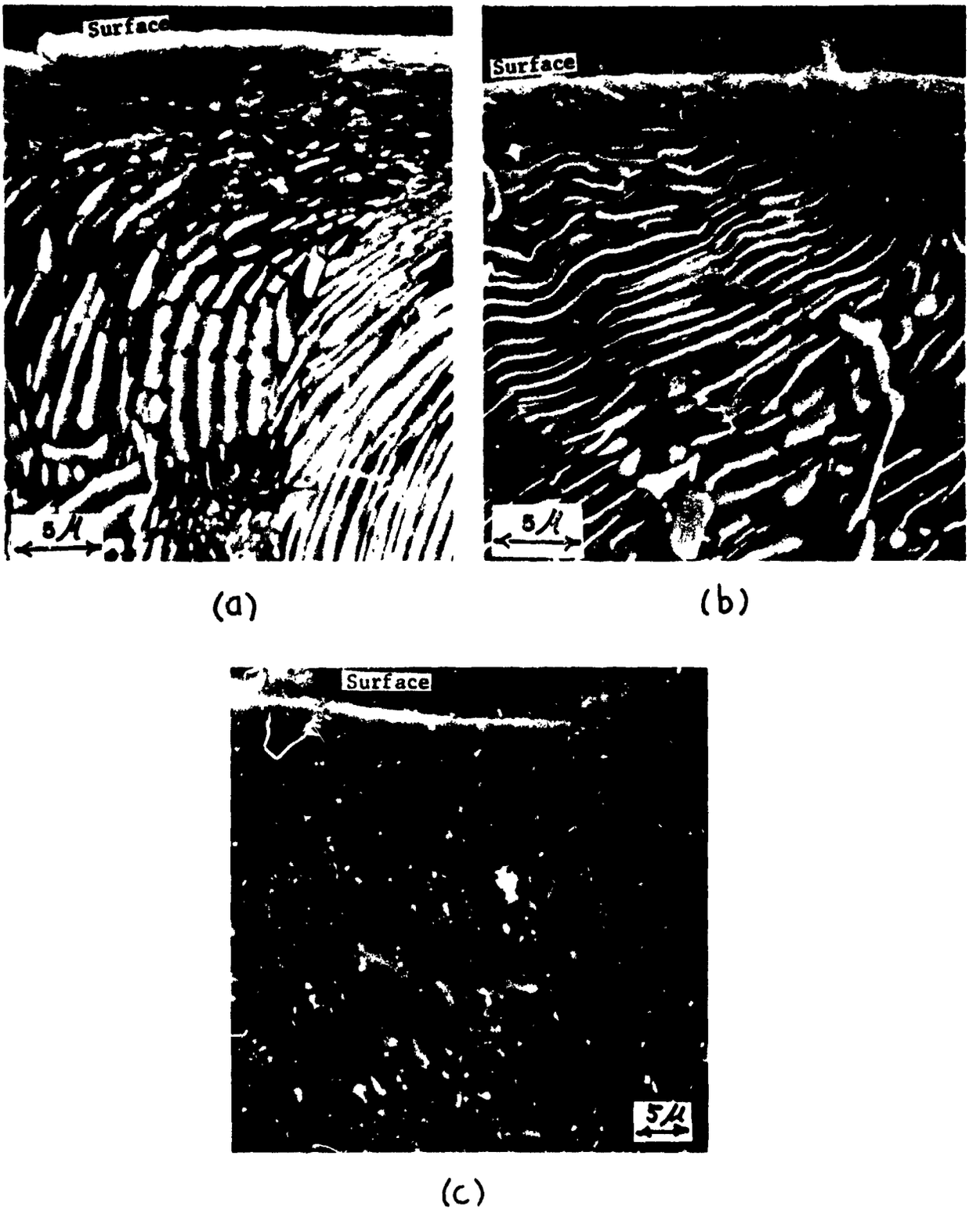

Figure 2.3

Subsurface deformation and crack formation: (a) AISI 1095 pearlitic steel tested under a normal load of 0.45 Kg for 15 min in argon; (b) AISI 1095 pearlitic steel tested under a normal load of 2.0 Kg for 15 min in air; (c) AISI 1020 spheroidized steel, tested under a normal load of 2.25 Kg for 30 min in argon.

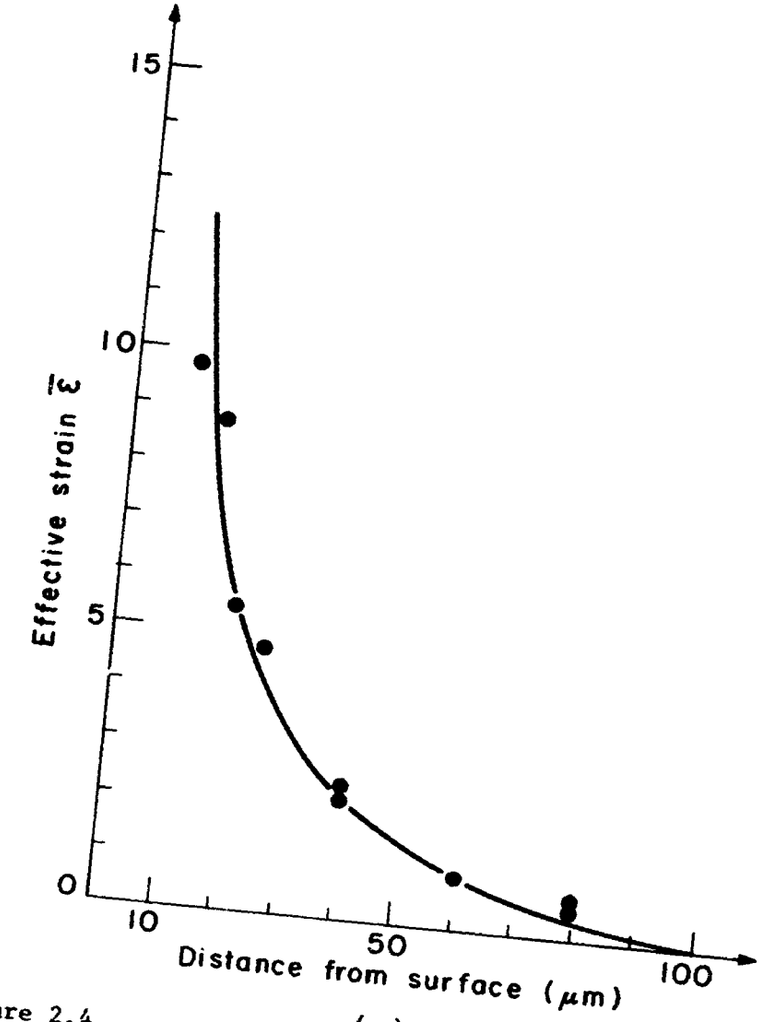

(a)

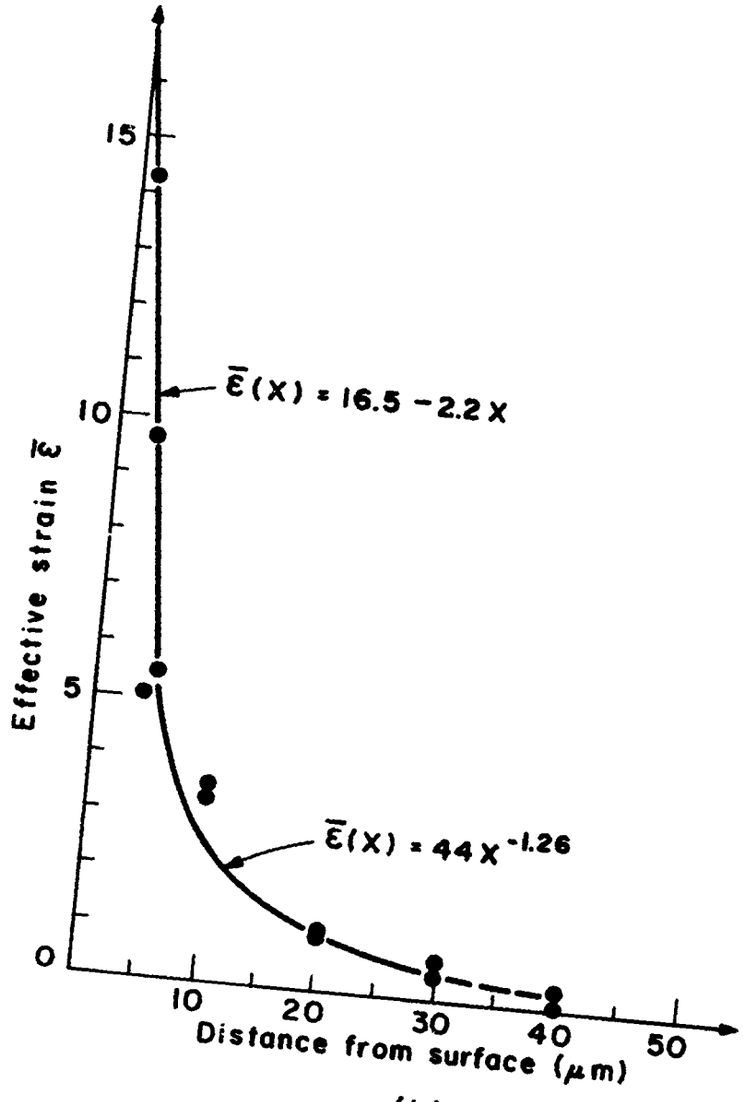

(b)

Figure 2.4

Subsurface strain variation obtained by grain shape measurements: (a) copper specimen tested under a normal load of 2.1 Kg and after a sliding distance of 68 m in argon; (b) AISI 1020 steel tested under a normal load of 2.4 Kg and a sliding distance of 180 m in argon.

The large strain gradient below the surface of a worn metal (such as the one shown in Fig. 2.4) has been also determined theoretically by using the finite element method. The analysis, however, is very approximate since the material was assumed to be isotropic. In a real situation metals acquire texture during the wear process[21-24], making the surface highly anisotropic and affecting the adhesion and surface traction. In the case of f.c.c. metals the plane of the surface after deformation is determined to be a (111) plane, whereas in b.c.c. metals it is a (011) plane. These are slip planes. In the case of h.c.p. metals, some claim that the (0001) plane is the surface plane after deformation[23], while others disagree[21]. This is the slip plane for all h.c.p. metals, although other slip planes are activated in metals with a c/a ratio larger than the ideal 1.63.

II 7) Wear Sheet Formation by Crack Nucleation and Propagation

a) General Observations

The large strain accumulated at the subsurface eventually causes void nucleation below the surface as shown in Fig. 2.5[25]. The micrograph is of a metallographically polished and etched section through the wear track (parallel to the sliding direction) and shows void nucleation and crack propagation between two adjacent inclusions below the surface. These cracks eventually propagate parallel to the surface, as shown in Fig. 2.6 for OFHC copper and AISI 1020 steel[25]. When the subsurface cracks reach a critical length, they become unstable and propagate to the surface to generate wear sheets on the worn surface. Fig. 2.7 shows a wear sheet lifting off a worn surface[26]. Upon further passage of the slider these sheets separate from the surface and generate loose wear particles. Some of these particles may fracture further if they get entrapped between the sliding surfaces. Fig. 2.8 shows some typical wear particles of different materials generated without lubricants under different normal loads. It is noted that the size of the particles depends on the material and the normal load. Most of the particles are in the form of sheets and some have fractured into smaller pieces.

b) Crack Nucleation

In bulk deformation of metals, crack nucleation is favored at the hard inclusion-matrix interface[27,28]. This is also true during delamination wear.

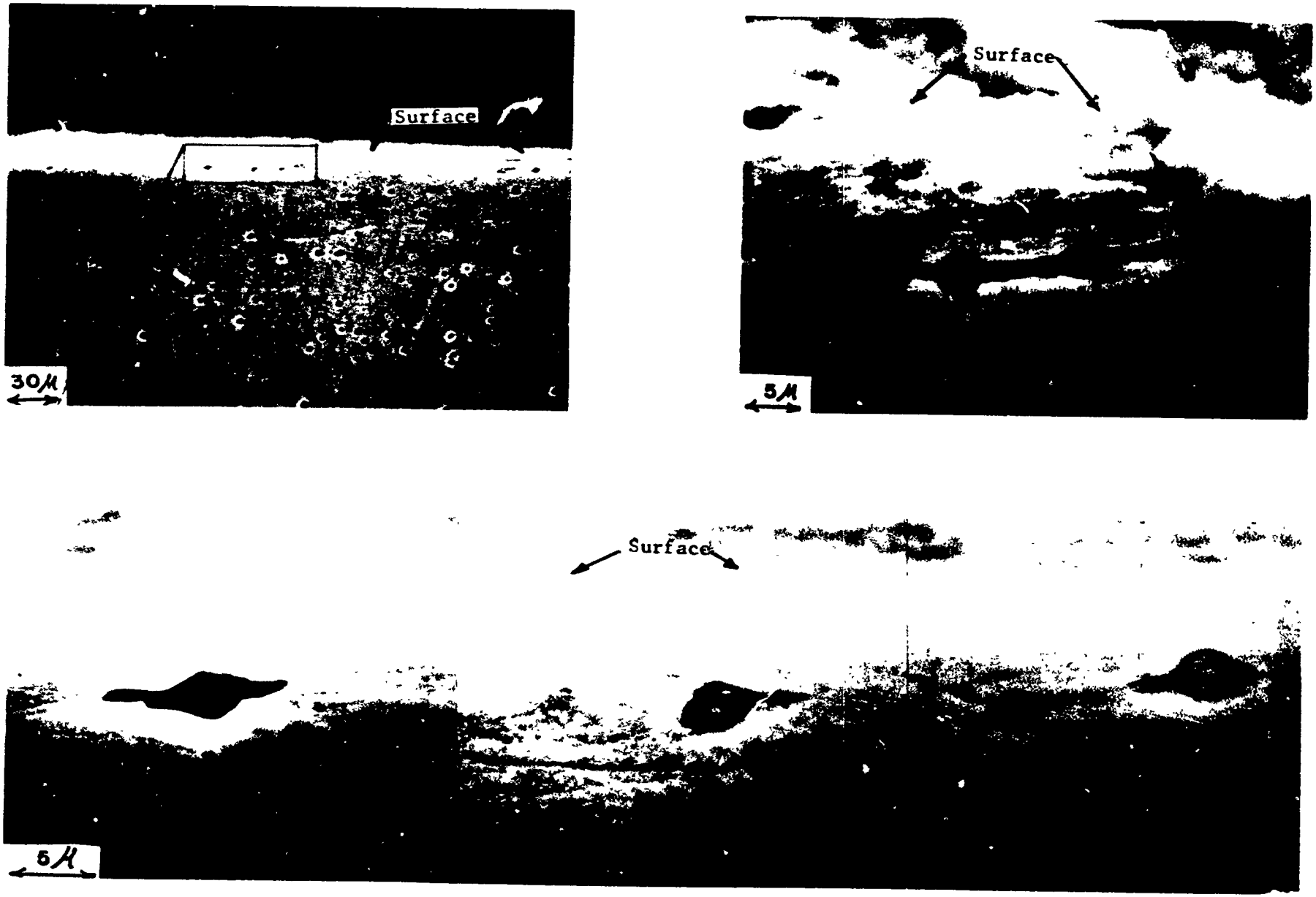

Figure 2.5

Subsurface void and crack formation in Fe-1.3% Mo specimen, tested under a normal load of 2.5 Kg and a sliding distance of 21 m in argon.

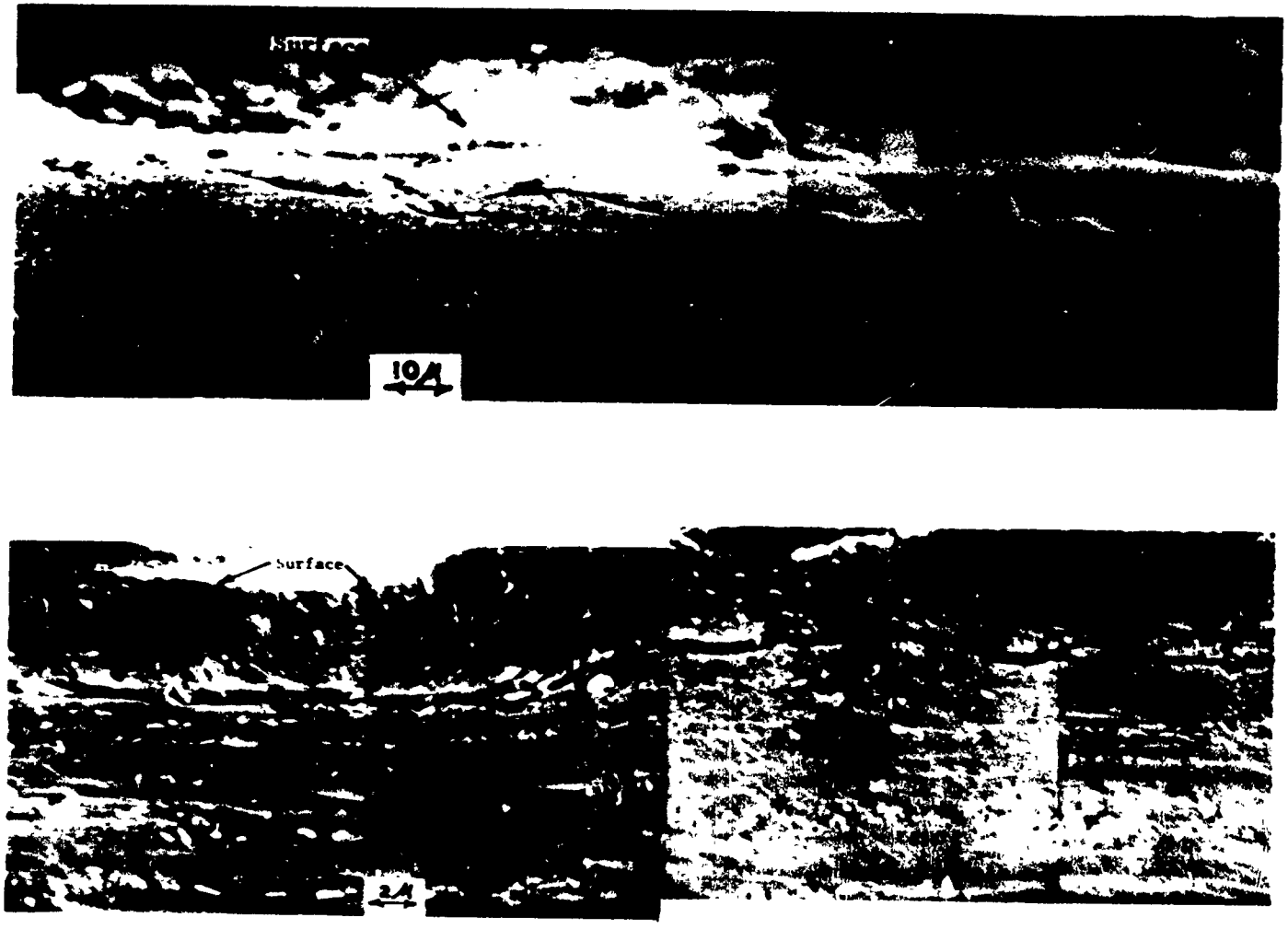

Figure 2.6

Subsurface crack formation in: (a) OFHC copper, tested under a normal load of 1.8 Kg and a sliding distance of 15 m; (b) AISI 1020 steel, tested under a normal load of 1.8 Kg and a sliding distance of 45 m.

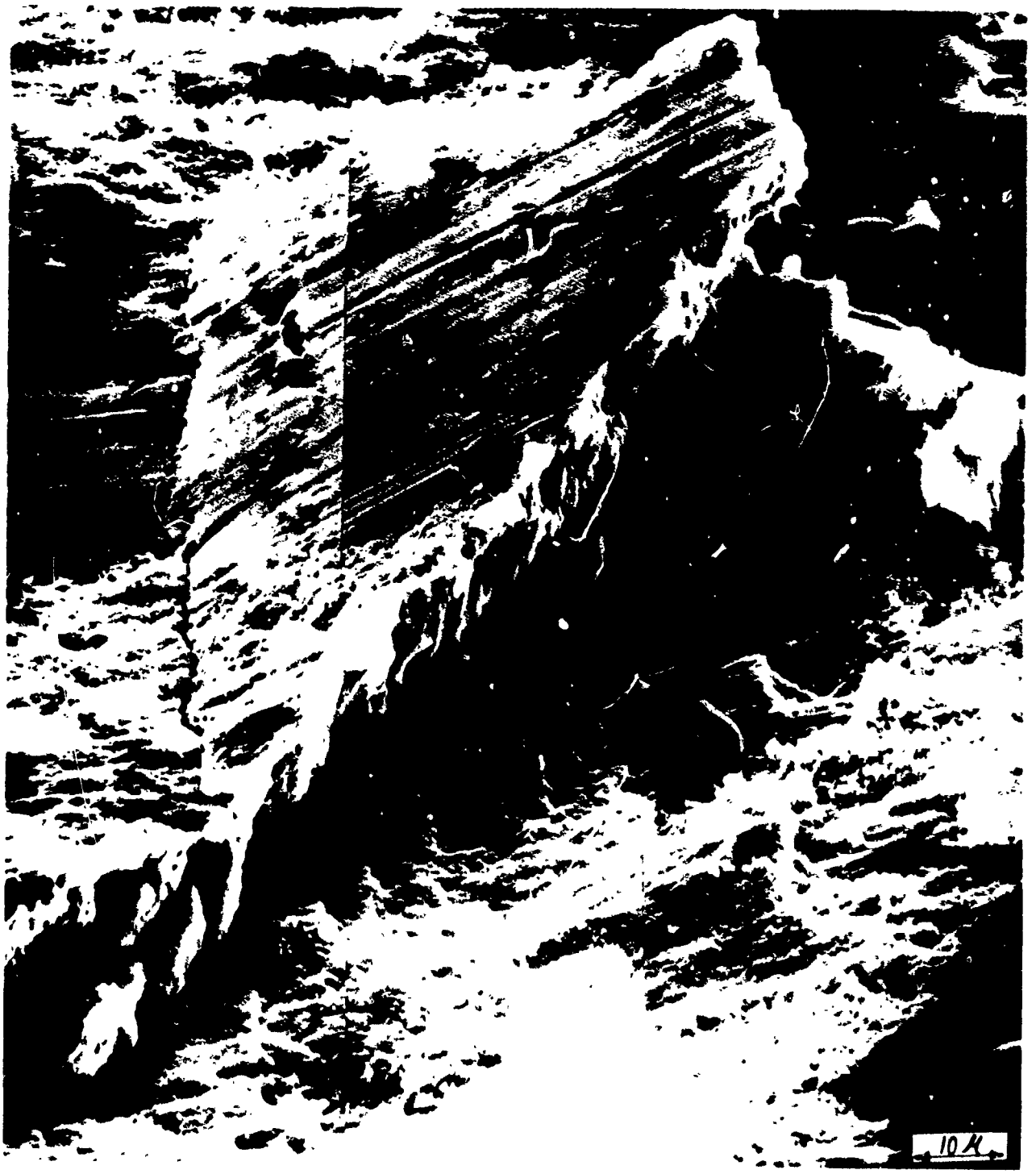

Figure 2.7

Wear sheet on the wear track of Fe-Mo specimen, tested under a normal load of 2.5 Kg and a sliding distance of 90 m.

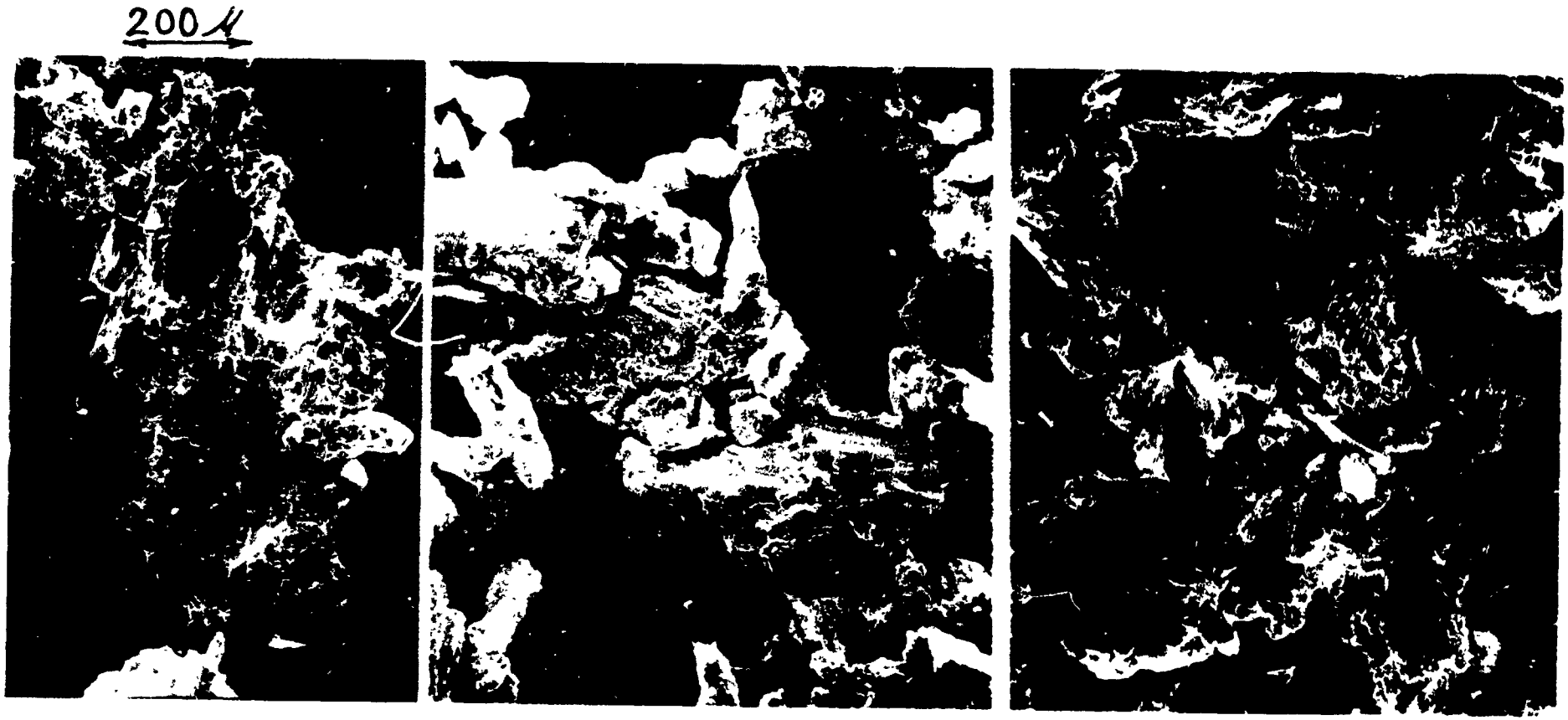

Figure 2.8a

Wear particles collected after tests in argon: AISI 1020 steel under a normal load of 2.25 Kg.

Figure 2.8b

Wear particles collected after tests in argon: AISI 1020 steel under a normal load of 0.40 Kg.

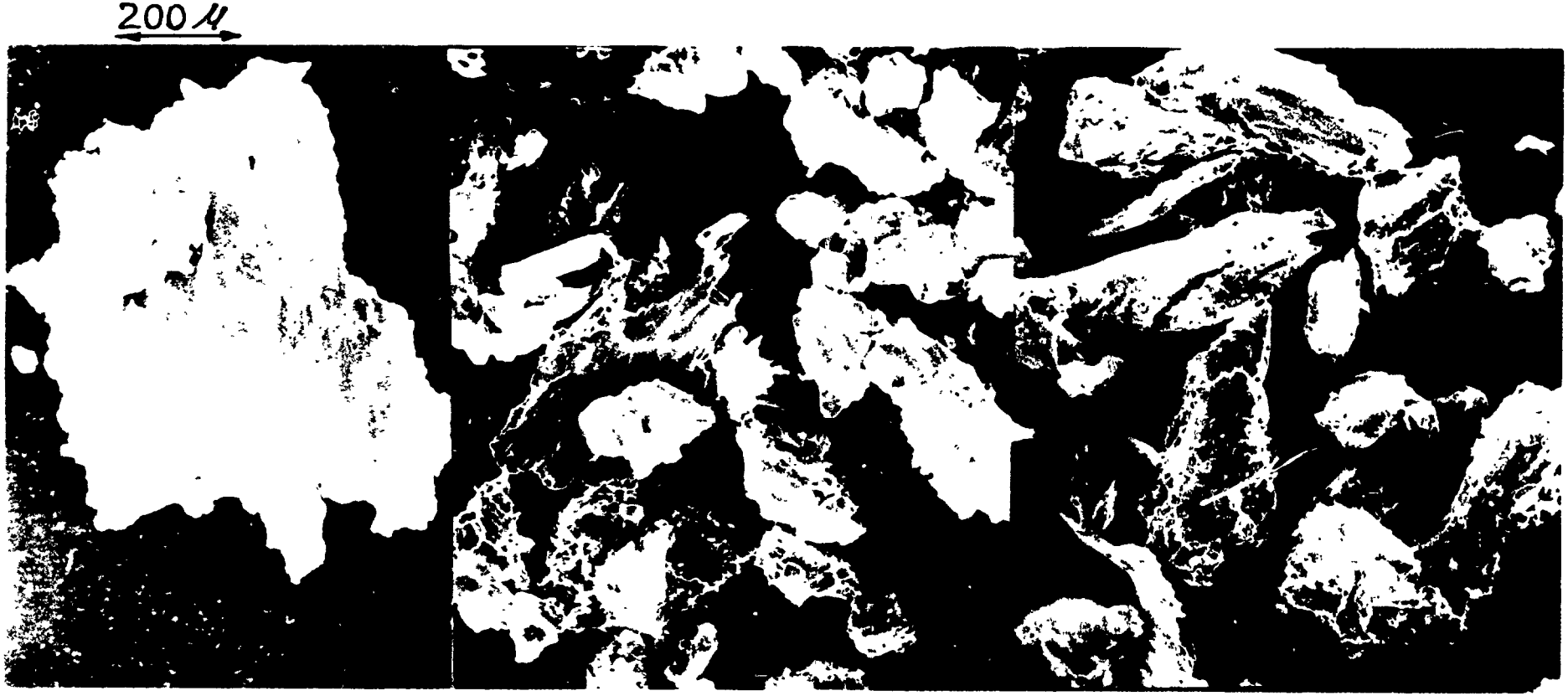

Figure 2.8c

Wear particles collected after tests in argon: AISI 4140 steel under a normal load of 2.25 Kg.

Figure 2.8d

Wear particles collected after tests in argon: AISI 4140 steel under a normal load of 0.40 Kg.

Figure 2.8e

Wear particles collected after tests in argon: AISI 52100 steel under a normal load of 4.5 Kg.

however, the wear process is unique in that there are two opposing mechanisms affecting crack nucleation: the high compressive state of triaxial loading very near the asperity contact suppresses the crack nucleation process, while the large plastic strain field promotes it. Since the hydrostatic pressure decreases with distance from the surface, cracks will nucleate at a depth below the surface where the condition for crack nucleation is satisfied.

The exact condition for subsurface crack nucleation during delamination is not known. However, there is evidence that the crack nucleation process does not differ, at least qualitatively, from those discussed for uniaxial bulk deformation by Argon, et al.[28,29] even though the total strain and the strain gradient are more severe in delamination wear than in bulk deformation. Cracks are most readily nucleated between adjacent large particles and more cracks are detected around large particles than around smaller ones. Crack nucleation is usually by the decohesion of the matrix-particle interface rather than by the fracture of particles in metals with equiaxial particles. In metals with elongated particles of large aspect ratios the fracture of particles is more prevalent. Crack nucleation is detected over the major portion of the plastically deformed region, well below the depth at which crack propagation occurs.

For crack nucleation around hard particles two conditions must be satisfied: the local stress must be equal to the strength of the particle-matrix interface or the cohesive strength of the particle; and the elastic strain energy released upon decohesion or fracture must be sufficient to supply the surface energy of the crack or the void. According to Argon, et al.[28], the energy condition is always satisfied by particles larger than 100Å in the case of normal bulk deformation; or conversely, voids cannot form around particles smaller than 100Å because the elastic energy released upon crack nucleation is less than the surface energy requirement. The interface stress between the particle and the matrix is developed due to the interfacial displacement incompatibility upon plastic yielding of the matrix[30]. The interface stress is greatly intensified when two inclusions are in such a close geometric proximity that the strain field of the matrix material between the particles is nearly homogeneous. In the case of delamination wear these interface tensile stresses are counterbalanced by the triaxial state of compressive stress existing underneath the surface. Because of this high hydrostatic pressure which retards void nucleation, large plastic deformation is required for crack

nucleation in delamination wear.

In zone refined-zone leveled iron with 500 ppm tungsten it was difficult to identify the region of crack and/or void nucleation. However, a few large cracks were detected very near the surface, indicating that cracks nucleated and that a very large strain is necessary for crack nucleation and/or propagation in metals with no inclusions[26]. The exact mechanism of crack nucleation in clean single phase metals is not known at this time. However, several plausible possibilities have been considered: vacancy formation during the large plastic deformation and subsequent coalescence to form a void, crack nucleation due to dislocation pile-ups at dislocation cells, and void formation at triple points due to the large local stress developed during deformation and texture development.

c) Crack Propagation

In general, crack nucleation does not guarantee crack propagation, since crack propagation requires either a negative hydrostatic pressure or presence of shear stress parallel to the surface. It has been found that a state of negative hydrostatic pressure may be present below the surface in the region behind a moving asperity[31], which may cause crack propagation in that region. The cracks may also propagate by the shear stress (tangential force) component of the subsurface stress distribution. However, the presence of large hydrostatic pressure under the contact might retard the process of shear crack propagation. In the next chapter the nature of subsurface crack propagation will be analyzed by examining the state of stress below the sliding surfaces.

Chapter III

MECHANICS OF DELAMINATION

III 1) Introduction

According to the delamination theory of wear, three processes must take place for wear to occur: deformation, crack nucleation, and crack propagation. Deformation and nucleation have been discussed in previous sections. This section will deal with crack propagation (qualitatively, since quantitative discussion is not yet possible).

The goal of this phase of the study of wear at M.I.T. is a criterion for crack propagation based on loading and material properties. With such a criterion, wear rates and part lives could be predicted. The formulation and analysis of criteria for crack propagation is a part of the study of fracture mechanics. Fracture mechanics deals with criteria for crack propagation in terms of material properties and the type and magnitude of stress acting throughout the body.

Thus it is necessary to know the state of stress present below the surface during sliding wear in order to apply existing fracture criteria or to formulate a new criterion. At present, an exact solution for the state of stress is not known; some approximate solutions are discussed below. Exact analytic solutions seem impossible, but numerical solutions are possible with minor extension of existing procedures. Numerical solutions are currently being sought by the M.I.T. wear research group, using the finite element method.

III 2) Investigation of Subsurface Stress and Displacement

The finite element method is discussed in Appendix A. The material being modelled is copper, with a yield point of 17 kg/mm^2, a Young's modulus of 28000 kg/mm^2, and a Poisson's ratio of 0.333. The material is idealized as an elastic-perfectly plastic body, and the von Mises yield criterion is used. The loading condition is assumed to be plane strain, and the load is applied by a 10 μm long rigid asperity. The body is assumed to be an infinite half-plane.

Using this model, stresses, strains and displacements may be found for loading and unloading by a stationary asperity in presence of both the normal and tangential loads acting at the contact. At this time, the

results for unloading are not yet available. However, notwithstanding the cyclic nature of the loading which occurs as asperities pass over each point, some qualitative conclusions may be drawn as to the possibilities of crack propagation.

Figures 3.1, 3.2, and 3.3 show, for three coefficients of friction μ, the state of stress underneath the asperity at nearly the maximum load the elastic-plastic solid can support (approximately the point at which the tangential applied stress is equal to the yield stress). Two double-headed vectors intersect at each point at which stress is evaluated. The vectors are in the directions of the principal stress axes; their lengths are proportional to the magnitudes of the principal stresses; and the arrowheads point inward for negative (compressive) principal stress and outward for positive (tensile) principal stress. A reference vector below the plot provides a scale for reading stress magnitudes. A capital P beside a point indicates plastic deformation.

III 3) Discussion

Crack propagation in bulk occurs when a tensile stress is applied perpendicular to the plane of the crack (i.e. mode I) and also under the action of shear stresses (i.e. modes II and III). Compressive loading perpendicular to the crack plane influences the plastically deformed region around a crack tip, but a hydrostatic compressive loading by itself cannot propagate the crack. These statements have been used to formulate mathematical fracture criteria, such as the critical stress intensity factor K_c and the J integral. However, the formulations either assume small plastic deformation, a small plastic zone, or no edge effects. None of these assumptions are justifiable in a sliding wear situation.

The general statements about the type of stress that can propagate a crack do apply to sliding wear. The out-of-plane shear mode III cannot be discussed here, because the plane strain assumption forbids out-of-plane shear. Mode III is unlikely, since the plane strain assumption is a good one.

As to the possibility of in-plane shear (mode II), this mode seems unlikely. In Figs. 3.1, 3.2, and 3.3 the principal shear directions (45° from the principal stress directions) are usually at a non-zero angle to the surface. Since cracks propagate by mode II along the principal shear directions, and since

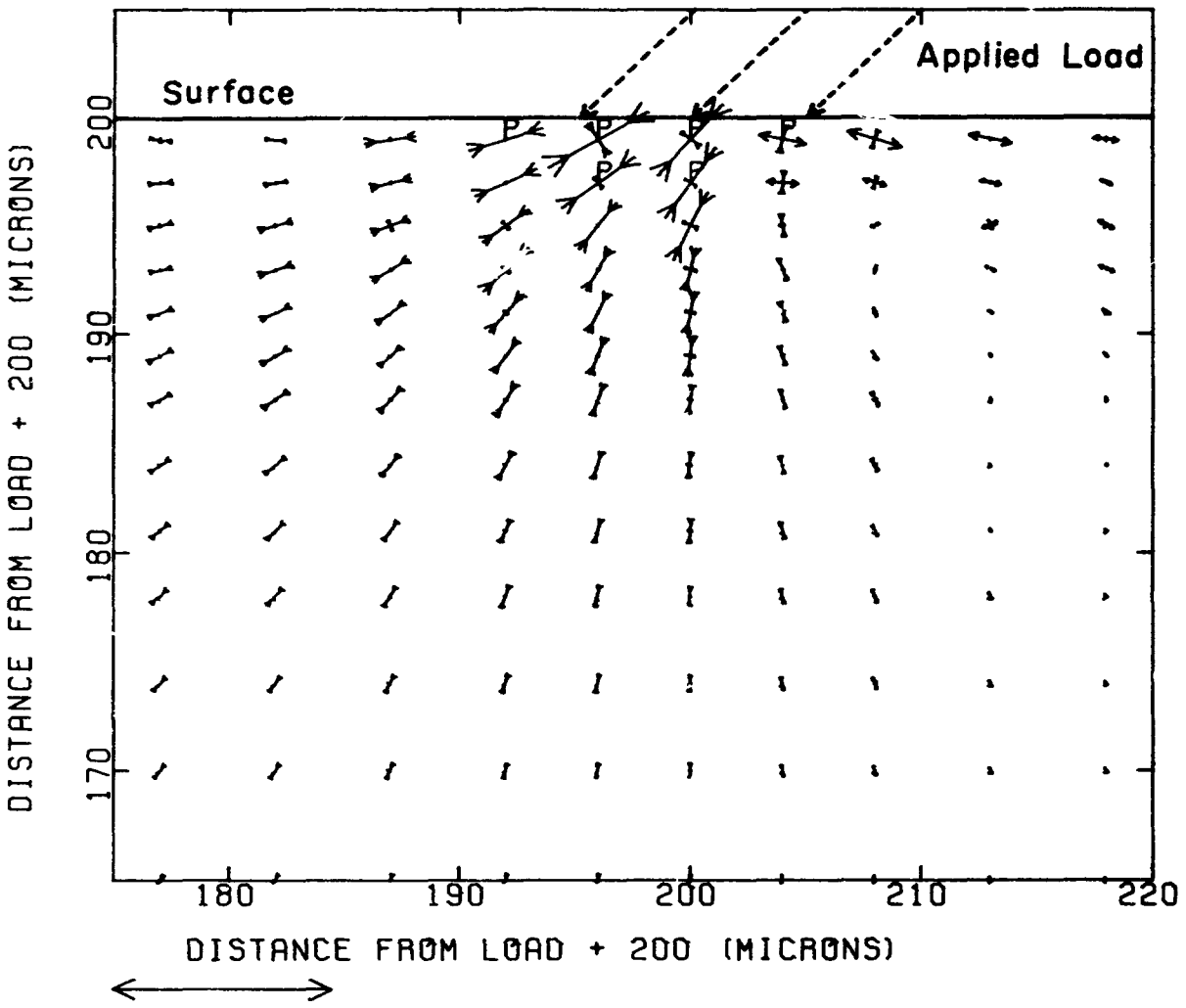

Figure 3.1

Stress field under a 10 μm asperity, μ = 1

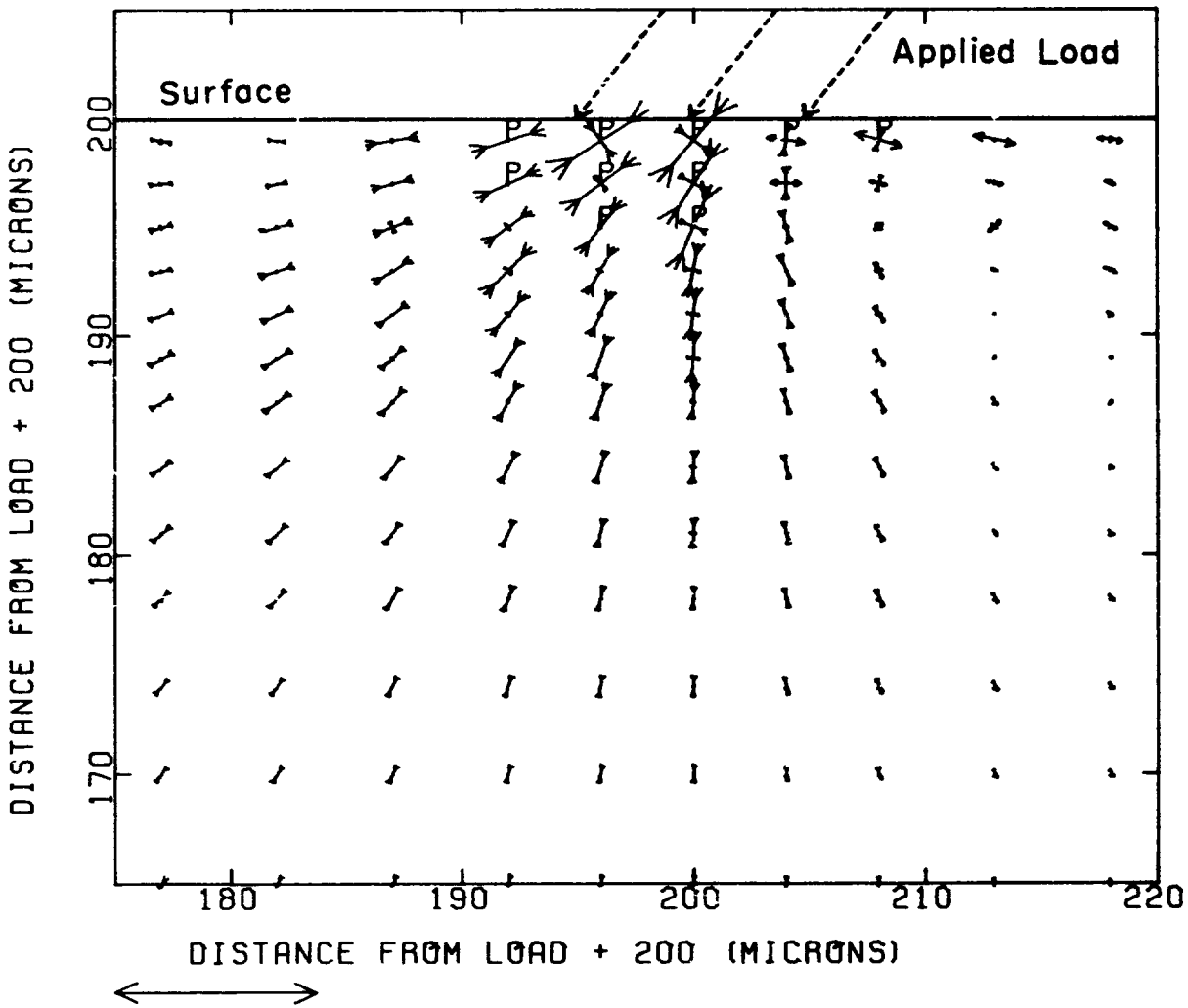

REFERENCE VECTOR LENGTH IS 5.0000 POUNDS * 10**-5 PER MICRON**2
PRINCIPAL STRESSES UNDER A 10 MICRON LONG ASPERITY, MU=3/4 (P INDICATES PLASTIC)

Figure 3.2

Stress field under a 10 μm asperity, $\mu = 3/4$

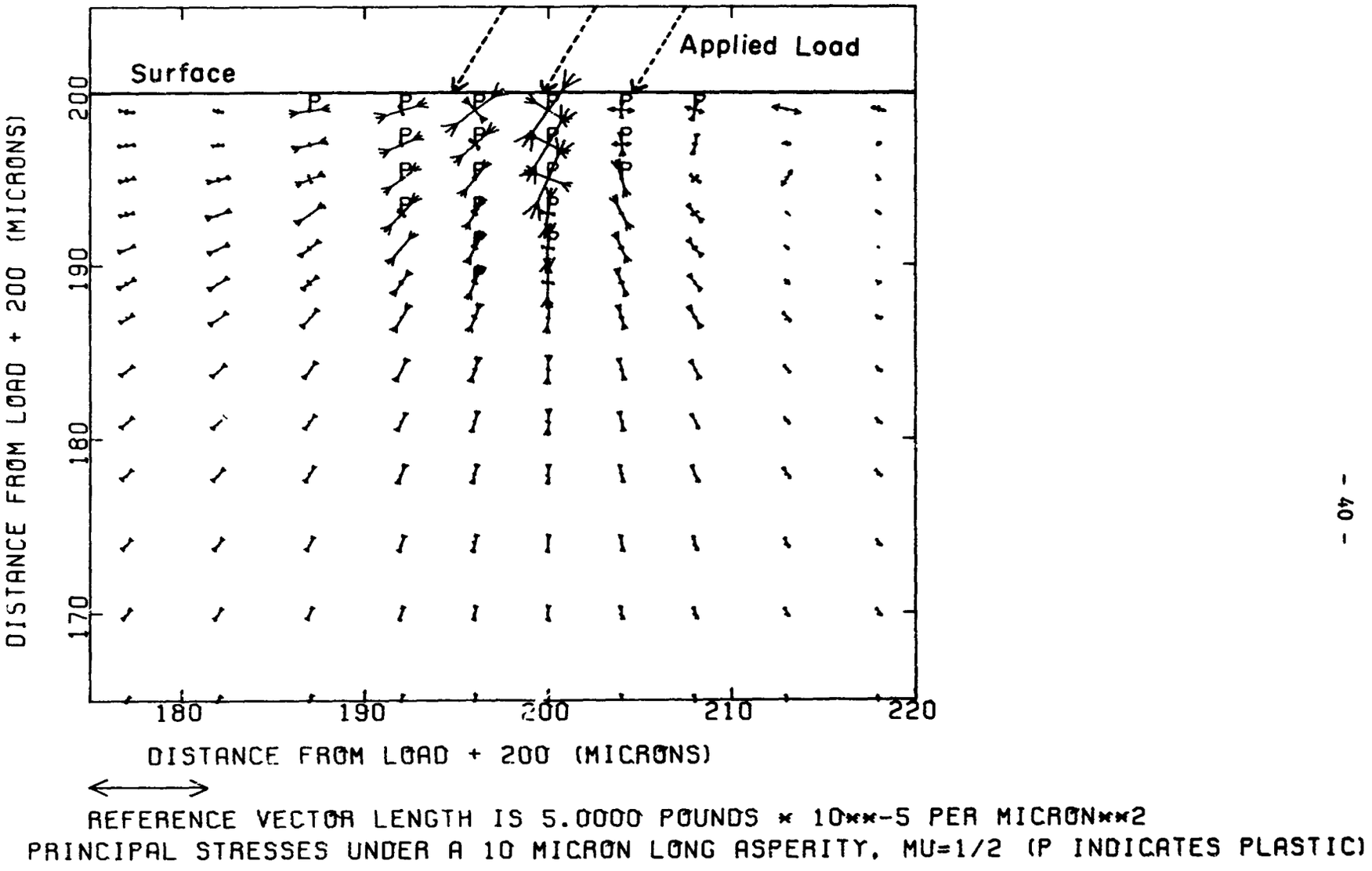

Figure 3.3

Stress field under a 10 μm asperity, $\mu = 1/2$

cracks have been observed only roughly parallel to the surface, mode II is unlikely. However, mode II is still possible. This mode will not be discussed further here, since it has been investigated and understood less than the more common tensile mode (mode I). Also, the discussion below shows that mode I is the most likely mode.

There is some evidence that subsurface cracks may propagate by a tensile (modeI) process during sliding wear. Assuming for the moment that a crack may nucleate anywhere, and assuming that all nucleated cracks have the same stress concentration factor and do not change the overall stress field appreciably, the crack which lies at the point of maximum tensile stress is most likely to propagate. For a given material, the position of the point of maximum tensile stress is a function of the total applied load and the coefficient of friction μ. If the assumptions above are at all reasonable, the depth of the maximum tensile stress should correlate well with the observed crack depth.

Figure 3.4 is a plot of observed crack depth and the depth of the maximum tensile stress perpendicular to the surface versus μ. The tensile stress depth was found by quadratic interpolation of the results shown in Figs. 3.1 and 3.2. The tensile zone is too shallow in Fig. 3.3 for interpolation. The stresses were evaluated at a load near to the maximum total load that the elastic-plastic solid can support (approximately the yield stress to half the yield stress as μ increases from $\frac{1}{2}$ to 1). The crack depths were measured from photographs of cross sections of various specimens.

By including work hardening or cyclic softening, the maximum load the solid can support would be increased. This would increase the magnitude and depth of the maximum tensile stress, and move the experimental points in Fig. 3.4 vertically. However, the relative positions of the experimental points (i.e. the slope of the line between them) is dictated by the mechanics of loading rather than the magnitude of the load, and would not change. The good correlation of slopes in Fig. 3.4 supports the hypothesis that cracks propagate parallel to the surface by a mode I mechanism at the point of maximum tensile stress perpendicular to the surface. Furthermore, it should be noted that the general trend is about the same as the experimentally determined wear coefficients vs. μ relation found by Rabinowicz as shown in Fig. 3.5.[32]

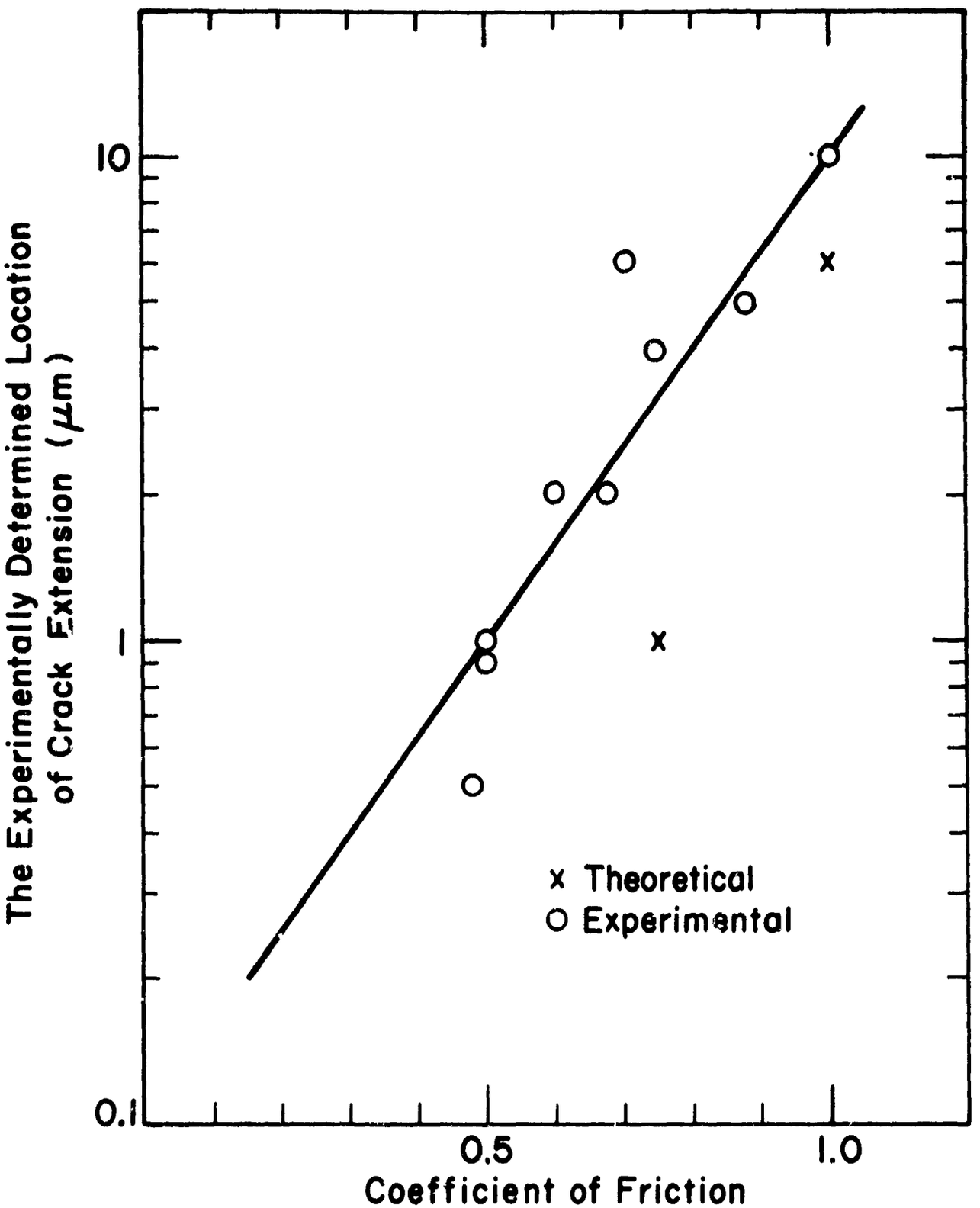

Figure 3.4

The experimental and theoretical relationship between crack depth and coefficient of friction.

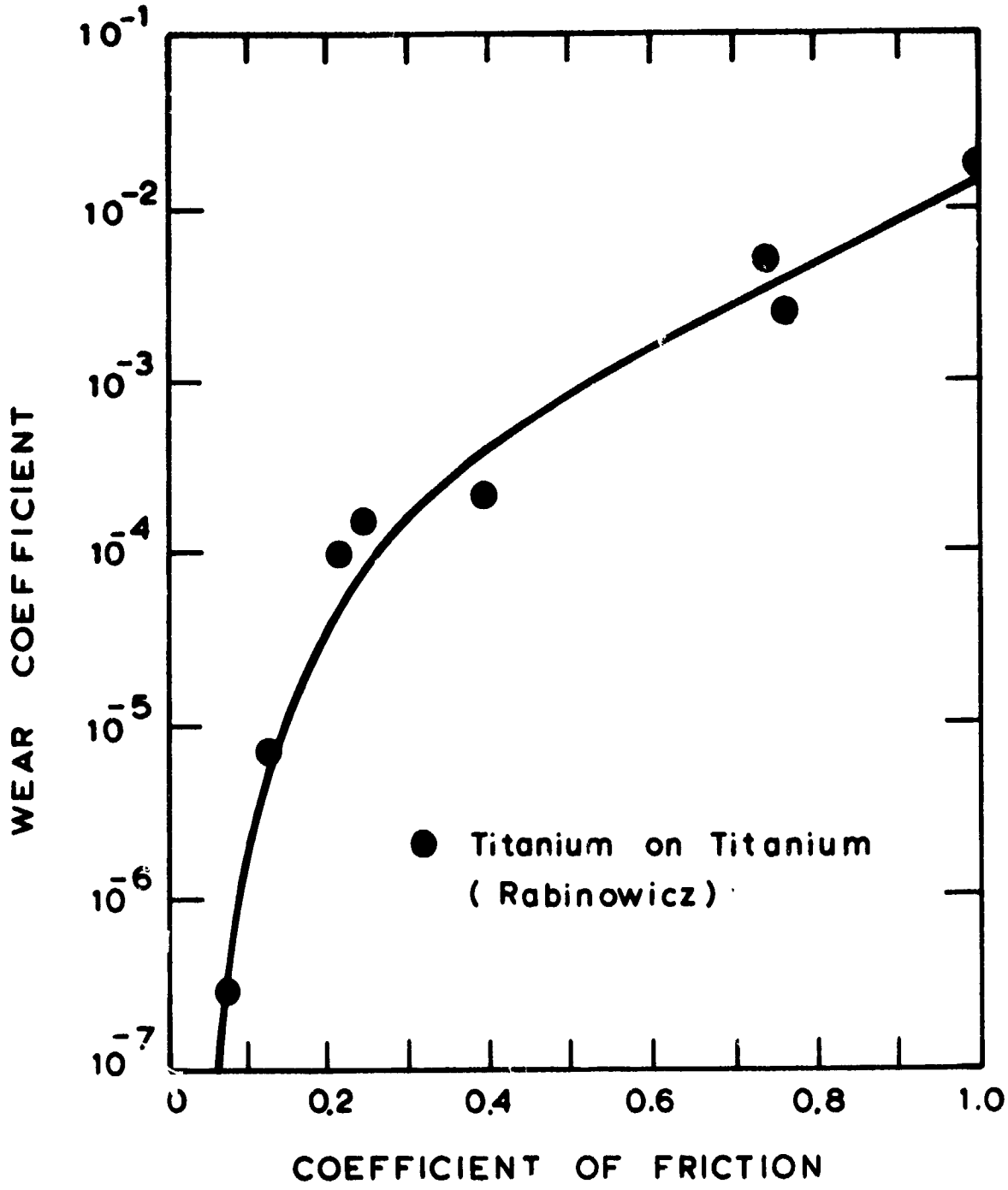

Figure 3.5

An experimental relationship between wear coefficient and coefficient of friction (adapted from Ref. 32).

The preceding discussion of tensile stress only considered the tensile stress perpendicular to the surface. In view of the large tensile stresses parallel to the surface in Figs. 3.1, 3.2, and 3.3, it seems surprising that cracks generally do not propagate perpendicular to the surface. However, the existence of the flow stress gradient would reduce the magnitude of those stresses since the soft surface layer could not support such large stresses parallel to the surface. In addition, the texture produced during sliding wear may favor crack propagation parallel to the surface. Experiments are now being carried out to investigate the possibility of cracks normal to the surface in brittle materials.

Further conclusions cannot be drawn until the cyclic loading condition has been considered, the "coarseness" of the model (distance between points at which stress is evaluated) has been decreased, and quantitative fracture criteria have been devised. It is difficult to use established fracture criteria, since all such criteria ignore edge and size effects which are certainly important in wear since the cracks are so near the surface and the plastic zone is so large.

III 4) Future Plans

Besides the aforementioned refinement of the grid and consideration of unloading, the material model must be revised in order to account for cyclic effects. Experimental work has been started which will lead to a constitutive equation which will include both cyclic softening and hardening. This equation will be used to define a yield criterion for finite element analyses of repeated passes of moving asperities.

It is certain that inclusions, second phase particles, and cracks will alter the stress field. Analyses are being performed which consider the effect of a rigid inclusion. We hope to be able to analyze the effect of cracks and inclusions in various positions in the body.

In summary, in order to fully understand wear, the mechanics of deformation, crack nucleation, and crack propagation must be clarified. To this end, the finite element method offers promise as a tool for finding stresses and strains in sliding wear. These stresses and strains, once found, can be used in fracture criteria to predict wear rates and part lives.

Chapter IV

ENERGY CONSIDERATIONS:
THE RELATION BETWEEN FRICTION COEFFICIENT AND WEAR RATE

IV 1) Introduction

An upper bound solution[4] based on Archard's adhesion model of wear predicts the external work done in sliding wear to be at least two to three orders of magnitude smaller than the measured external work. This has been explained by proponents of the adhesion theory by assuming that wear particles transfer from one surface to the other before coming loose. Although transfer occurs for some metals (e.g. gold and copper), it is very limited in others (e.g. steel). There is no evidence that sufficient transfer occurs to account for the external work in any case.

Any theory which describes a physical phenomenon must be consistent with the laws of thermodynamics such as conservation of energy. An approximate analysis presented in this chapter shows that the delamination theory of wear does satisfy the energy conservation laws. It follows that friction and wear are related, since the friction coefficient contributes to the external work and wear is related to the internal plastic energy since it is caused by subsurface deformation.

The energy conservation analysis is used to find an order of magnitude approximation to the relationship between friction coefficient and wear rate. The model is overly simplified, since sufficient information for a detailed model is unavailable, yet it yields surprisingly good results. The model shows that the coefficient of friction is related to the wear factor by the constitutive relation for a cyclically loaded metal, the experimentally determined strain field near the wearing surface, and the thickness of the delaminated sheet.

IV 2) Analysis of the Unlubricated Case

It is clear that the early stages of wear of a surface consist of the plastic deformation of surface asperities and subsequent removal of these deformed asperities by a fatigue process. However, the wear rate associated with the removal of these asperities is low and the surface at this time has a polished appearance and the surface is still usable.

A sliding surface becomes rough and unusable when wear occurs by the delamination process which is caused by sub-surface crack nucleation and propagation following the deformation of the surface layer.[25,26,33-35]

When the wear process reaches a steady state condition, the depth of the plastically deformed zone reaches a constant value for a given set of sliding conditions[35]. The equivalent plastic strain in the metal when the steady state wear condition is reached differs from metal to metal. The experimental measurements made by Agustsson[20] using the technique of Dautzenberg and Zaat[36] show that the plastic strain gradient in steel could be approximated by a combination of linear and exponential empirical functions. The plastic strain in copper was so large that it could not be measured quantitatively very near the surface.

The equivalent plastic strain $\bar{\epsilon}^p$ in annealed AISI 1020 steel specimens, which have undergone a delamination wear process, was approximately determined to be [20]

$$\begin{aligned} \bar{\epsilon}^p &= \epsilon_0 - \alpha x = 16.5 - 2.2x \quad \text{for} \quad 0 \leq x \leq x_c \\ \bar{\epsilon}^p &= \epsilon_1 x^{-\beta} = 44x^{-1.26} \quad \text{for} \quad x \geq x_c \end{aligned} \tag{1}$$

where the x-axis is perpendicular to the surface as shown in Fig. 4.1. The unit of x is μm. The depth at which both functions have the same value and yield the same slope is given by

$$x_c = \left(\frac{\beta\epsilon_1}{\alpha}\right)^{\frac{1}{1+\beta}} = \left(\frac{1.26 \times 44}{2.2}\right)^{\frac{1}{2.26}} = 4.17\,\mu m \tag{2}$$

The plastic strain is accumulated in several cycles, each cycle corresponding to the passage of one asperity. If N_f such cycles of loading are required for delamination to occur, then the total equivalent plastic strain before delamination is

$$\bar{\epsilon}^p = \sum_{i=1}^{N_f} \Delta\bar{\epsilon}_i^p \tag{3}$$

where $\Delta\bar{\epsilon}_i^p$ is the net plastic strain generated during the ith cycle.

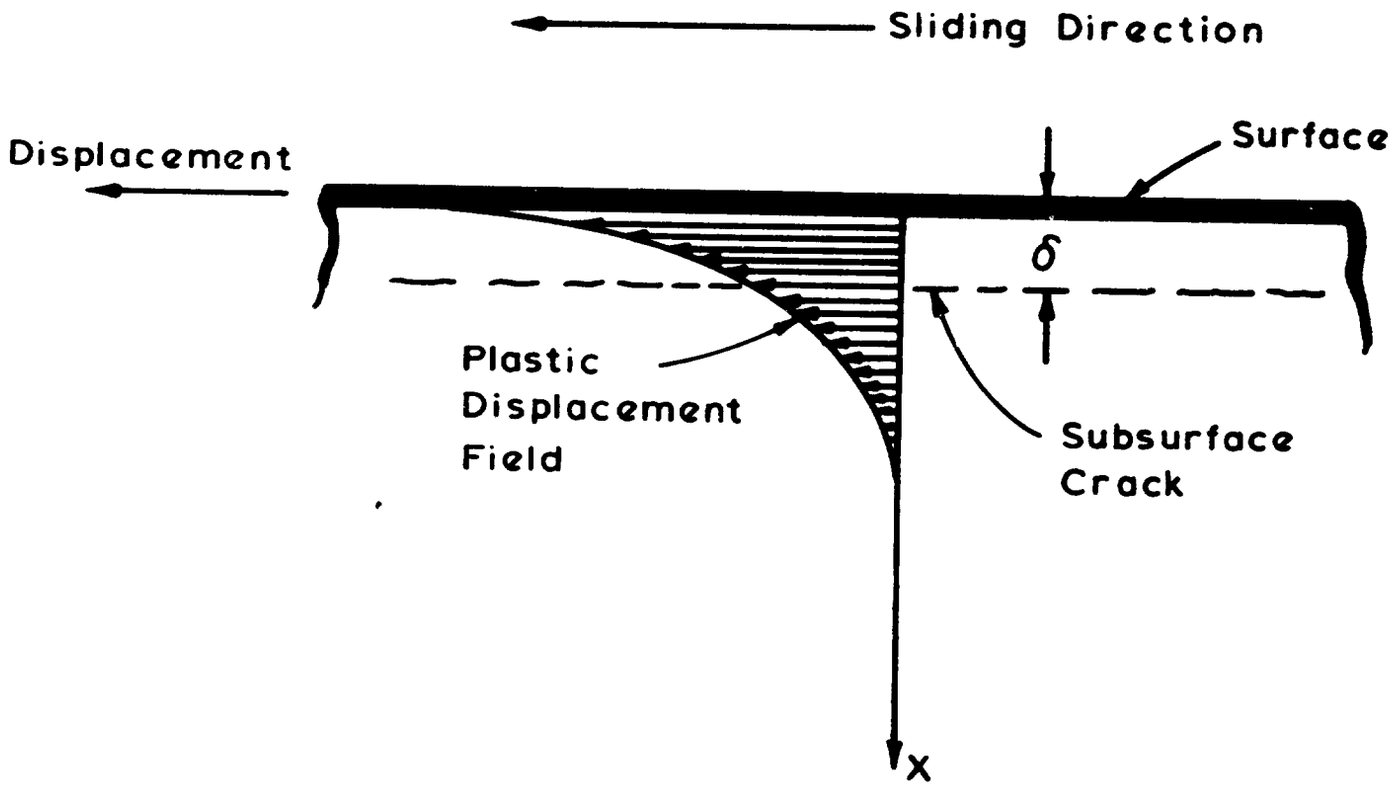

Figure 4.1

Schematic repr.sentation of displacement field below a plastically deformed worn surface.

An energy argument will be used to relate the internal energy due to plastic deformation to the external work done by the surface traction. In order to be able to determine the plastic work done in generating a permanent deformation $\bar{\epsilon}^p$, the work done per cycle may be summed over the entire loading history as

$$W^p = bl \sum_{i=1}^{N_f} \int_0^{\infty} \int_0^{\bar{\epsilon}_i} \bar{\sigma}\, d(\bar{\epsilon}_i)\, dx \tag{4}$$

where b is the average width of the wear sheet, ℓ is the average length of the wear sheet, $\bar{\sigma}$ is the equivalent stress, $\bar{\epsilon}_i$ is the total equivalent strain the material undergoes and N_f is the total number of loading cycles that the material has experienced at the time of delamination. Both $\bar{\sigma}$ and $\bar{\epsilon}$ are functions of the depth x. The total equivalent strain $\bar{\epsilon}_i$ is not the same as the net permanent strain $\Delta\bar{\epsilon}_i^p$ per cycle.

At this time there is no solution available for $\bar{\epsilon}_i$ and $\Delta\bar{\epsilon}_i^p$. A similar problem has been investigated by Merwin and Johnson[37] for rolling contact problems by considering only the effect of normal stress. The problem we are interested in solving differs from the Merwin-Johnson problem because of the tangential load acting on the surface. The major conclusion of the Merwin-Johnson solution is that the subsurface material can deform plastically and the plastic strain can accumulate when the normal load exceeds a critical value. It was shown that whenever the shear stress τ_{xy} exceeds the shear flow stress of the metal the plastic strain accumulates, based on the assumption that the material relaxes elastically until the residual stresses satisfy the boundary condition. The possibility that the material may undergo secondary plastic flow upon unloading was not considered by Merwin and Johnson. We are in the process of analyzing the deformation of metals under more realistic assumptions using a finite element method.

Another reason for the plastic strain accumulation may be the peculiar behavior of metals under cyclic loading. When a metal is subjected to cyclic loading, it either softens or hardens as shown in Fig. 4.2[38]. Cold worked metals usually undergo cyclic softening, while annealed metals may first undergo cyclic hardening followed by cyclic softening. After each cyclic loading there is a residual permanent strain $\Delta\bar{\epsilon}_i^p$, which is much smaller

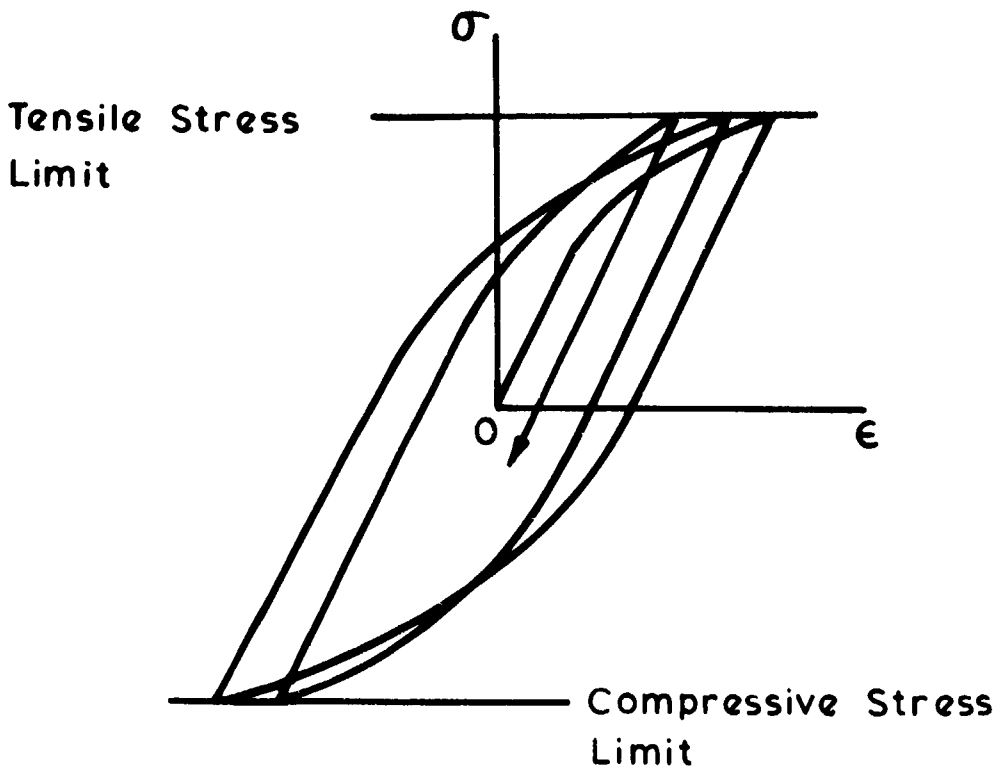

Figure 4.2a

Stress-strain curves for constant stress cycles (adapted from Ref. 38): cyclic hardening.

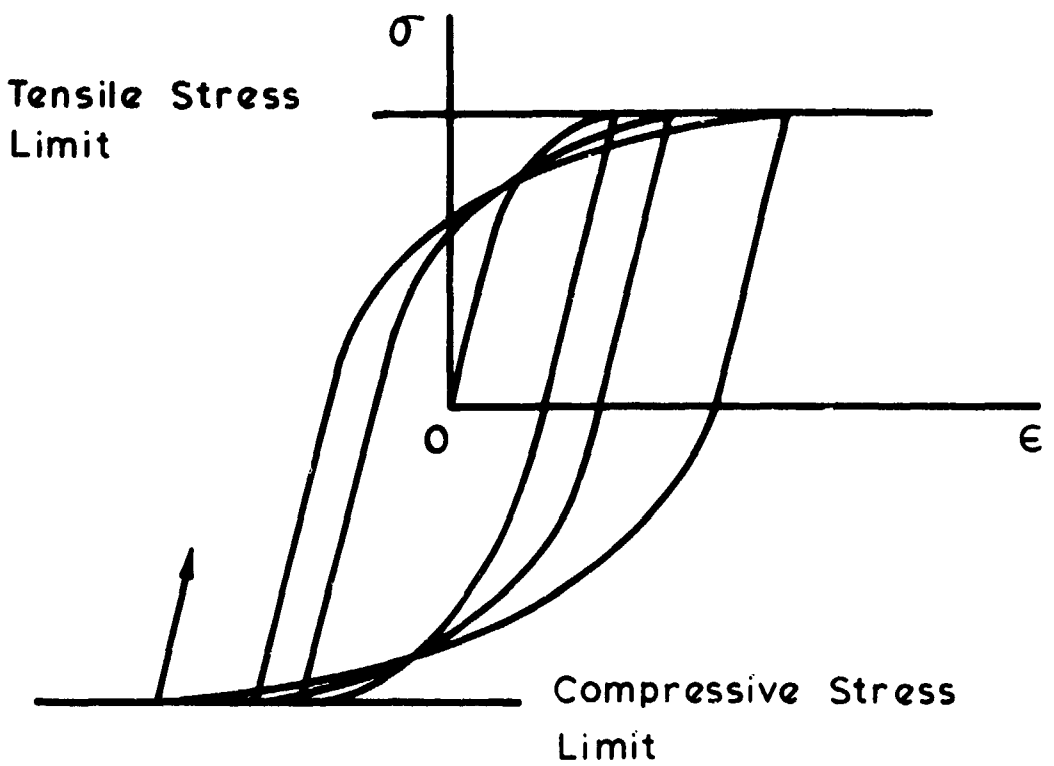

Figure 4.2b

Stress-strain curves for constant stress cycles (adapted from Ref. 38): cyclic softening.

than the maximum strain amplitude $\bar{\varepsilon}_i$ of that cycle, as illustrated in Fig. 4.3. For cyclically softening materials $\Delta\bar{\varepsilon}_i^p$ increases with repeated loading, whereas it decreases with cycling for cyclically hardening materials.

The stress-strain history of the metal near the surface is different depending on its distance from the surface. For the elastic semi-infinite solid loaded by a concentrated load the Boussinesq[87] solution states that the metal very near the surface experiences a reversed compression-tension stress, while the material below it may only experience compressive loading and unloading. There can also be secondary plastic flow upon unloading due to the residual stress.[39] A possible stress-strain history is given in Fig. 4.3 which is plotted in terms of the maximum resultant shear stress τ and the resultant shear strain γ. It should be noted that $\bar{\sigma}$ and $\bar{\varepsilon}$ always remain positive by definition and that the absolute value of τ is nearly equal to $\bar{\sigma}/2$ and that of γ is nearly equal to $\bar{\varepsilon}/2$.

As a first approximation to the problem one may assume that

$$\bar{\sigma} = \bar{\sigma}_0 = \text{constant} \tag{5}$$

Substituting eqn. (5) into eqn. (4), the latter may be written as

$$\begin{aligned} W^p &= (bl) \sum_{i=1}^{N_f} \int_0^{\infty} \int_0^{\bar{\epsilon}_i} \bar{\sigma}_0 \, d(\bar{\epsilon}_i) \, dx \\ &= (bl) \sum_{i=1}^{N_f} \int_0^{\infty} \bar{\sigma}_0 \, \bar{\epsilon}_i \, dx \end{aligned} \tag{6}$$

Let the ratio m_i of the total equivalent strain $\bar{\varepsilon}_i$ to the net plastic strain per cycle $\Delta\bar{\varepsilon}_i^p$ be defined as

$$m_i = \frac{\bar{\epsilon}_i}{\Delta\bar{\epsilon}_i^p} \tag{7}$$

and as a first approximation let mi=m, where m is a constant independent of x. Substituting Eq. (7) into Eq. (6), we obtain

$$W_p = m \, \bar{\sigma}_0 \, (bl) \sum_{i=1}^{N_f} \int_0^{\infty} \Delta\bar{\epsilon}_i^p \, dx \tag{8}$$

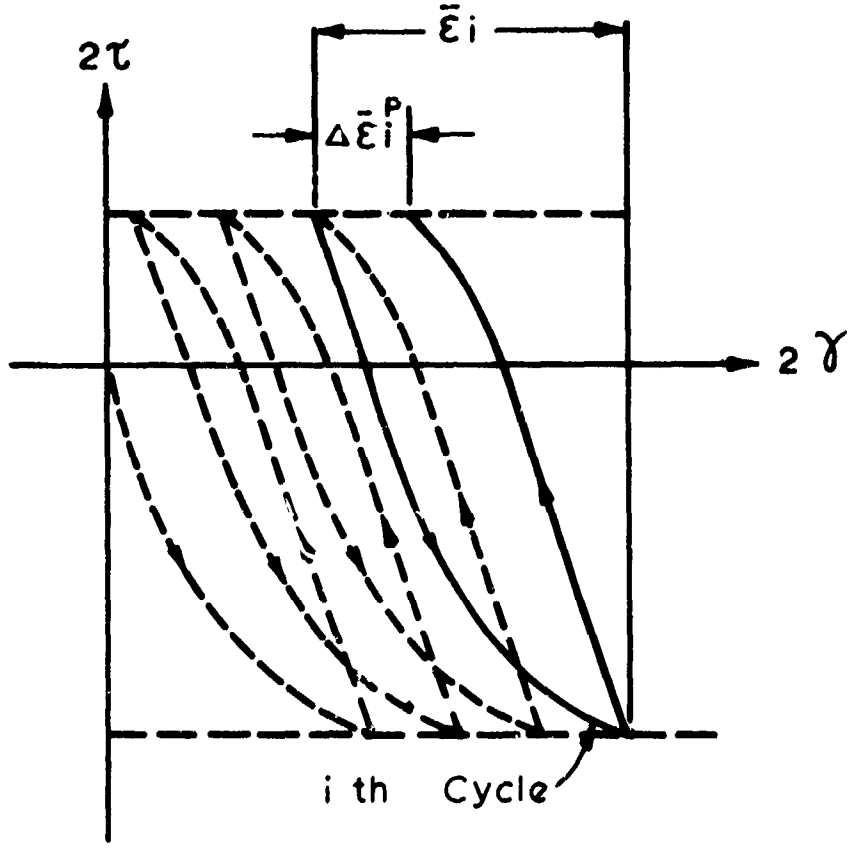

Figure 4.3

Stress-strain history of a cyclically loaded metal; the i-th cycle is shown by the solid line.

Using Eq. (3), Eq. (8) may be written as

$$W_p = m\,\bar{\sigma}_0\,(bl)\int_0^{\infty}\bar{\epsilon}^p\,dx \tag{9}$$

After a wear sheet of thickness δ is delaminated, the additional work necessary to delaminate the next layer ΔW^p is given by

$$\Delta W^p = m\,\bar{\sigma}_0\,(bl)\left[\int_0^{\infty}\bar{\epsilon}^p\,dx - \int_{\delta}^{\infty}\bar{\epsilon}^p\,dx\right]$$

$$= m\,\bar{\sigma}_0\,(bl)\int_0^{\delta}\bar{\epsilon}^p\,dx \tag{10}$$

If $\delta < x_c$, the first of Eqs. (1) may be substituted into Eq. (10) as

$$\Delta W^p = m\,\bar{\sigma}_0\,(bl)\int_0^{\delta}(\epsilon_0 - \alpha x)\,dx = m\,\bar{\sigma}_0\,(bl)\left[\epsilon_0\delta - \frac{\alpha\delta^2}{2}\right] \tag{11}$$

If $\delta > x_c$, Eqs. (1) may be substituted into Eq. (10) as

$$\Delta W^p = m\,\bar{\sigma}_0\,(bl)\left[\int_0^{x_c}(\epsilon_0 - \alpha x)\,dx + \int_{x_c}^{\delta}\epsilon_1 x^{-\beta}\,dx\right]$$

$$= m\,\bar{\sigma}_0\,(bl)\left[\epsilon_0 x_c - \frac{\alpha x_c^2}{2} + \frac{\epsilon_1}{1-\beta}\left(\delta^{1-\beta} - x_c^{1-\beta}\right)\right] \tag{12}$$

The frictional work done by an external agent (i.e., slider) W^e in removing the wear sheet of dimension (δbl) is

$$W^e = \frac{1}{n}\int_0^{S_0} F\,dS = \mu L S_0/n \tag{13}$$

where S_0 is the distance slid to generate n wear sheets, μ is the coefficient of friction, and L is the normal load. Some of the work done is used to generate a new surface for the newly delaminated sheet, but this surface energy is expected to be one to two orders of magnitude smaller than the work consumed during plastic deformation. Equating Eq. (13) to Eq. (11) or Eq. (12), we obtain

$$\mu L S_0 = n\,m\,\bar{\sigma}_0\,(bl)\,\delta\left[\epsilon_0 - \frac{\alpha\delta}{2}\right] \quad \text{if } \delta < x_c \tag{14}$$

$$\mu L S_0 = n\,m\,\bar{\sigma}_0\,(bl)\left[\epsilon_0 x_c - \frac{\alpha x_c^2}{2} + \frac{\epsilon_1}{1-\beta}\left(\delta^{1-\beta} - x_c^{1-\beta}\right)\right]$$

$$\text{if } \delta > x_c \tag{15}$$

Eq. (14) and Eq. (15) may be re-written as

$$\mu = m\,\bar{\sigma}_0 \left[\epsilon_0 - \frac{\alpha\delta}{2}\right]\left(\frac{nbl\delta}{LS_0}\right) \quad \text{if } \delta < x_c \tag{16}$$

$$\mu = m\,\bar{\sigma}_0 \left[\epsilon_0 \frac{x_c}{\delta} - \frac{\alpha x_c^2}{2\delta} + \frac{\epsilon_1 \delta^{-\beta}}{1-\beta}\left(1 - \left(\frac{x_c}{\delta}\right)^{1-\beta}\right)\right] \frac{nbl\delta}{LS_0} \tag{17}$$

$$\text{if } \delta > x_c \tag{17}$$

where (nblδ) =V is the volume of worn material. Using the definition of the wear factor κ, which is valid during the steady state wear process, i.e.,

$$\kappa = \frac{V}{LS_0} \tag{18}$$

Eq. (16) and Eq. (17) may be written as

$$\frac{\mu}{\kappa} = m\,\bar{\sigma}_0 \left(\epsilon_0 - \frac{\alpha\delta}{2}\right) \quad \text{if } \delta < x_c \tag{19}$$

$$\frac{\mu}{\kappa} = m\,\bar{\sigma}_0 \left[\epsilon_0 \frac{x_c}{\delta} - \frac{\alpha x_c^2}{2\delta} + \frac{\epsilon_1 \delta^{-\beta}}{1-\beta}\left(1 - \left(\frac{x_c}{\delta}\right)^{1-\beta}\right)\right] \tag{20}$$

$$\text{if } \delta > x_c$$

It should be noted that (μ/κ) under dry sliding conditions is only a function of material properties. However, Eq. (20) does not imply that there is in general a linear relationship between μ and κ, because a constant, assumed stress distribution was used in the calculation. Since the integral of Eq. (12) goes only from 0 to δ, the constant stress assumption is equivalent to assuming an elastic-perfectly plastic material stress field.

A numerical example may be given using the cyclic softening data of Morrow, et al,[40] for AISI 1045 steel. As shown in Fig. 4.4, the ratio m lies somewhere between 250 and 500. Assuming the following values for AISI 1045 steel

$$m = 375$$
$$\bar{\sigma}_0 = 175{,}000 \text{ p.s.i.}$$

if δ=2μm, the ratio (μ/κ) can be computed, using Eq. (19), to be 6.6×10^{12} Kg/m^2. If δ=8μm, the ratio (μ/κ) can be computed using Eq. (20) to be 3.9×10^{12} Kg/m^2. Typical friction and wear data for AISI 1045 steel yield

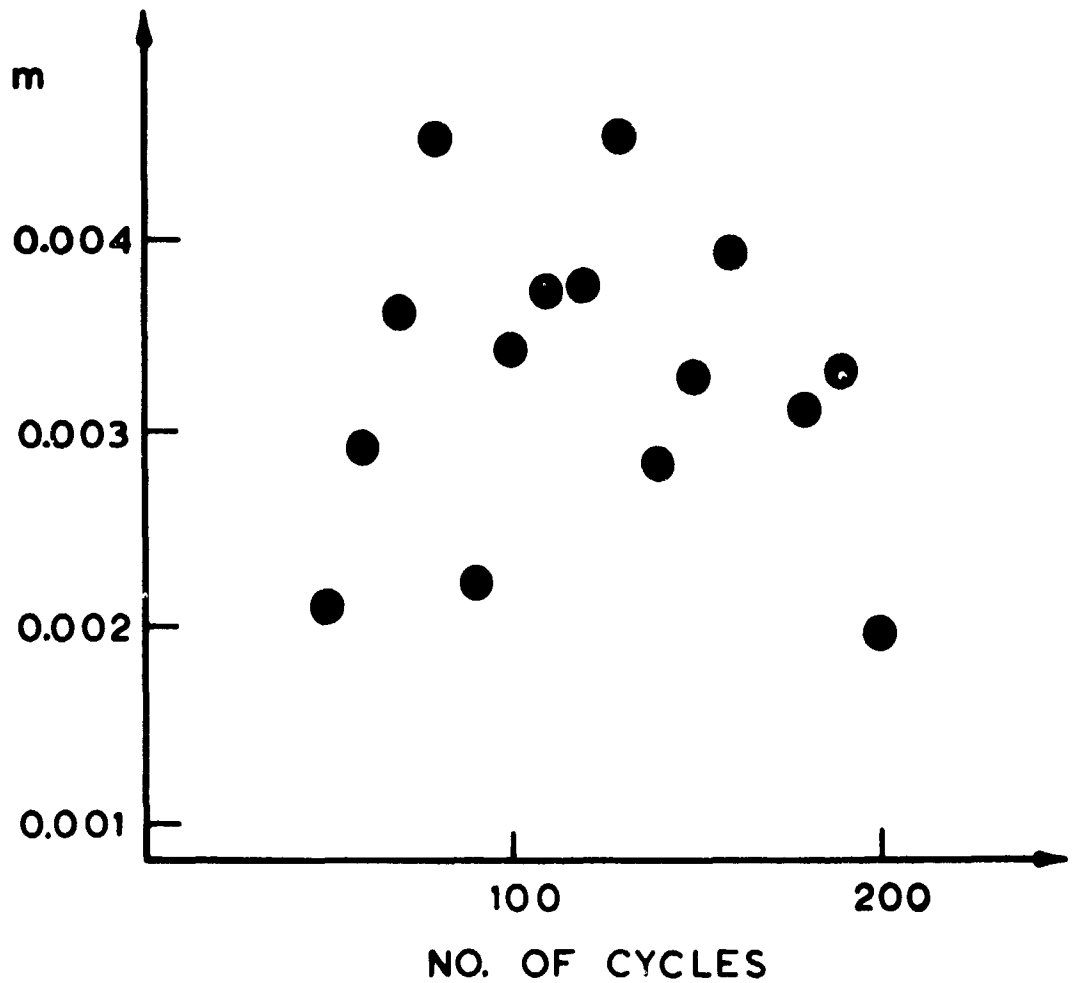

Figure 4.4

The ratio m = $\tilde{\varepsilon}_i / \bar{\Delta}\varepsilon_i^p$ for AISI 1045 steel (data obtained from Ref. 40).

the following values:*

$$\mu = 0.6$$
$$\kappa = 1.31 \times 10^{-13} \ m^2/Kg$$
$$\mu/\kappa = 4.58 \times 10^{12} \ Kg/m^2$$

The theoretical (μ/κ) ratio is surprisingly close to the experimental value. Although the data were not obtained from the same specimens and therefore the calculation is not reliable, it shows that it agrees within an order of magnitude.

The foregoing analysis indicates that considering the approximate nature of material characterization, the agreement is quite reasonable. It should be pointed out that the value used for $\bar{\sigma}_0$ may be too large for a cyclically softening metal near the surface. When the mechanics of the surface deformation is properly taken into account, the agreement may be better.

The implications of the above crude analysis for the dry sliding case are the following:

a) μ and κ are related to each other by material properties and are proportional to each other in a normal range of sliding conditions.

b) Once the deformation characteristics, the crack nucleation and propagation under the influence of surface traction, and the frictional coefficient of metals are known, the wear behavior may be predicted.

c) The basic hypothesis of the delamination theory, i.e., the wear caused by sub-surface deformation and crack nucleation and propagation, is reasonable, since it can account for the energy dissipated.

d) At a given value of μ, the metal with small α and large m, $\bar{\sigma}_0$, ε_0 and ε_1 wears less.

IV 3) Analysis of the Lubricated Case

When there is a lubricant between the sliding surfaces, the interface phenomenon is much more complicated and defies a simple analysis. The difficulty lies in taking into account the energy dissipated in deforming the lubricant. The complicated nature of the problem is illustrated here through a simple analysis.

---

*These values were obtained from a wear test on AISI 1045 steel with a BHN of 370. The specimen was 0.6 cm diameter cylinder rotating in an argon gas atmosphere against a fixed specimen of the same material with its axis perpendicular to it. The normal load was 0.45 Kg.

Part of the external work done is used to deform the lubricant. When a viscous fluid is used as a lubricant, the work done to deform the lubricant ΔW^f is conv ted into thermal energy. The energy balance requires that

$$\Delta W^e = \Delta W^p + \Delta W^f \tag{21}$$

which may be re-written and simplified, for $\delta < x_c$, as

$$\mu = \kappa \cdot m \bar{\sigma}_0 \left(\epsilon_0 - \frac{\alpha\delta}{2}\right) + \rho c_p \left(\frac{V_f}{S_0}\right)\frac{\Delta T_{ad}}{L} \tag{22}$$

where V_f is the volume of the fluid sheared by the sliding action of the slider, ρc_p is the volumetric heat capacity of the fluid, and ΔT_{ad} is the temperature rise of the fluid under adiabatic conditions. The determination of ΔT_{ad} is not straightforward, since heat transfer from the fluid to metals and vice versa is difficult to isolate. If ΔT_{ad} can be determined, the wear factor can again be determined once the coefficient of friction is known.

IV 4) Limitations of the Analysis

The foregoing analysis assumed that the history of cyclic deformation is analogous at all x except for the magnitude of the stress and strain. The role of residual stress and strain was not properly taken into account. It also did not consider the variation of material properties as a function of depth. Many of these questions must be answered before the analysis given here can be established on a firm foundation.

IV 5) Conclusions

The work done by the surface traction can be accounted for based on the delamination theory of wear. However, much work has to be done before the wear rate and the coefficient of friction can be determined theoretically based on the basic properties of materials.

Chapter V

MICROSTRUCTURAL EFFECTS IN DELAMINATION WEAR

V 1) Introduction

According to the delamination theory, sliding wear of metals is controlled by the mechanical properties of the surface and the microstructure of the subsurface, since they control the processes of deformation, crack nucleation and propagation. If the microstructure of a metal is modified in a manner which increases the hardness (flow stress) alone without increasing crack nucleation sites, the wear rate will decrease. This reduction in wear is expected because the subsurface deformation of the material with a higher hardness is less, thus resulting in a lower rate of crack nucleation and propagation. On the other hand, if the modification of the microstructure increases the number of void nucleation sites (second phase particles etc.) without increasing the hardness, similar reasoning predicts that the wear rate will increase. In most commercial metals, addition of second phase or inclusions strengthens the material, i.e. microstructural changes affect both the hardness and the number of crack nucleation sites.

For the present study three metal systems were chosen to explicitly show the influence of microstructure on the sliding wear of metals. The alloy systems were copper-tin solid solutions, internally oxidized copper-chromium and copper-silicon solid solutions, and steels. The hardness of the copper-tin solid solutions was increased by increasing the tin content within the solubility range. Since this alloy was free of second phases or inclusions, the effect of hardness on wear was isolated. In the internally oxidized systems the hardness did not increase appreciably by increasing the number of incoherent SiO_2 and Cr_2O_3 particles, but the number of crack nucleation sites was effectively increased. Therefore, the effect of second phase particles was isolated with this system. The third alloy system, iron solid solutions containing inclusions and low carbon steels, was chosen to combine the effect of both the hardness and the number of second phase particles, since by increasing the number of inclusions and cementite particles the hardness was also increased. Additionally, steels with different heat treatment conditions were used to show the effect of second phase particle morphology on the wear behavior.

V 2) Experimental Procedure

Cylinder-on-cylinder wear tests were conducted as described in Appendix D. The stationary pins were made from AISI 52100 steel for all tests. The specimens were rotated at a surface speed of 180 cm/min. The Cu-Sn and steel specimens were tested under normal loads of 1.81 Kg and 0.45 Kg, respectively; whereas the internally oxidized samples were tested under normal loads ranging from 0.22 to 2.25 Kg. All tests were run at room temperature in an argon atmosphere without any lubricants.

V 3) Copper-Tin Solid Solutions

Solid solution specimens having four different tin concentrations (0, 1.5, 3.5 and 6 at %) were prepared as described in Appendix B to be free of any second phase or inclusion particles. By increasing the solute (tin) concentration, the hardness of the material increased linearly, as shown in Fig. 5.1. The strengthening by the addition of solute in this type of material is caused by the substitutional mechanism. The linear relationship between the hardness and the solute content (Fig. 5.1) has also been observed by Fleisher.[41,42]

The results of wear tests on the copper-tin solid solutions are presented in Fig. 5.2. The figure shows that the steady state (delamination) wear rate decreases with the addition of tin solute. This inverse dependence is caused mostly by the increase in hardness (Fig. 5.1) and partly by the decrease in friction coefficient (Fig. 5.3) as the tin concentration is increased. The steady state wear rate is plotted in Fig. 5.4 vs. the original hardness of the worn material. It can be seen that the wear rate depends inversely on the hardness. This dependence was expected because a material with a higher hardness (flow stress) deforms less and is subjected to a lower rate of crack nucleation and propagation. Even though these materials do not contain any observable inclusions, subsurface cracks generate and lead to delamination. The exact mechanism of crack nucleation and propagation in clean metals is not known yet; some possible mechanisms were suggested in Chapter II.

As was shown previously, the friction coefficient and the wear rate are related because of the energy balance (Chapter IV) and the mechanics of delamination (Chapter III).

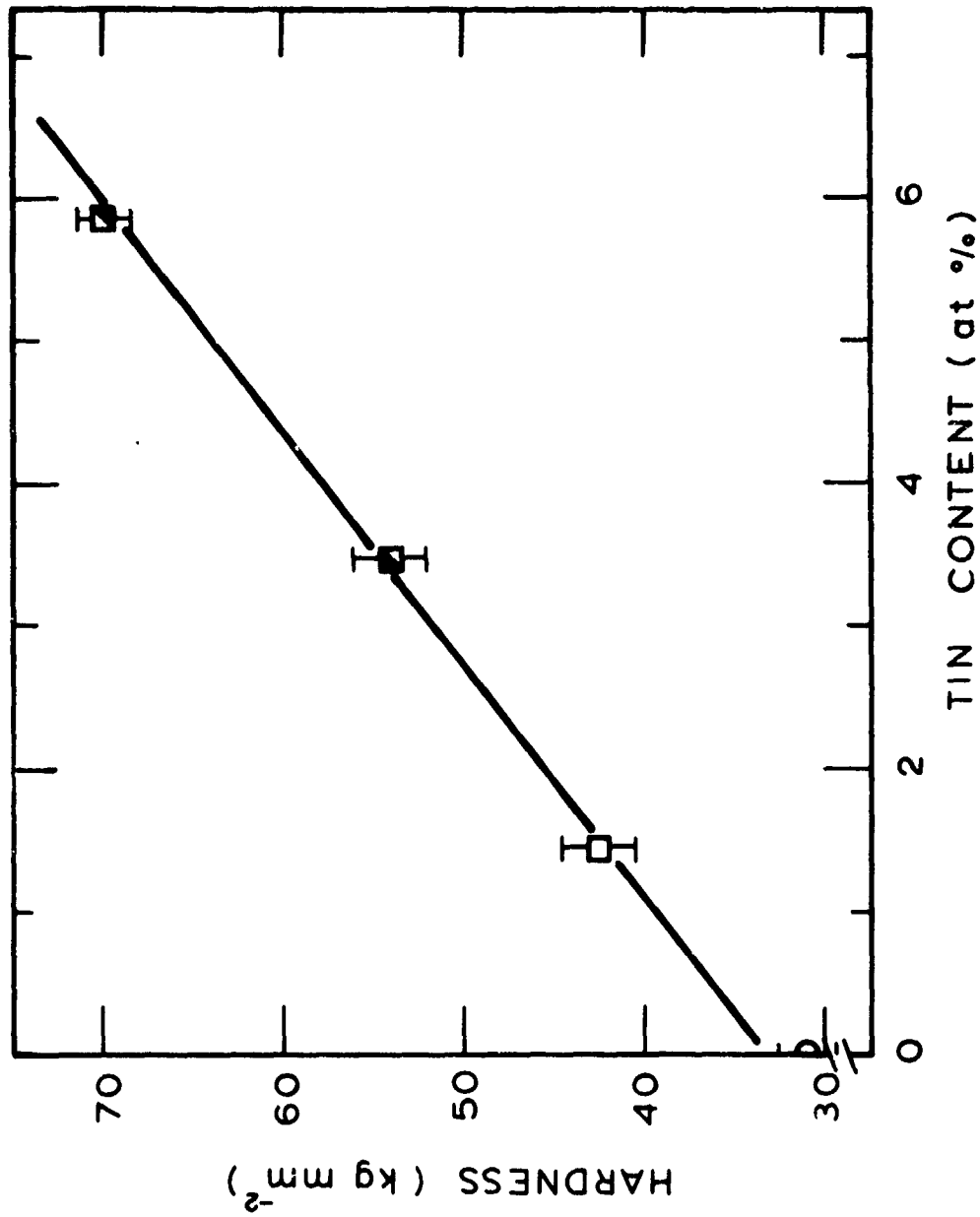

Figure 5.1

The influence of composition on the hardness of copper-tin solid solutions.

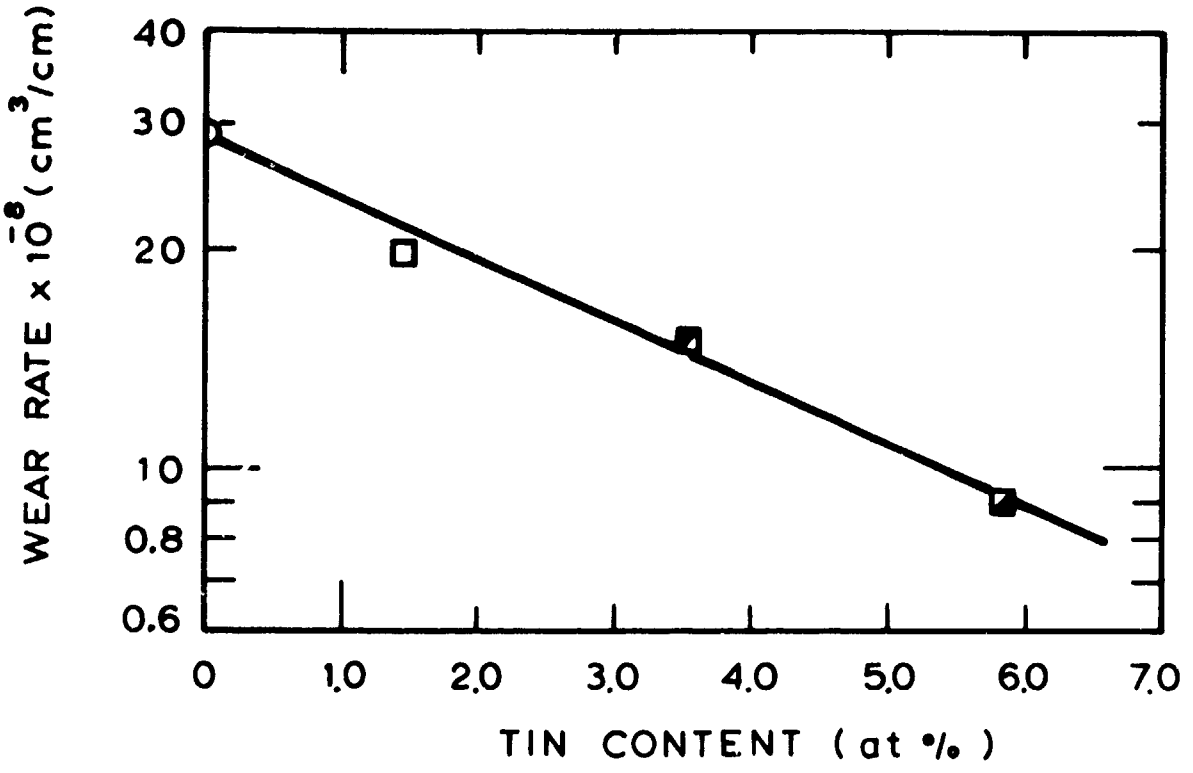

Figure 5.2

Wear rate of copper-tin solid solutions as a function of tin content.

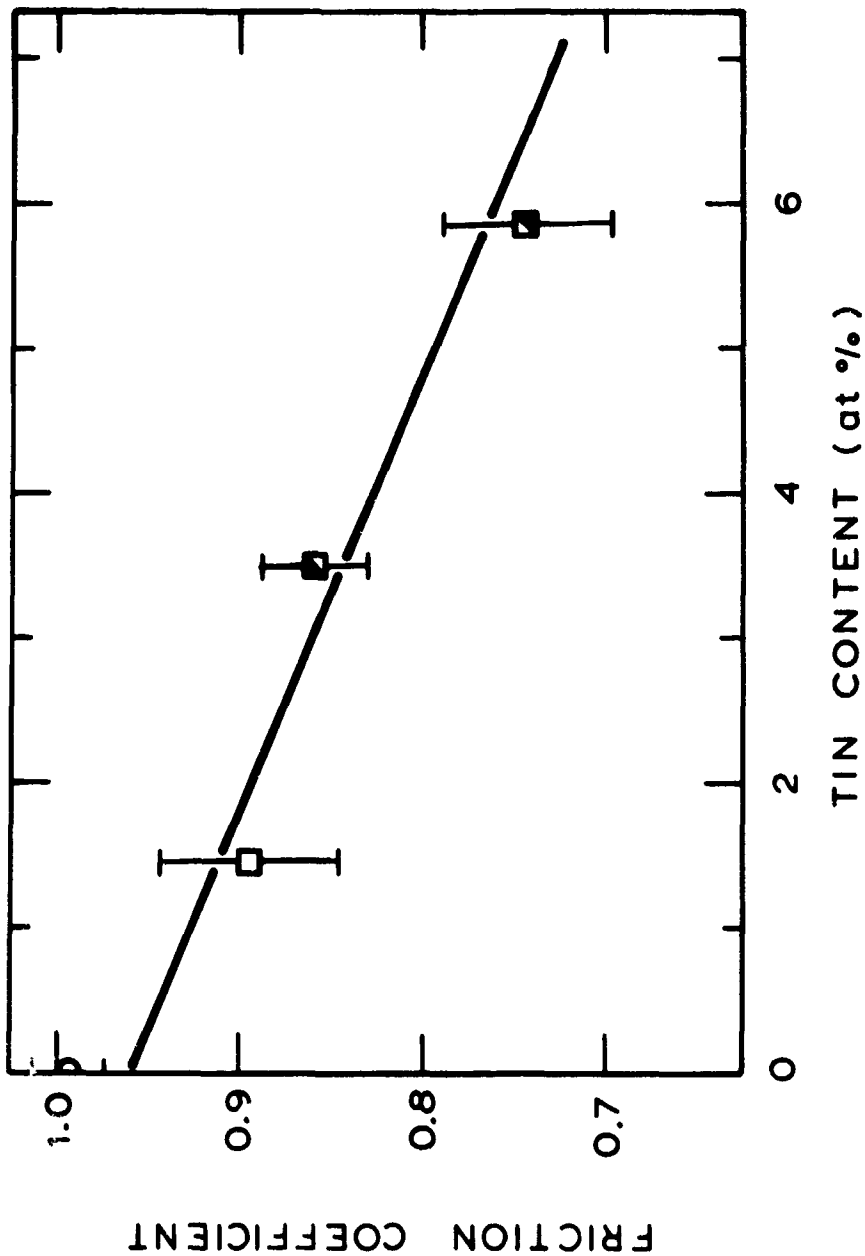

Figure 5.3

Reduction of friction coefficient by tin addition.

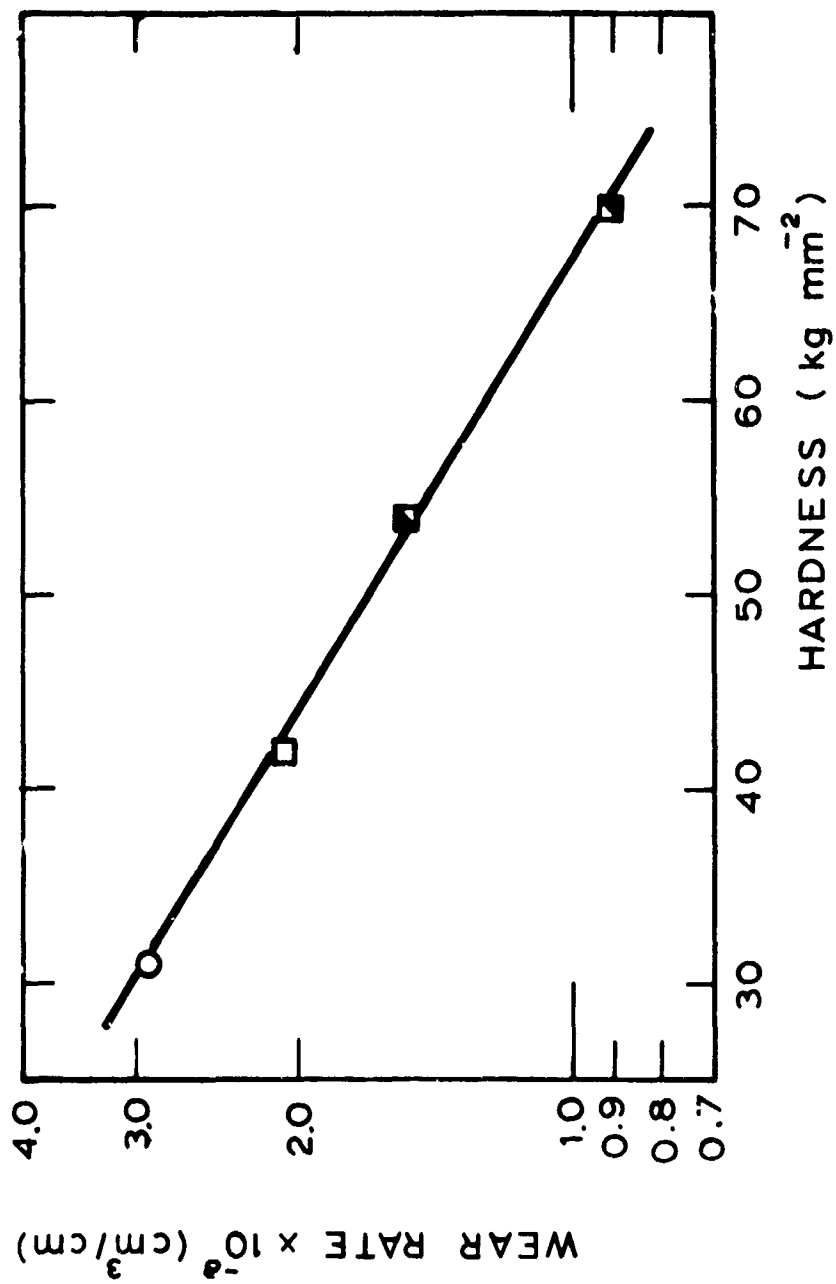

Figure 5.4

Reduction of wear by increasing hardness of copper-tin solid solutions.

Since the friction coefficients in the wear tests on copper-tin solid solutions were not constant, the decrease of wear by addition of the tin may be partially due to the decrease of friction coefficient. This dependence is shown in Fig. 5.5, where wear rates and wear coefficients are plotted vs. the friction coefficients. The wear coefficient is used primarily because it is a dimensionless quantity representing the wear behavior.

V 4) Internally Oxidized Copper Alloys

In order to show the effect of inclusions on wear, internally oxidized copper-chromium and copper-silicon alloys were used. The copper-chromium specimens contained 0.18% chromium, whereas the copper silicon specimens had 0.5 and 1.0% silicon. Details of alloy preparation are given in Appendix C. The oxide content of these alloys, which ranged from 0.45% to 7.30%, did not cause a large change in the hardness of the alloys as indicated in Table C.1. Therefore, this class of alloys is suitable for studying the effect of inclusions on wear.

The wear tests were run for 30 min. (54 m of sliding) under different normal loads. Fig. 5.6, which is a plot of weight loss and the normal load for the alloys tested, indicates that the wear rate increases with the oxide content. This is more evident from Fig. 5.7a which shows the inverse of wear coefficients, an index of wear resistance, plotted versus the volume fraction of oxide particles. The relationship between the wear resistance and volume fraction is very similar to the fracture strain vs. volume fraction of particles for uniaxial fracture testing.[43-46]

Fig. 5.8b which is a plot of friction coefficients vs. the volume fraction of particles for the internally oxidized copper alloys, indicates that friction decreases with the increase in the number of particles. The wear coefficients and the friction coefficients are plotted in Fig. 5.8 for these samples. The figure shows that wear depends inversely on friction. This relationship (which is the reverse of the expected dependence) indicates the important influence of inclusions on wear; i.e., reduction in friction coefficients increases the wear rates because of larger number of crack propagation sites in the internally oxidized alloys.

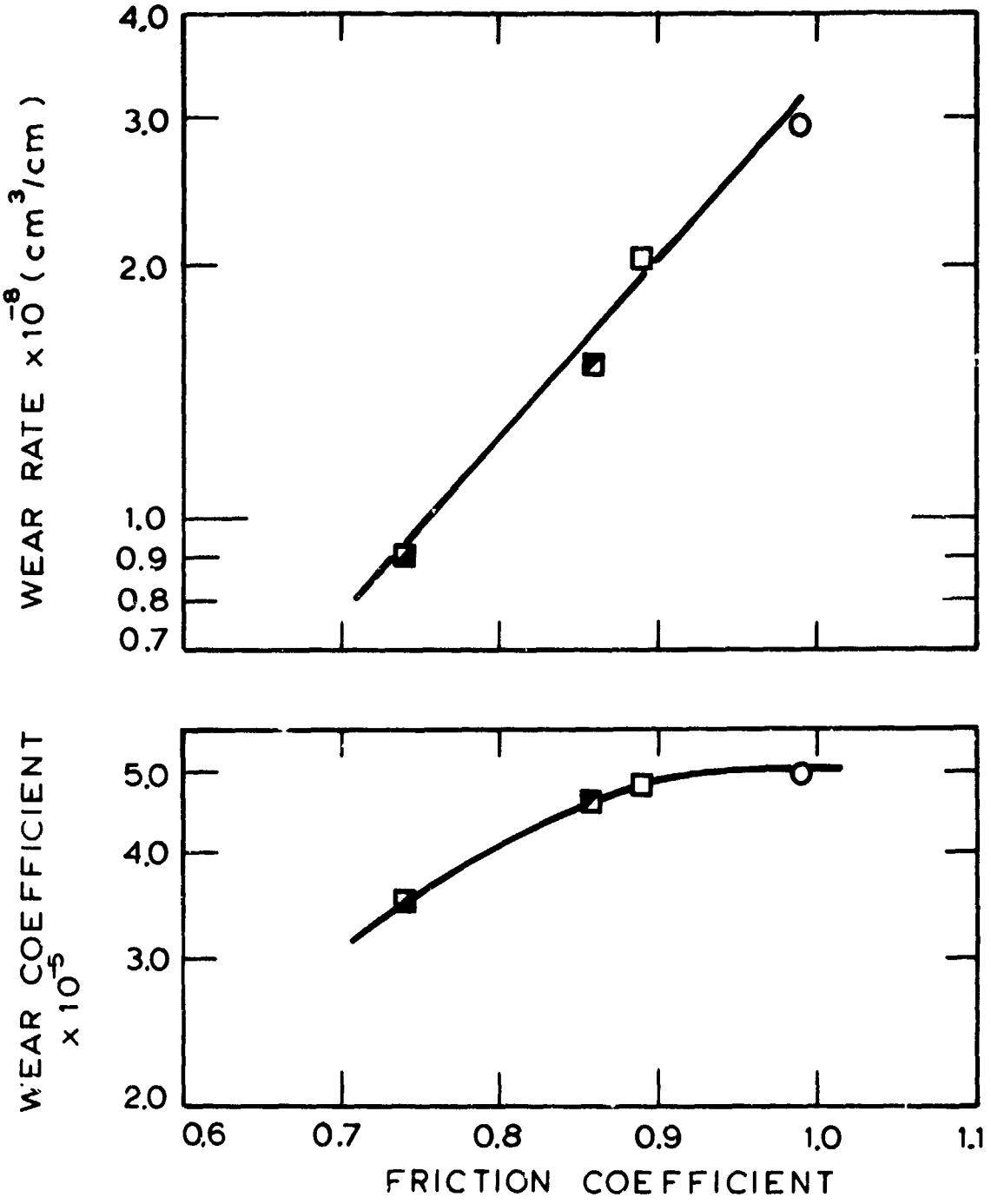

Figure 5.5

Dependence of wear coefficients and wear rates on friction coefficient. (Wear coefficients must be multiplied by 3.)

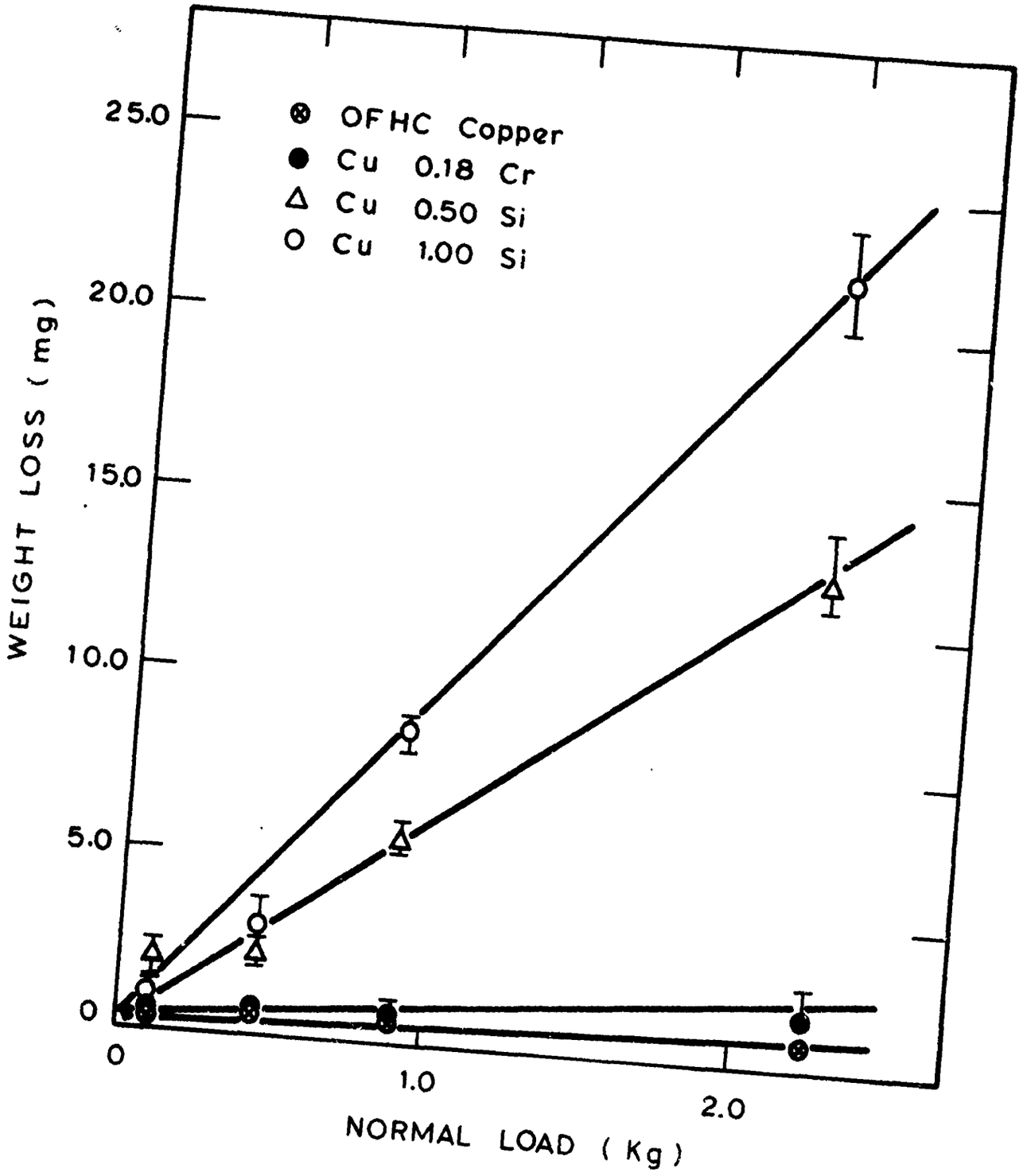

Figure 5.6

Weight loss of Copper and internally oxidized Cu-Cr and Cu-Si alloys vs. normal load for 30 min. tests.

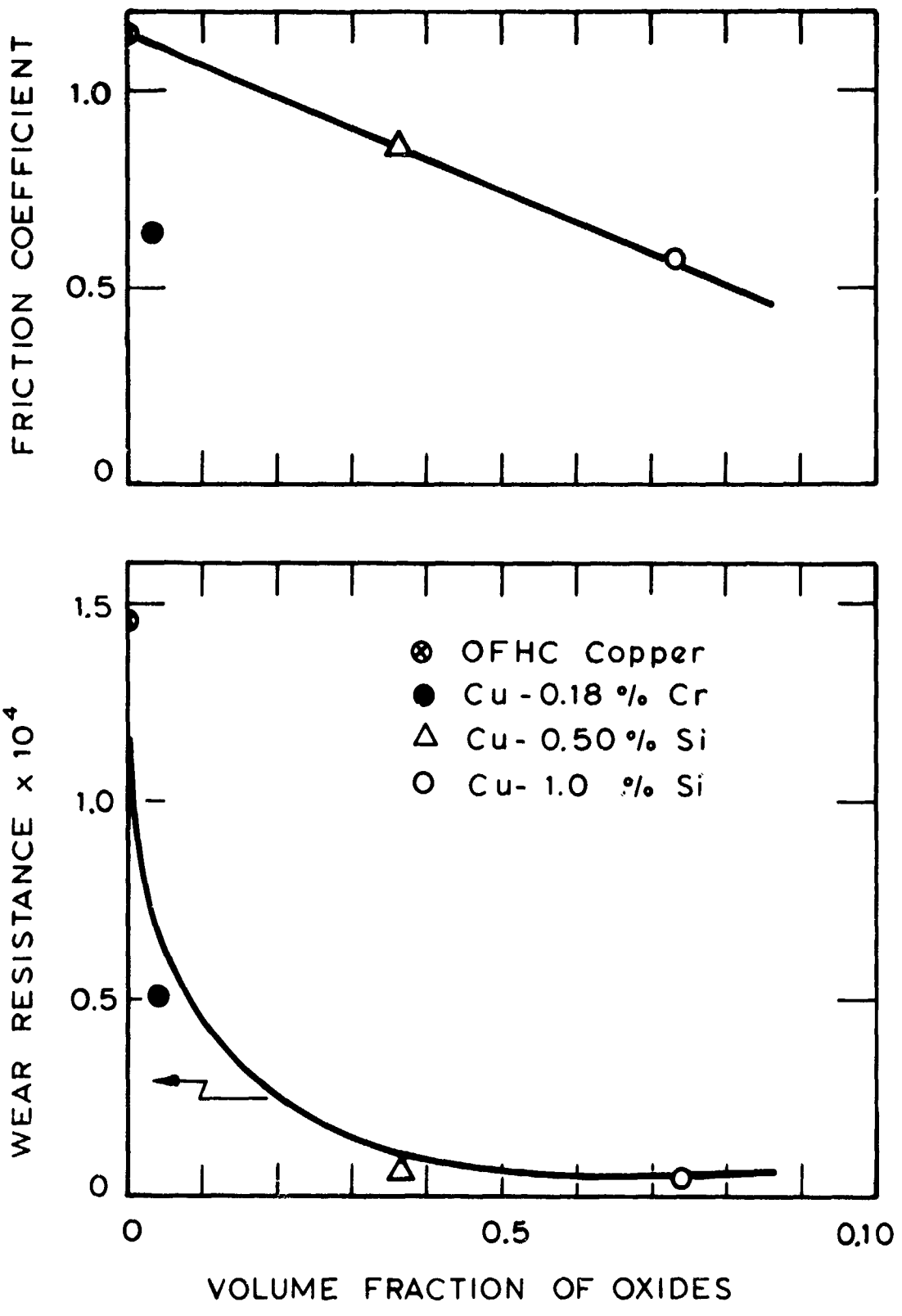

Figure 5.7

Wear resistance and friction coefficients vs. the volume fraction of oxide particles.

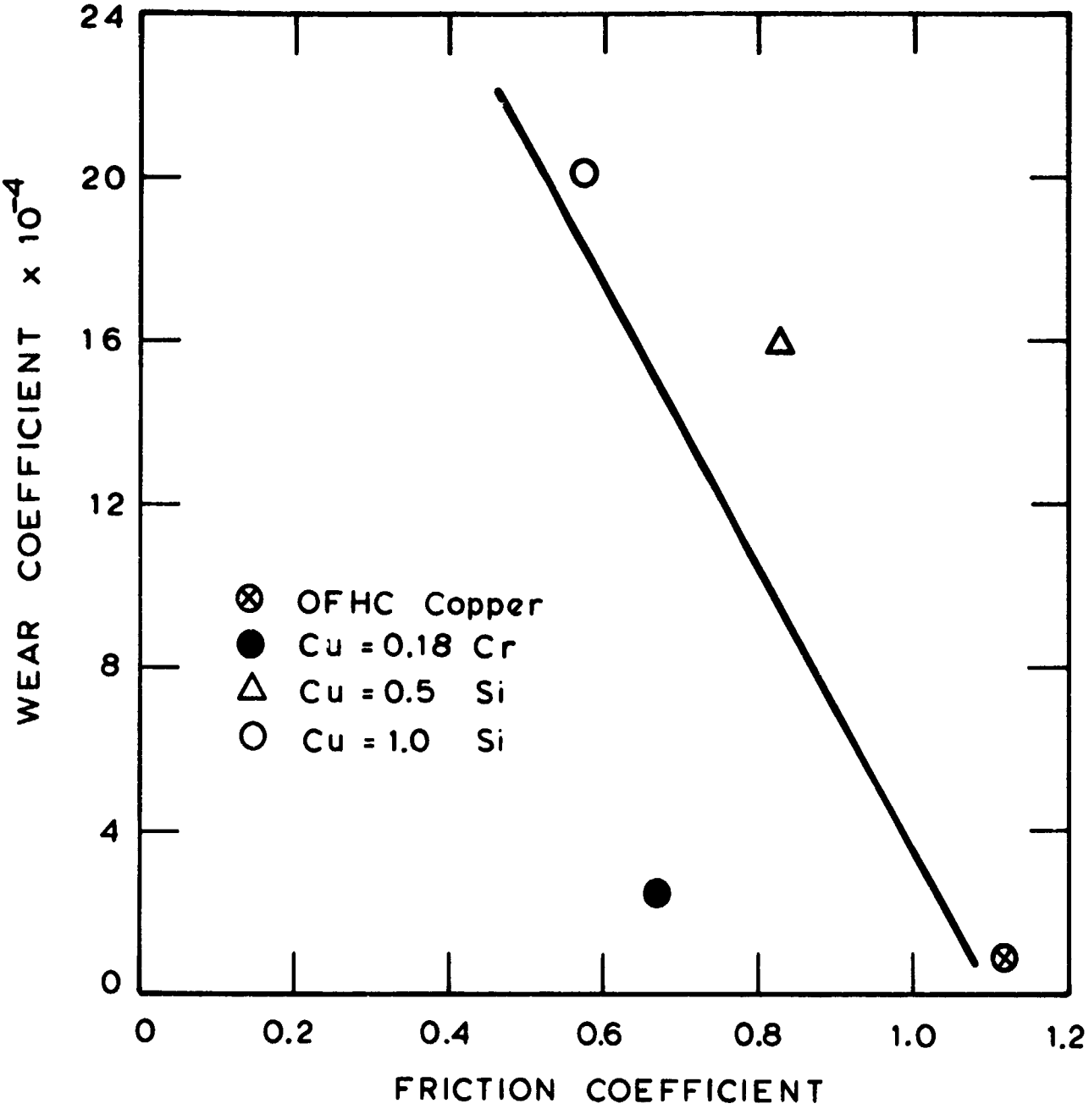

Figure 5.8

Wear coefficient vs. friction coefficient for internally oxidized copper alloys.

The similarity of Fig. 5.7a to uniaxial fracture strain vs. volume plots indicates that a relationship between uniaxial tension ductility and wear resistance exists. Therefore, it may be assumed that any metallurgical parameter which affects ductility will also have an influence on the wear resistance. Particle size, spacing (and hence volume fraction) of particles, and coherency of particles with the matrix are the most important metallurgical variables affecting ductility. The degree of coherency (i.e. the matrix/particle bond strength) is an important variable in void nucleation. It has been shown [81] that by slight alloy addition the matrix/particle interface can be strengthened and the ductility can be increased. Coherence of particles with the matrix increases as the particle size is decreased. Therefore, void nucleation and wear in metals containing second phase particles can be decreased by either alloying to strengthen the bond or by decreasing the size of the particles to increase coherency. Also, as discussed in Chapter II, void nucleation may not be possible for very small particles (less than 100 Å) due to the lack of sufficient elastic energy.

The next important parameter influencing ductility is the particle size. Theoretical analyses by Gurland[83] and Ashby[82] indicate that ductility increases as particle size is decreased. Experimental results obtained for internally oxidized metals[84] support these theoretical analyses; whereas the results obtained for spheroidized steels[85] are contrary to the theories. This is perhaps due to the complete lack of coherency (presence of a bond strength) in the internally oxidized metals as compared with some coherency in steels.

The results presented here confirm the predictions of the delamination theory. By increasing the number of inclusions the wear rate should increase, provided that the hardness (flow stress) is not increased. Accordingly, when only the hardness is increased, the wear rate decreases as was shown for copper solid solutions. These two alloy systems are very specialized and were selected to show the separate effect of hardness and inclusion content on sliding wear. In most commercial metals however, these two effects are present simultaneously.

V 5) Iron Solid Solutions and Steels

In order to investigate the combined effect of hardness and inclusions on wear, pure iron, iron-ruthenium and iron-molybdenum solid solutions and

AISI 1018, 1045 and 1095 steels were used. The pure iron was zone-refined and practically contained no inclusions. The iron solid solutions had a number of inclusions of 1-2.5μm (40-100μin) in diameter. The heat treatment and the metallurgical variables of these metals are listed in Table 5.1

The volume fraction, f, and the particle size, d, of the inclusions in iron solid solutions were determined by using approximately 2000 points of intersection on 4 micrographs of each sample. The volume fraction of cementite in steels were determined from the stoichiometric relation. These were then used to determine the mean free path, λ, by the following relation:[43]

$$\lambda = \frac{2d}{3f}(1-f).$$

The steels were heat treated to have three types of carbide structure. AISI 1018 steel was tested in the spheroidized and pearlitic conditions, AISI 1045 was tested after spheroidization and AISI 1095 was tested in the spheroidized, pearlitic, and bainitic conditions. The heat treatment was also varied to obtain fine and coarse structures.

The wear tests were conducted for different sliding distances in order to find the steady state wear coefficient for each material. Table 5.1 lists the wear coefficients and the friction coefficients for the materials tested. The table indicates that the wear coefficients for iron solid solutions increase with increasing volume fraction of inclusions. This is more evident from Fig.5.9a which plots the inverse of the wear coefficients, an index of wear resistance, versus the volume fraction of inclusions and hard second phase particles for iron and spheroidized steels. Wear resistance decreases with increasing volume fraction of particles down to a minimum value of wear resistance at 0.07 volume fraction. Beyond this value, wear resistance increases with the volume fraction.

The relationship which exists between wear resistance and volume fraction at low volume fractions is in fact similar to the fracture strain vs. volume fraction curves[43-46] obtained for fracture in uniaxial tension or torsion testing. This similarity is not surprising because the mechanism of void and crack formation in delamination and in tensile or torsional fracture are similar even though the states of stress and strain are quite dif-

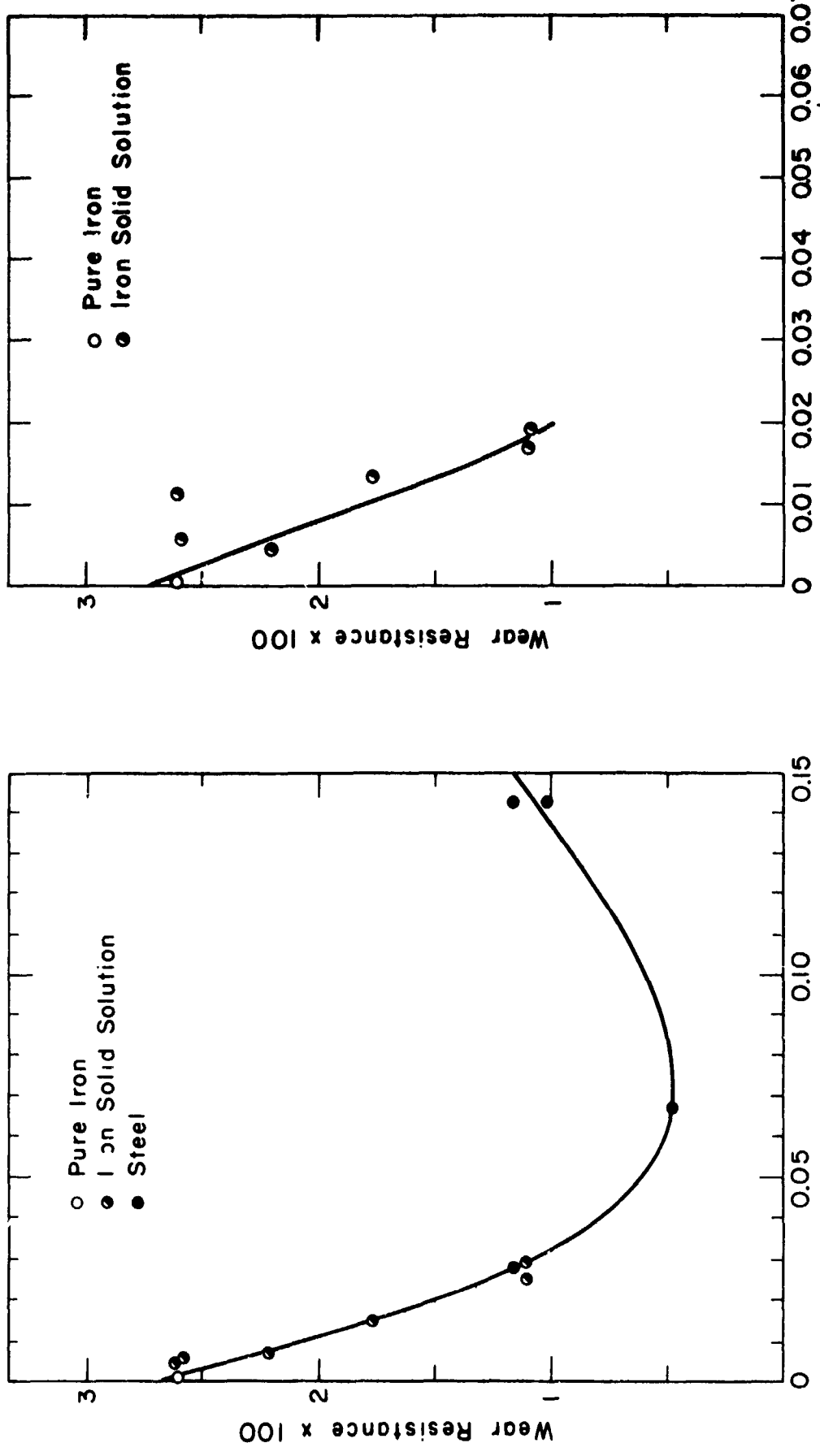

Figure 5.9

The effect of volume fraction and mean free path on the wear resistance (1/k = SL/3WH) of iron and spheroidized steels.

Table 5.1 Iron Solid Solutions and Steels: Metallurgical Variables and Experimental Results.

Materials	Heat Treatment and Metallurgical Variables					Experimental Results	
	Heat Treatment	Brinell Hardness (Kg/mm^2)	Volume Fraction	Mean Free Path (μm)	Average Particle Size (μm)	Wear Coefficients $x10^{-3}$	Friction Coefficients
Pure Iron	700°C 1 hr	35	0.0004	850	0.5	3.81	0.80
Iron Solid Solutions							
Fe-200ppm Ru	700°C 1 hr	37	0.004	89	0.6	3.81	0.82
Fe-0.06% Mo	"	45	0.004	177	1.0	3.81	0.76
Fe-0.75% Mo	"	51	0.007	232	2.4	4.56	0.84
Fe-1.3% Mo	"	60	0.015	68	1.5	5.61	0.76
Fe-2.7% Mo	"	74	0.025	60	2.3	8.97	0.78
Fe-4.3% Mo	"	75	0.030	52	2.3	8.97	0.80
AISI 1018 Steel							
Finely Spheroidized	900°C 15min, oil quenched 400°C 1 hr	110	0.020	9	0.4	8.88	0.86
Pearlitic	700°C 24 hrs	75	"	-	---	8.43	0.82
AISI 1045 Steel							
Finely Spheroidized	900°C 15min, oil quenched 400°C 1 hr	175	0.067	3	0.4	22.14	0.85
AISI 1095 Steel							
Finely Spheroidized	900°C 15min, oil quenched 400°C 1 hr	190	0.142	2	0.4	9.72	0.85
Partially Spheroidized	as received	162	"	-	---	8.52	0.83
Fine Pearlitic	600°C 1 hr	157	"	-	---	7.41	0.76
Coarse Pearlitic	650°C 21 hrs	130	"	-	---	6.27	0.80
Bainitic	700°C 1 hr	190	"	-	---	28.14	0.83

ferent. In both of these cases cracks are nucleated at the inclusions or second phase particles and lowering the volume fraction of particles increases both the ductility and the wear resistance.

It is observed from Fig. 5.9a that at higher volume fractions, wear resistance increases with increasing the volume fraction. This is possible due to the increased flow stress of the material which allows less plastic deformation and thus reduces the rate of void formation under the sliding conditions similar to the case of copper tin solid solutions.

The wear resistance may also depend on the mean free path. (Fig. 5.9b) A similar relationship has been reported for the fracture of steels in torsion testing.[45] However, it is difficult to separate the effect of the mean free path from the volume fraction, since they are not independent when the particle size is kept nearly constant. The wear behavior may depend on both the volume fraction and the mean free path, if the volume fraction controls the subsurface void and crack nucleation and if the mean free path influences the rate of crack extension between the voids around the particles. Theoretical analysis of McClintock[86] has shown that uniaxial fracture strain depends on the logarithm of interparticle spacing, other variables remaining constant.

The wear coefficients which are listed in Table 5.1 for steels, indicate that the wear behavior depends on the morphology of the second phase particles. Among the various structures studied for AISI 1095 steel, coarse pearlite and bainite had the lowest and the highest wear coefficients, respectively. It was also found that the spheroidized steels had larger wear coefficients than pearlitic steels.

The particle morphology has been found to influence the fracture behavior under uniaxial and torsional loading conditions in contradiction to the way it effects the wear behavior. Rosenfield et al.[46] and Lemmon and Sherby[45] have reported a better ductility for spheroidized steels than pearlitic steels, because the pearlite plates fracture preferentially at lower strains than that required for crack formation in the spheroidized steels. This may be reversed under sliding conditions because of the presence of the large hydrostatic compression very close to the surface. It was observed (Fig. 2.3) that many of the pearlite plates behave plastically under the large hydrostatic compression and deform rather than fracture. Therefore, the subsurface crack formation by pearlite fracture may be retarded under sliding conditions, resulting in a lower wear coefficient.

Despite these inherent similarities between fracture and delamination, there are basic differences, primarily in the states of stress and strain. In tensile or torsional fracture testing, the state of loading is uniaxial tension or shear and the strains are uniformly distributed. Sliding contacts, on the contrary, experience a unique loading condition which is a combination of shear and hydrostatic compression. The deformation under these conditions is not uniform with depth and is confined to a thin surface layer. The large hydrostatic compression which exists near the surface could greatly alter the ductility and fracture properties of the surface layer. The effect of hydrostatic compression on ductility has been studied under uniaxial tension[47] and shear deformation[48]. These investigations show that ductility increases in the presence of high hydrostatic compression. The increase of ductility is shown to result from suppression of void nucleation at the particle/matrix interface[49]. This retardation of crack formation under high hydrostatic compression together with the softness of the surface[3] may explain the excessively large subsurface deformation[20], which occurs before delamination.

V 6) Summary

The results of this chapter substantiate the predictions of the delamination theory concerning the role of microstructure on sliding wear. Therefore it may be concluded that wear of metals may be decreased by elimination of void nucleation sites, by increasing the hardness of the material, or by the combination of these two procedures.

Chapter VI

DELAMINATION IN OTHER WEAR PROCESSES

VI 1) Introduction

The preceding chapters confirmed the delamination theory for the case of sliding wear. Delamination occurs because of the presence of tractions on the contacting surfaces. Therefore, delamination may be expected to be present in other types of surface phenomena, if normal and tangential forces are present at the surface. This chapter considers three types of wear in which delamination may have an influential role.

VI 2) Fretting Wear

Fretting wear occurs between two tightly fitting surfaces when there is a small amplitude oscillating slip between them. The early stage of fretting wear[3,50,51] is caused by the wear mechanisms postulated by the delamination theory of wear. Once the wear particles are generated, they may oxidize and act as abrasive particles between the surfaces, accelerating the wear process. However, the critical stage of fretting wear is the generation of wear particles by the delamination process. The micrograph in Fig. 6.1, which was taken by Waterhouse[50], shows the fretted surface of Ti-7Al-4V alloy tested in air at 107 cycles per second under a mean stress of 147 MN/m^2 and alternating stress of 83.5 MN/m^2. It can be seen that the wear particles are in the form of thin sheets.

One of the unique and controversial phenomena observed in fretting wear is the dependence of the wear rate on the amplitude of the oscillatory motion, as shown in Fig. 6.2.[52] In terms of the delamination theory of wear, the decrease in the wear rate at low amplitudes can be explained by noting that cracks cannot link together between two inclusions (i.e. crack nucleation site) when the plastic strain is small. Fretting wear rate depends on the microstructure since the distance between crack nucleation sites vis-a-vis the amplitude of oscillating slip is the rate determining process. Once the amplitude of oscillating slip is sufficient to link the cracks together, the early stage of fretting wear is not any different from sliding wear.

One of the major problems associated with fretting wear is fretting fatigue. Since fretting fatigue is initiated at cracks generated by fretting

Figure 6.1

Micrograph of a fretted Ti-6Al-4V surface (Ref. 50).

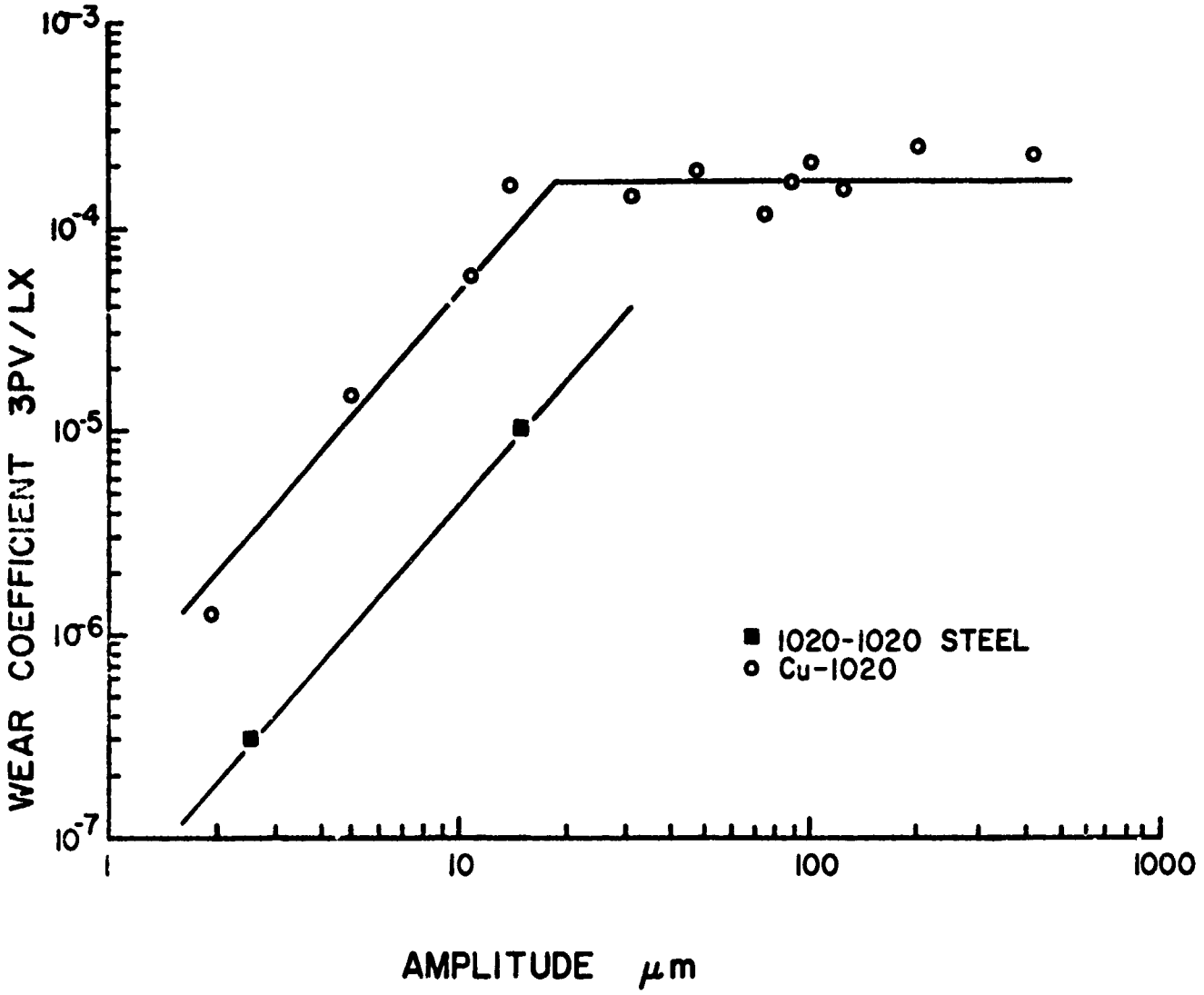

Figure 6.2

Fretting wear coefficient vs. the amplitude of oscillation (Ref. 52).

wear, fretting fatigue can be prevented if fretting wear can be reduced. Although lubrication of the interface is a possible solution, in some applications lubricants cannot be applied. Fretting fatigue may also be prevented by plating a hard substrate with a thin layer of softer metal to minimize the delamination wear as has been discussed earlier[13,14] and in Chapter VIII. Such experimental results for fretting fatigue were recently reported by Ohmae, et al.[53], but the importance of the thickness of the plated layer was not recognized by them.

The environmental effect on fretting was recently discussed by Van Leeuwen in terms of the delamination theory of wear [54]. He postulated that since water may oxidize bare metal according to the following reactions

$$Fe \rightarrow Fe^{2+} + 2e$$

$$Fe^{2+} + 2\ H_2O \rightarrow Fe\ (OH)_2 + 2H^+$$

the resulting hydrogen ions or protons could be transported by the dislocations as Cottrell clouds, as they move from a region near the surface into the subsurface region to pile up at hard particles. The dislocations would then deposit the hydrogen at the interface between the matrix and the obstacle and cause hydrogen embrittlement cracking at that location. This transport of hydrogen by dislocation motion, rather than by thermaly activated diffusion , would then explain the accelerated fretting-corrosion in a water-containing environment.

VI 3) Abrasive Wear

Abrasive wear can be caused either by hard abrasive particles entrapped between two sliding surfaces or by the asperities of a hard surface sliding on a soft surface. The abrasive wear volume is, to a first approximation, proportional to the normal load and the distance slid, and inversely proportional to the hardness. Many wear processes change into abrasive wear when loose wear particles are generated.

The mechanism of abrasive wear consists of two modes of material removal: cutting of the surfaces by hard loose particles or asperities on the mating surface, and delamination by subsurface deformation. The surface traction associated with the cutting action deforms the surface layer which

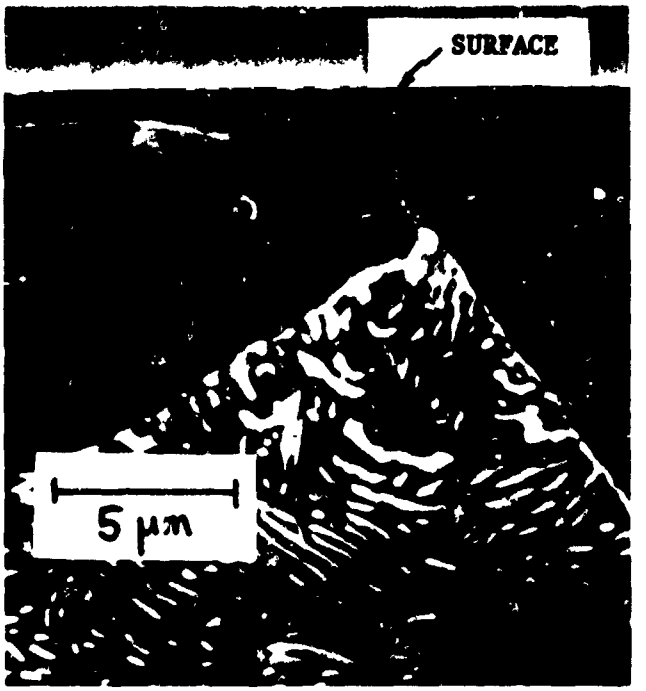

Figure 6.3

Subsurface deformation and void formation in abraded AISI 1020 steel.

causes subsurface crack nucleation and propagation as shown in Fig. 6.3. The figure shows a micrograph of a section perpendicular to the abraded surface of an annealed AISI 1018 steel pin (diameter 0.64cm) which was subjected to abrasive action by abrading against 240 grit SiC abrasive paper at a speed of 6.3 cm/sec and a normal load of 0.4 kg. Depending on the sharpness and hardness of the abrasive particles, either the delamination or the cutting action may be the dominating mechanism. The harder the surface the less will be the cutting action. When the delamination mechanism dominates, the microstructural effects discussed for sliding wear should be equally applicable.

VI 4) Erosive Wear

When a metal surface is gradually worn by the action of particles impinging on the surface, it is called erosion by solid particle impingement. This is a problem and arises in pipes which transport solid particle slurries, gas turbines, and aircraft propellers. Finnie[55] and Bitter[56] proposed wear mechanisms for this type of wear caused by solid particle impingement. Finnie's model assumes that each one of the solid particles acts as a cutting tool when it strikes the surface, removing some of the surface material. Bitter[56] proposed that the normal velocity component of the impinging solid particle causes wear by a fatigue process, while the tangential components cause wear by deformation.

Fig. 6.4 shows micrographs of the surface of 2024-T4 aluminum impacted at various speeds at an impingement angle of 45°. It should be noted that the material is displaced a great deal but very little material has been removed by actual cutting action. Fig. 6.5 shows aluminum specimens impacted at 280 m/sec at room temperature and at 150 m/sec at 200°F. The specimen impacted at the higher speed shows signs of melting[57], but the evidence is not conclusive. The specimen impacted at 200°F shows "mud" cracks (similar to cracks formed in drying mud), indicating that the surface has undergone oxidation at a high temperature or melted. Fig. 6.6 shows the cross sectional view of the subsurface cracks in copper and steel. It should be noted that the cracks tend to be perpendicular to the direction of impact and that subsurface cracks exist at a finite distance away from the surface. The subsurface cracks extend deeper in the specimen impacted perpendicular to the surface. The mechanics of the surface deformation is such that we have a maximum deformation at the surface. Since crack nucleation is not favored

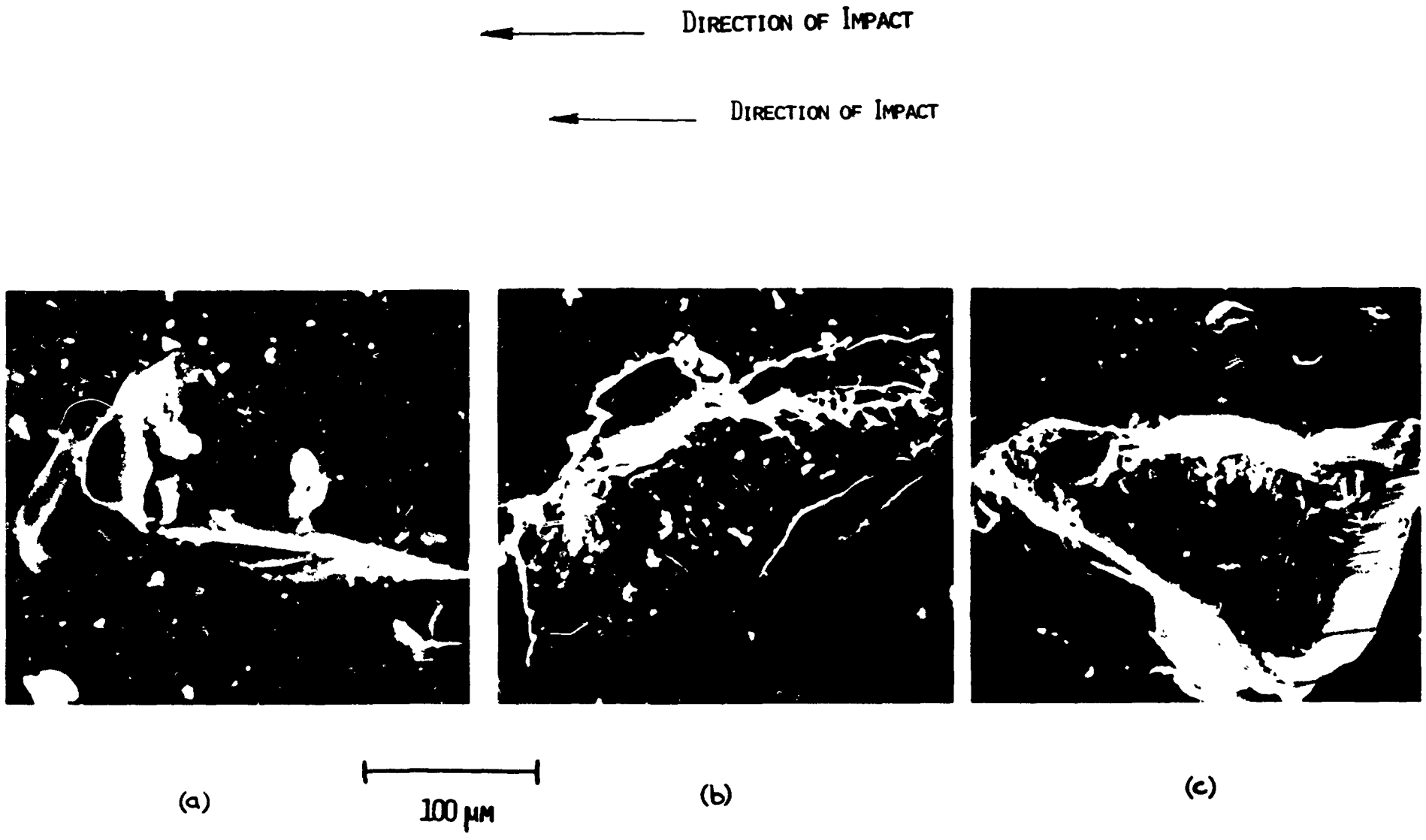

Figure 6.4

Erosion surface of 2024-T4 aluminum impacted at different speeds by SiC particles at impingement angle of 45^{o} (Ref. 57): (a) impact speed of 32 m/sec; (b) impact speed of 156 m/sec; (c) impact speed of 310 m/sec.

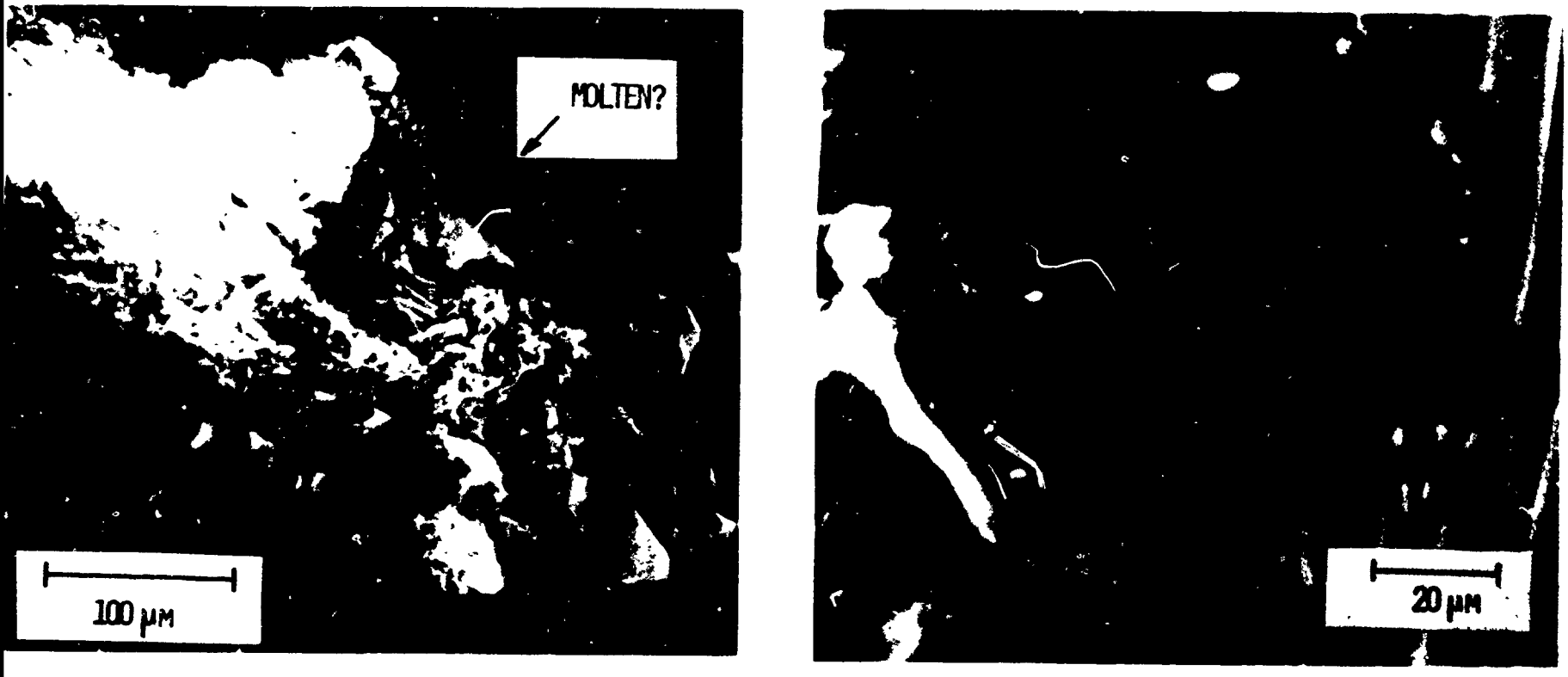

(a) (b)

Figure 6.5

Erosion surface of 2024 aluminum impacted at different temperatures by SiC particles at impingment angle of 90° (Ref. 57): (a) 17° F, 280 m/sec; (b) 200° F, 150 m/sec.

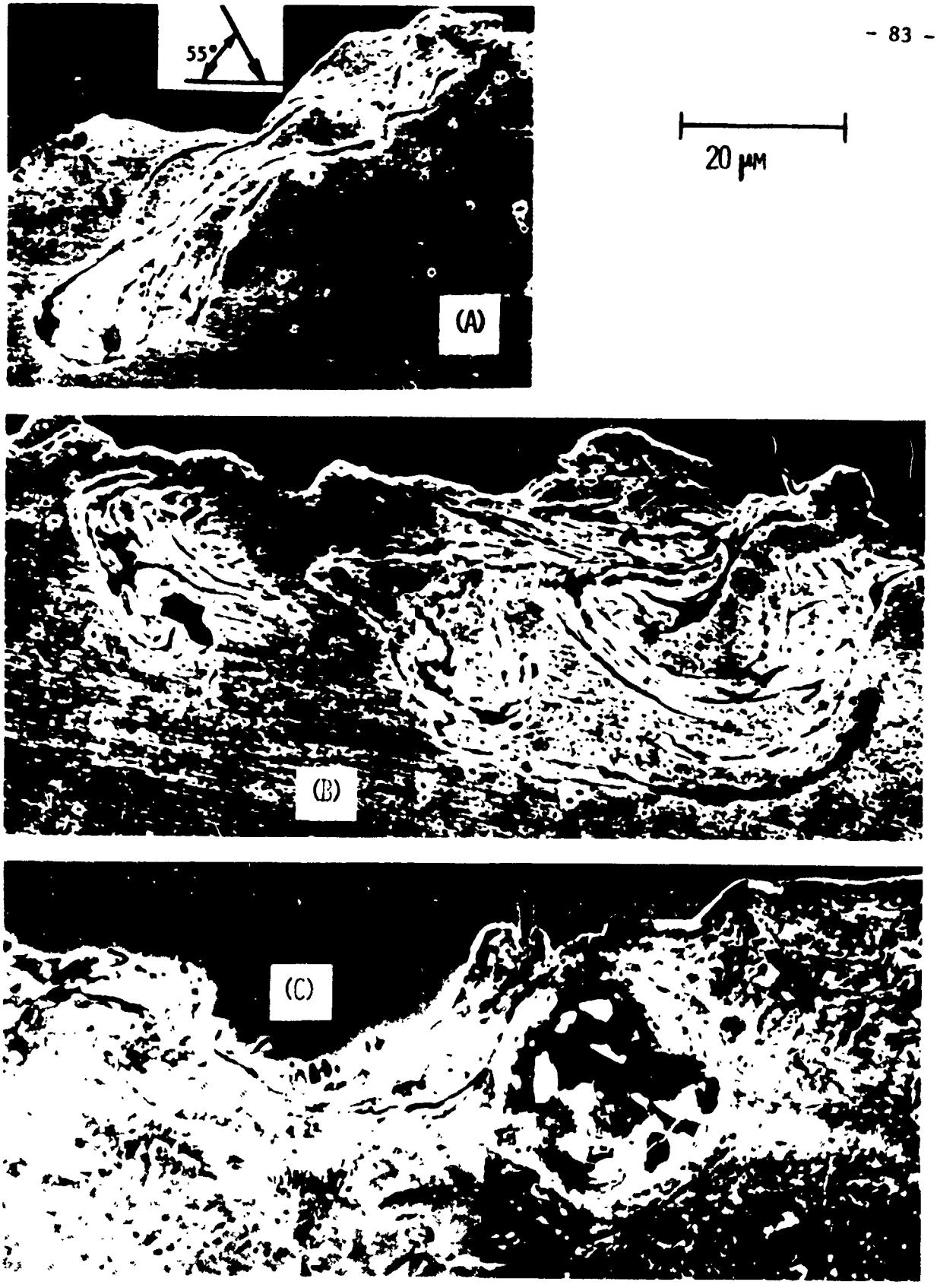

Figure 6.6

Surface damage in erosive wear: (a) copper, 254 μm SiC particles, impacted at 55°, 105 m/sec; (b) same as (a) except the impact angle is

wherever there is a high hydrostatic pressure, cracks will tend to nucleate underneath the impacted surface. Since crack propagation is similarly affected by the hydrostatic pressure, the depth of stable crack propagation will vary depending on the position of the material relative to the interface between the particle and the surface and on the direction of particle motion. It should be noted that the mechanism of erosion by liquid particle impingement seems to be quite different from the case considered here.[58]

Chapter VII

SURFACE ROUGHNESS AND INTEGRITY EFFECTS ON SLIDING WEAR

VII 1) Introduction

It has been recognized for some time that the surface roughness and waviness affect the wear characteristics of unlubricated and boundary lubricated surfaces. However, the exact nature of this effect has not been clarified. In fact, it appears that in most instances the machining specifications for sliding surfaces are left to empiricism. When the tolerance between the sliding surfaces is large, one can normally avoid the problem by "running-in" the surface, which is equivalent to letting the surface reach an equilibrium steady state wear situation. For some critical applications where the tolerance is extremely important (such as in bearings), this practice cannot always be used.

The purpose of this chapter is to provide further insight into the "run-in" process and to discuss the merits of having either rough or smooth surface in sliding applications. The effect of surface roughness and surface "quality" on sliding wear are examined, and it is shown that measurements of the surface roughness alone is not sufficient to characterize the quality of a sliding surface. According to the delamination theory of wear such factors as microstructural damage are equally important.

The phenomenon of "run-in" which is generally observed in early stages of sliding interactions, refers to the large wear rates observed on the initiation of sliding. After this transient stage, the wear rate is reduced and becomes constant. Sasada et al.[59,60] attribute this behavior to the transfer of wear particles from one surface to the other, followed by oxidation of both surfaces to reduce the wear rate. This explanation can only be true in air and not under lubricated conditions or in an inert atmosphere; yet "run-in" is also observed under these conditions. Queener et al.[61] correlated this behavior to the removal of the original surface asperities and showed that under lubricated conditions "run-in" wear depends on the original surface roughness.

Although some[62] have tried to explain the steady state wear in terms of interactions and fracture of asperities, there is convincing evidence[31] that the subsurface deformation, and crack nucleation and propagation processes are the rate controlling mechanisms. The fact that there is always a steady state deformation field in the subsurface corresponding to the steady state wear, indicates that the steady state wear behavior can only be explained in terms of the delamination theory of wear.

VII 2) Review of Previous Investigations

According to the delamination theory of wear, sliding wear of metals at low speeds occurs by the following mechanisms:

1. Plastic deformation and fracture of the original asperities (i.e., original machining marks).
2. Plastic deformation of the subsurface by the traction existing at the contact area.
3. Void and crack formation in the deformed subsurface.
4. Subsurface void growth and crack extension.
5. Generation of long subsurface cracks nearly parallel to the surface.
6. Crack extension to the surface to generate wear sheets.

According to this theory the roughness and integrity (i.e., subsurface deformation and damage) of machined surfaces can affect only the initial wear behavior but not the steady state delamination process. In a previous study[63] it was shown that the effect of original surface roughness on wear was different depending on the normal load (Fig. 7.1). Under large loads* (0.3 kg), the rougher surfaces resulted in a larger initial weight loss associated with the volume of the initial surface asperities (Fig. 7.1a). However, once the original machining marks were removed and steady state delamination was observed, the wear rate of all surfaces were equal. When the wear tests were conducted under lower normal loads (0.075 kg), it was found that the rough surfaces had lower initial wear than smooth surfaces (Fig. 7.1b). This was due to the fact that delamination of the smooth surfaces began on the initiation of sliding; whereas delamination of the rough surfaces was delayed until the original

*Pin on disk geometry, AISI 52100 steel pin, 4.7 m/min average sliding speed, argon gas environment.

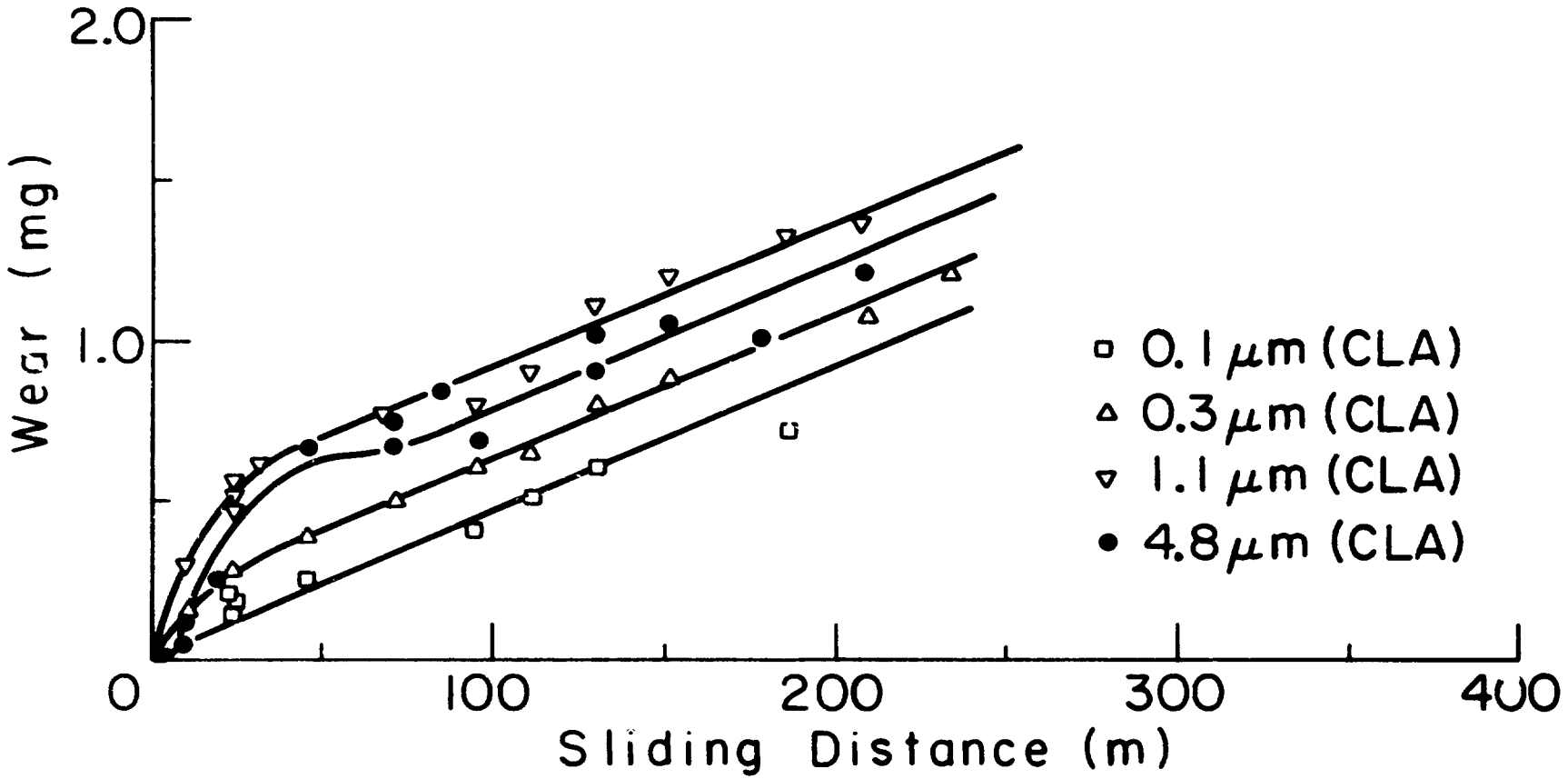

Figure 7.1a

Weight loss as a function of sliding distance for AISI 1020 steel (pin on disk geometry): under a normal load of 0.30 Kg.

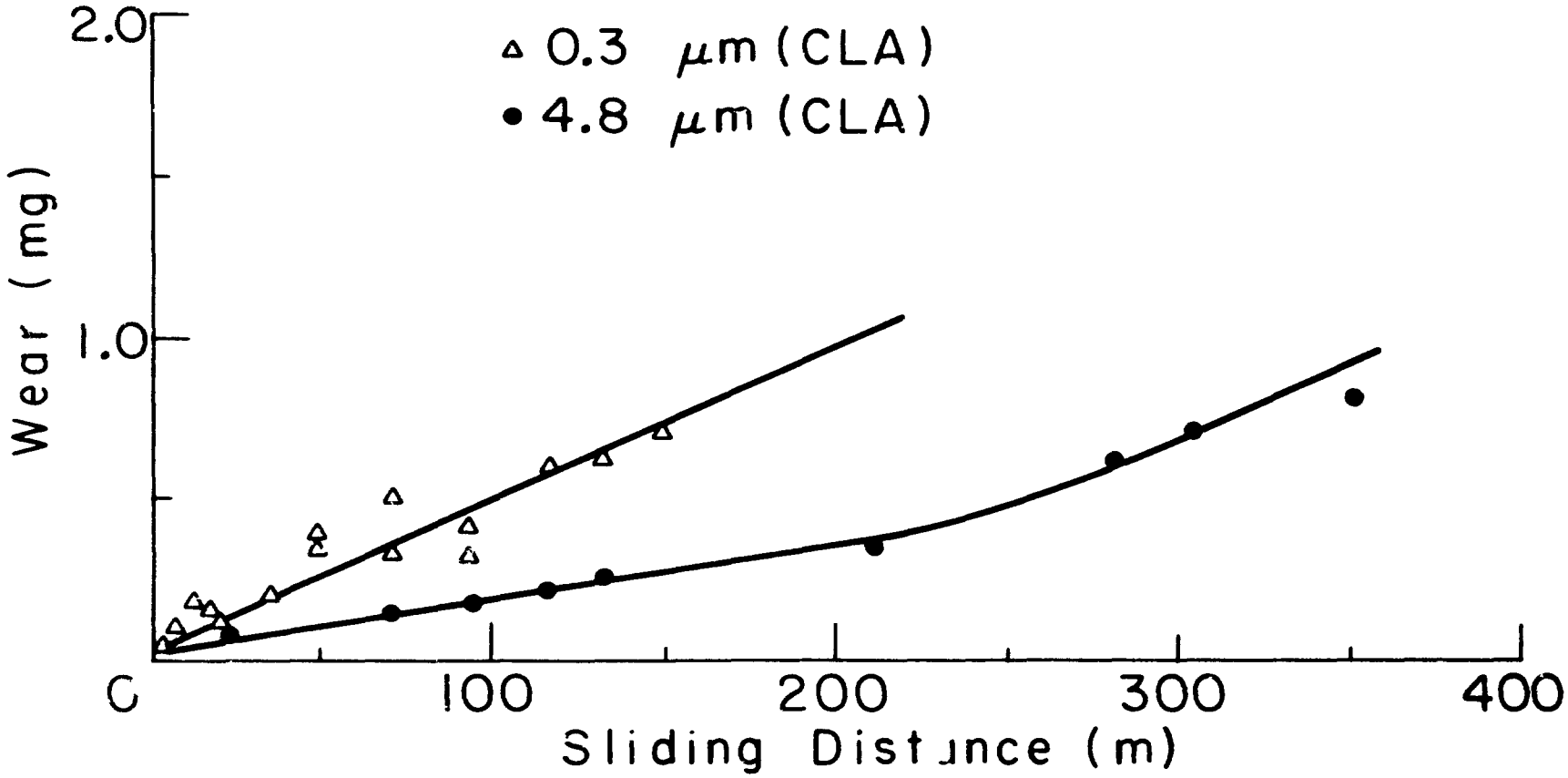

Figure 7.1b

Weight loss as a function of sliding distance for AISI 1020 steel (pin on disk geometry): under a normal load of 0.075 Kg.

machining marks were removed. During steady state delamination the wear rate of both surfaces were equal. Since the rate of the removal of asperities was much lower than the delamination rate, the rough surfaces had smaller weight losses than smooth surfaces. This phenomenon was not observed under larger loads because the contact stress was sufficient to remove the original asperities almost immediately and initiate delamination.

The transient wear process and delamination of a rough surface, is schematically shown in Fig. 7.2. The initial weight loss is associated with the deformation and removal by fracture of the tops of asperities (steps 1-5). The amount removed depends on the strength of the material, the surface fraction and the size of the asperities. However, when all of the original asperities are removed, the rate of delamination (steps 5-6) does not depend on the surface finish as observed in Fig. 7.1.

The wear track of the coarsest surface finish specimen after a two minutes test (10m of sliding) is shown in Fig. 7.3. The deformation of the asperities at the side of the track (Fig. 7.3a) and the occurance of delamination in the center of the track (Fig. 7.3b) is observed. Note that some machining marks are still present across the track. Due to the large size of asperities in this case, the whole track has not yet reached steady state delamination.

VII 3) Experimental Procedure

Wear tests were carried out on a lathe using a cylinder on cylinder testing geometry. The specimens were rotated at a surface speed of 1.8 m/min and the stationary AISI 52100 pins (0.6cm in diameter) were pushed against the specimens by a normal load of 0.106 and 0.850 kg. A series of tests were carried out with the slider moved manually parallel to the axis of the specimen. This was performed under a load of 0.907 kg for 10 passes. The tests were run under argon flowing at a rate of 10 ℓ/min into a chamber surrounding the contacting surfaces. All tests were run dry and at room temperature.

The material tested was commercial cold rolled AISI 1018 steel (hardness 84 kg/mm^2) and 70/30 brass (hardness 46 kg/mm^2), 0.6 cm in diameter. A variety of surface finishes were generated by turning. The surface finishes ranged from 1.2 to 10.4 μm (CLA). These specimen finishes were generated by turning at 319 rpm with a 0.13 mm depth of cut at various feed rates. Some specimens were prepared with cutting tools having a range of positive and negative rake

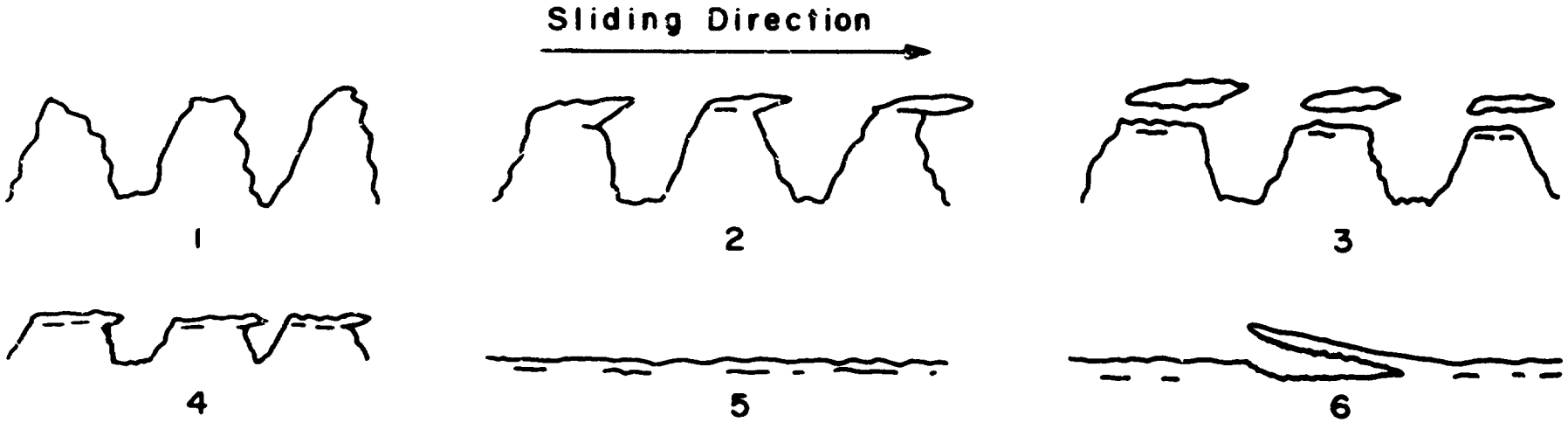

Figure 7.2

Schematic representation of the delamination process during sliding wear; asperity deformation and fracture 1-5, subsurface crack nucleation, propagation, and wear sheet formation 5-6.

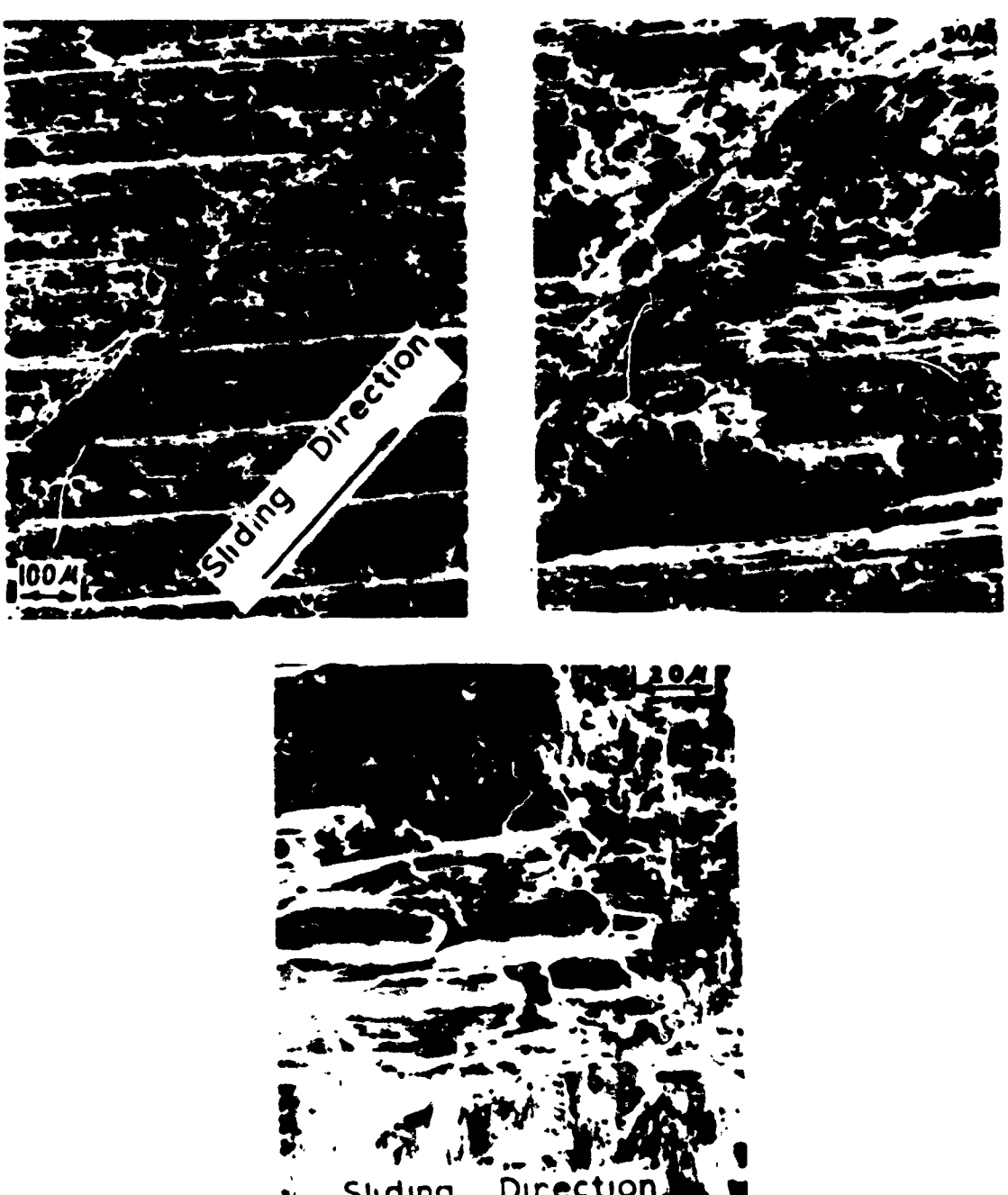

Figure 7.3

Wear track of 4.3 µm (CLA) surface finish AISI 1020 steel speciment (pin on disk geometry), under a normal loac of 0.30 Kg after 10 m sliding distance: (a) asperity deformation on the edge of the wear track, and delamination at the center, (b) delamination at the center of the wear track.

angles to study the effect of subsurface damage generated by machining. Another series of specimens were prepared by orthogonal turning[64] using tools with positive and negative rake angle lubricated with lard oil. The cutting forces for these tests were recorded and measured.

VII 4) Surface Roughness

The process of asperity deformation during the initial stages of sliding is shown in Fig. 7.4. The sliding was perpendicular to the machining marks in Fig. 7.4a and parallel in Fig. 7.4b. It is clearly observed that the rough surface (i.e., 3.4 μm CLA) has become smooth at the wear track, and there is no evidence of adhesive or transferred particles.

The results of wear tests on samples with varying roughness and normal loads are presented in Fig. 7.5. It is shown that under a load of 0.850 kg (Fig. 7.5a), the rough surfaces have a slightly larger wear than the smoother surface. The small difference in weight loss is probably due to the larger weight of the original asperities of the rougher surfaces. However, once the asperities are removed and steady state delamination is reached, the wear rate of all surfaces is the same.

Fig. 7.5b shows that under 0.106 kg normal load, the smoother surface has a larger wear than the rough surface. However, the final steady state delamination rate of both surfaces is the same. The difference in wear is due to the difference in the time delay before the onset of delamination. The 1.2 μm CLA surface starts delaminating after 9 m of sliding, where delamination of the 2.7 μm CLA surface begins after 32 m of sliding.

The result of these tests show that the surface roughness does not affect the steady state wear rate, but only influences the initial wear behavior of machined surfaces. The fact that the rough surfaces under low loads have smaller wear than smooth surfaces has interesting practical implications in the preparation of sliding surfaces. These results suggest that sliding surfaces will last longer under low contact stresses if they are made rough. Furthermore, under normal sliding conditions where lubricants are used, the rough surfaces will also retain the lubricant and the wear behavior may be improved even further.

It should be emphasized that the rough surface is better than the smooth surface only if there is no subsurface damage associated with machining. Otherwise the large asperities delaminate catastrophically and produce large

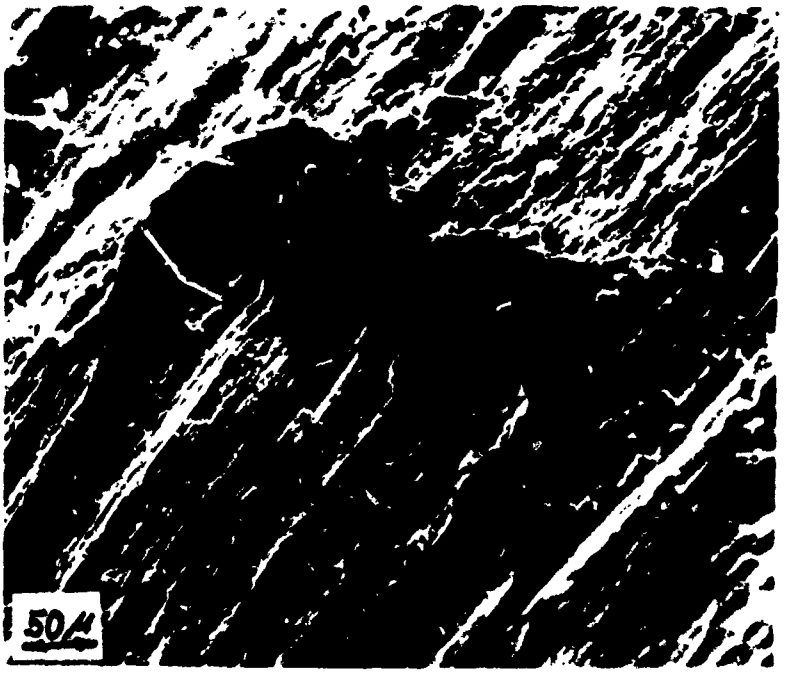

(a)

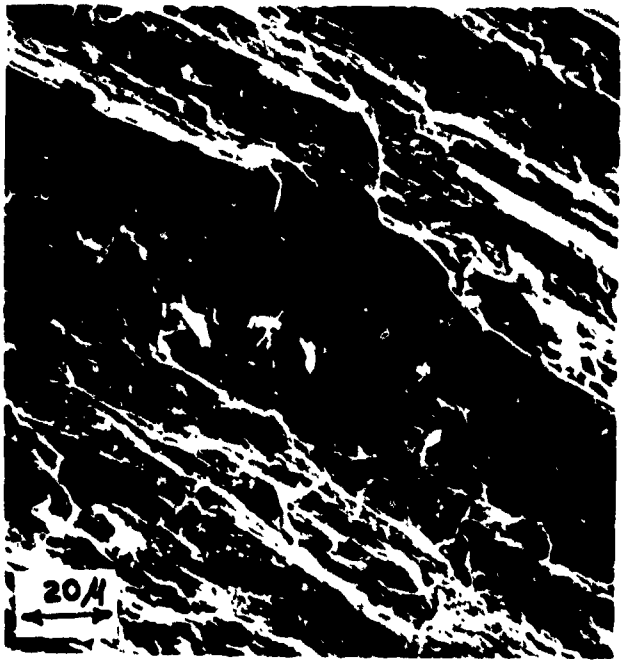

(b)

7.4 Plastic deformation of original asperities for AISI 1018 steel (cylinder on cylinder). (a) Sliding perpendicular to the machining marks, 2.0 μm (CLA) surface finish, under a normal load of 0.91 Kg for 10 passes. (b) Sliding parallel to the machining marks, 3.3 μm (CLA) surface finish, under a normal load of 0.35 Kg after 0.25 m of sliding.

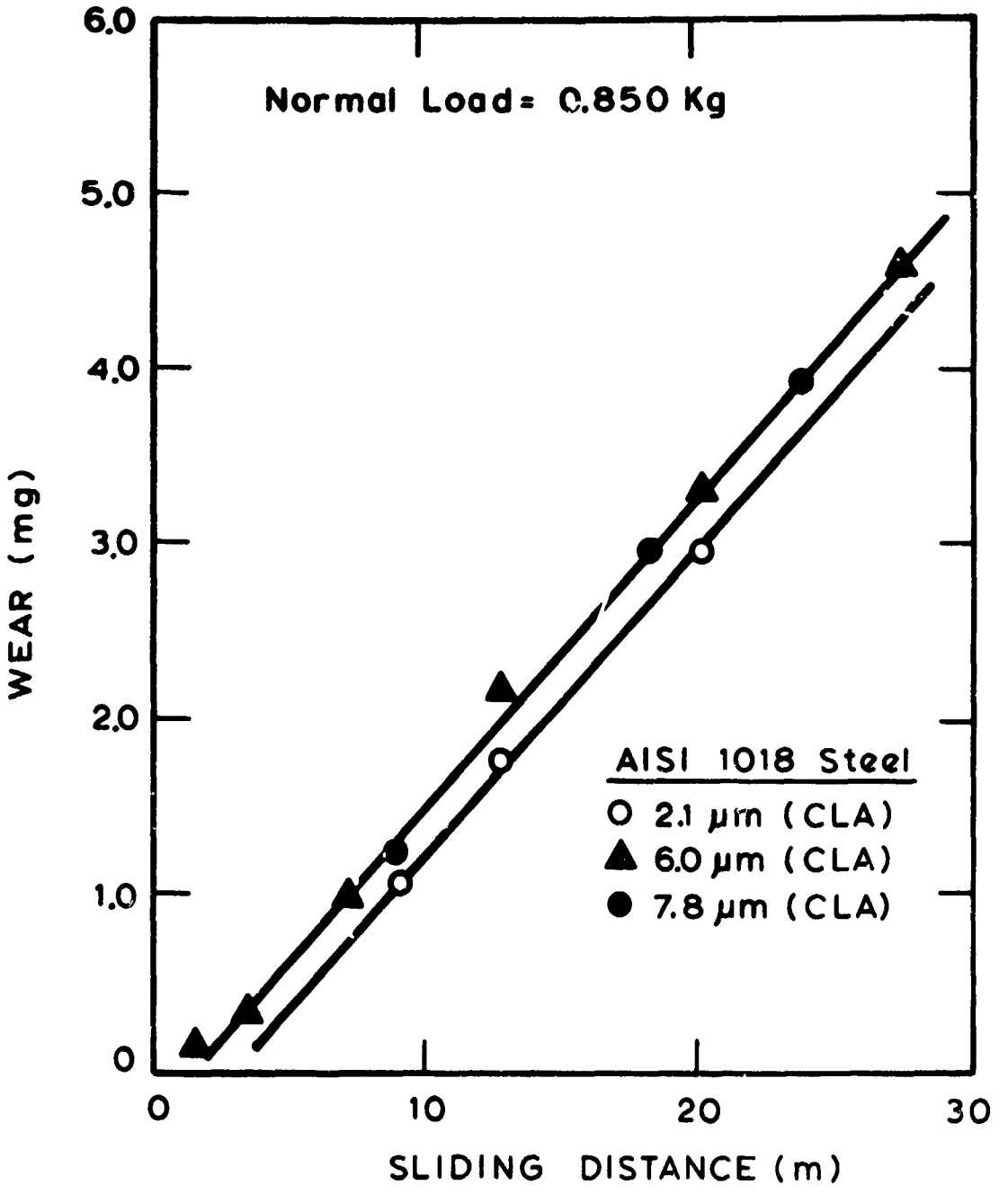

Figure 7.5a

The effect of original roughness of machined surfaces on weight loss: normal load of 0.850 Kg.

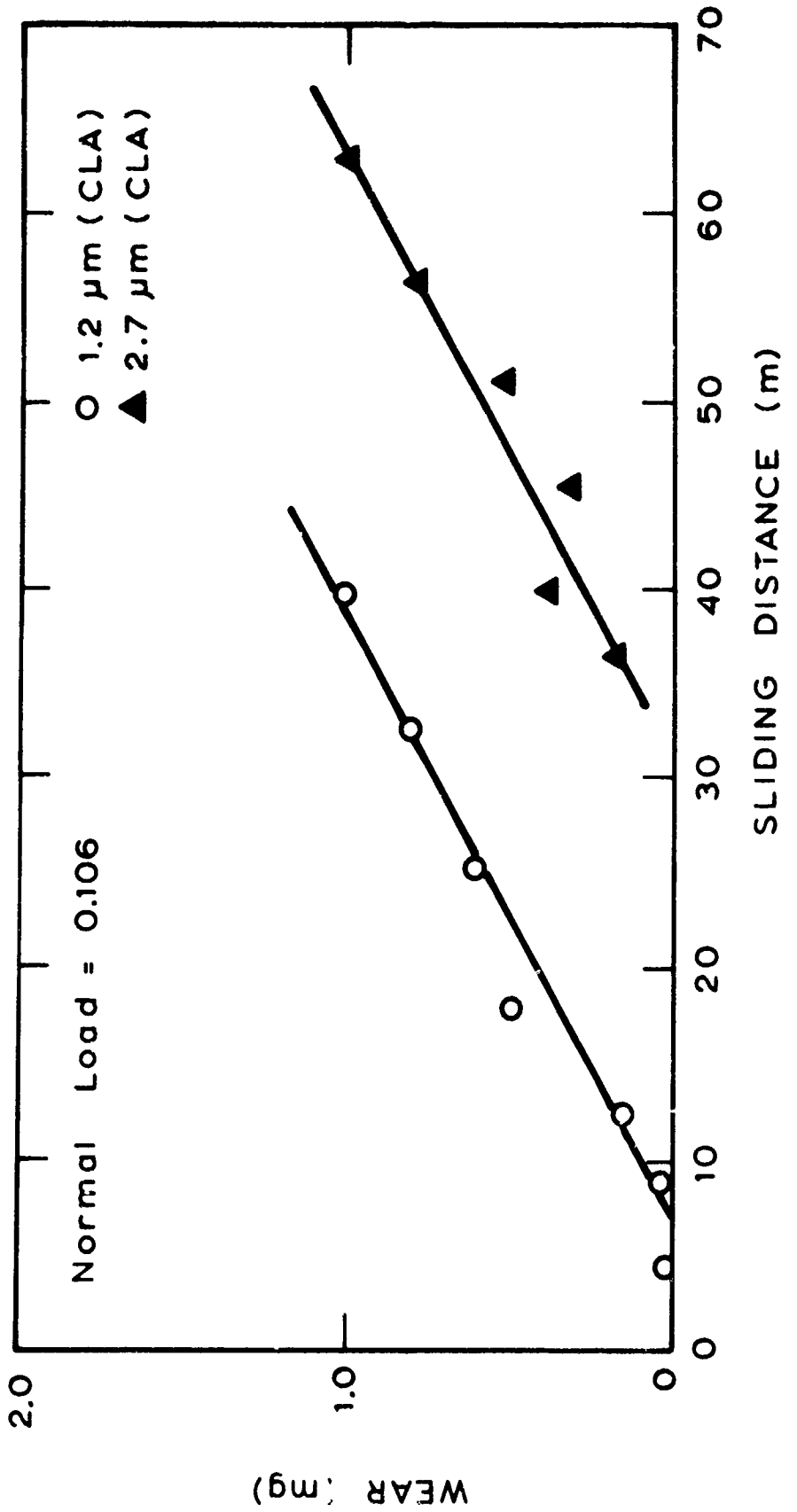

Figure 7.5b

The effect of original roughness of machined surfaces on weight loss: normal load of 0.106 Kg.

wear particles which could then cause abrasive wear of the sliding components. This was observed when specimens generated by a worn tool were wear tested under low (0.075 kg) normal loads. In these specimens the wear data was very scattered and the delayed delamination associated with rough surfaces was not observed.

VII 5) The Effect of Surface and Subsurface Damage

According to the delamination theory the sliding wear of metals occurs by subsurface deformation, void and crack nucleation and propagation. Therefore, if the prepared surface contains any subsurface damage (i.e., deformation, voids and cracks), one would expect a large initial wear rate. This is shown in Fig. 7.6 for an as-drawn surface vs. a polished surface. The initial weight loss of the as-drawn surface was higher because of the surface damage generated during drawing as shown in Fig. 7.7a. (The as-drawn surface was lighly polished with a 4/0 emery paper to remove the surface oxides.) The polished surface was prepared by polishing off 0.06 mm with No. 2 emery paper and a final polish with a 4/0 emery paper. This process generated a relatively damage-free surface as observed in Fig. 7.7b, leading to a lower volume loss than for the as-drawn specimen.

The effect of subsurface damage generated by machining on wear is shown in Fig. 7.8. The two series of specimens were machined using a sharp and a chipped cutting tool, shown in Fig. 7.9. The chipped tool was still capable of producing fine surface finishes and from a machinist's point of view was still useful. The difference in the initial weight loss of the two series of specimens is due to the larger subsurface damage generated by the chipped tool (10 μm deep) as compared to that of the sharp tool (2 μm deep), observed in Fig.7.10a and 7.10b, respectively. It is interesting to note that the subsurface deformation caused by the chipped tool was sufficient to generate wear sheets (Fig. 7.11) on the machined surface.

A recent investigation[65] has shown that burnished surfaces have lower wear rates than unburnished surfaces. This would be consistent with the present result if burnishing does not induce subsurface deformation and crack formation. In burnishing the asperities are deformed and fractured and some of the surface damage is removed resulting in a surface with a smaller degree of subsurface damage and lower wear rates.

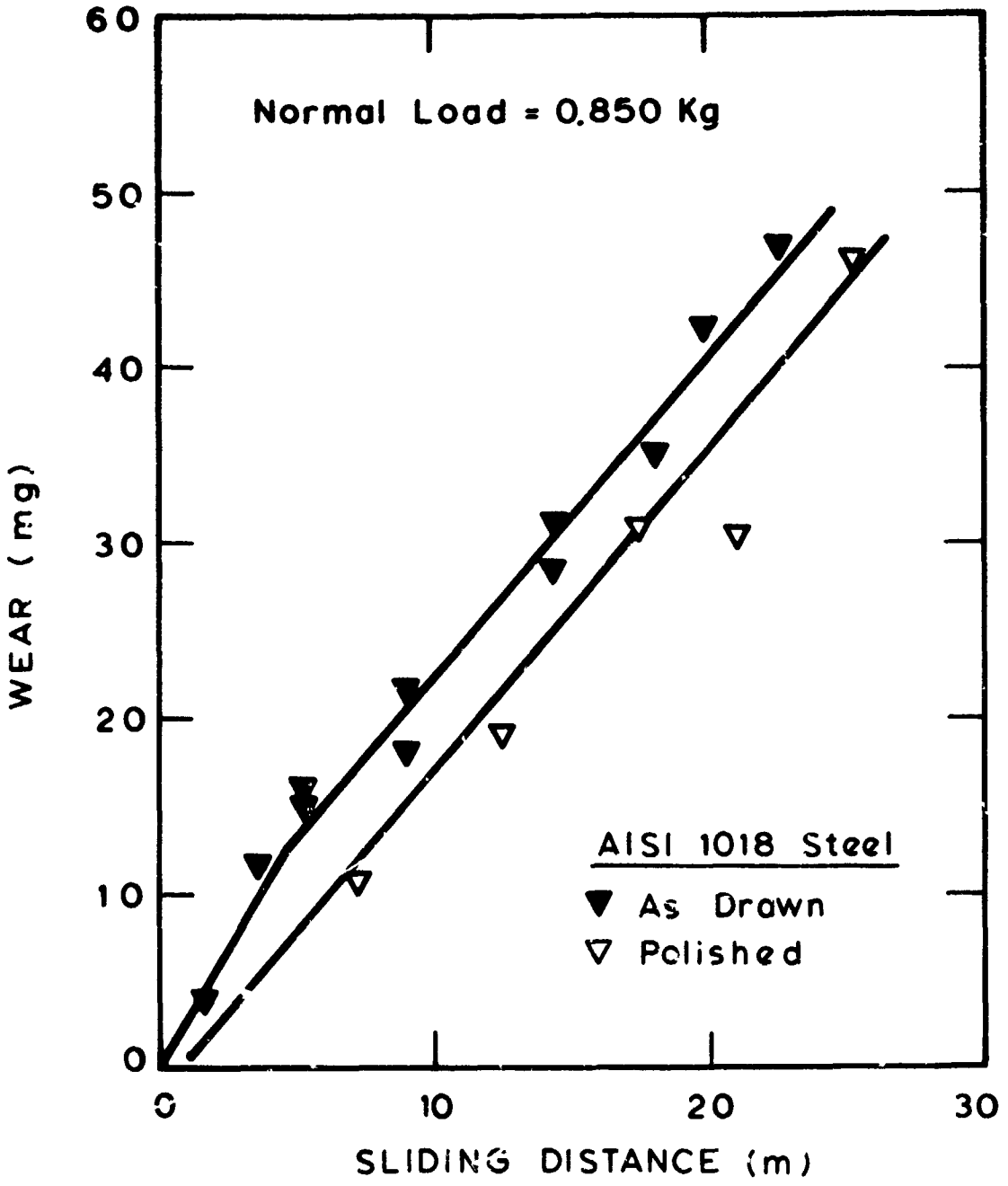

Figure 7.6

The effect of as-drawn material on wear of 1018 steel under a normal load of 0.85 Kg.

(a)

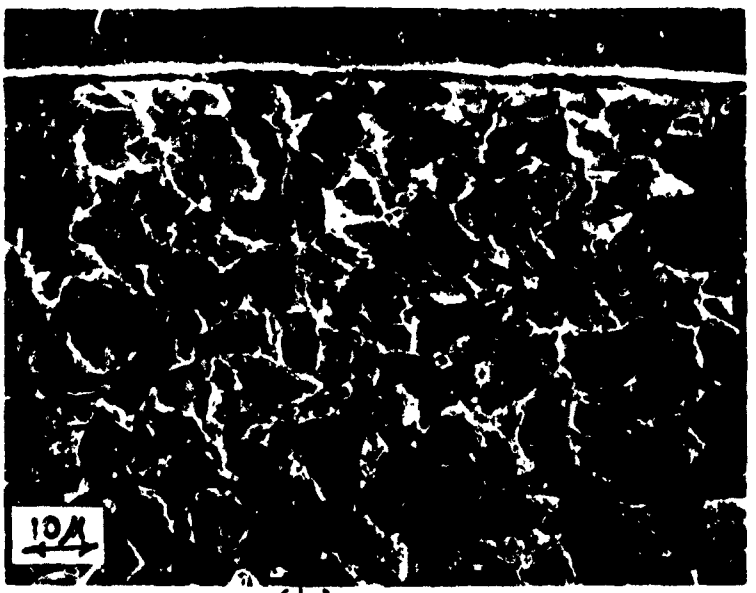

(b)

Figure 7.7

Sections perpendicular to the surface showing typical microstructure of 1018 steel: (a) as drawn; (b) after polishing.

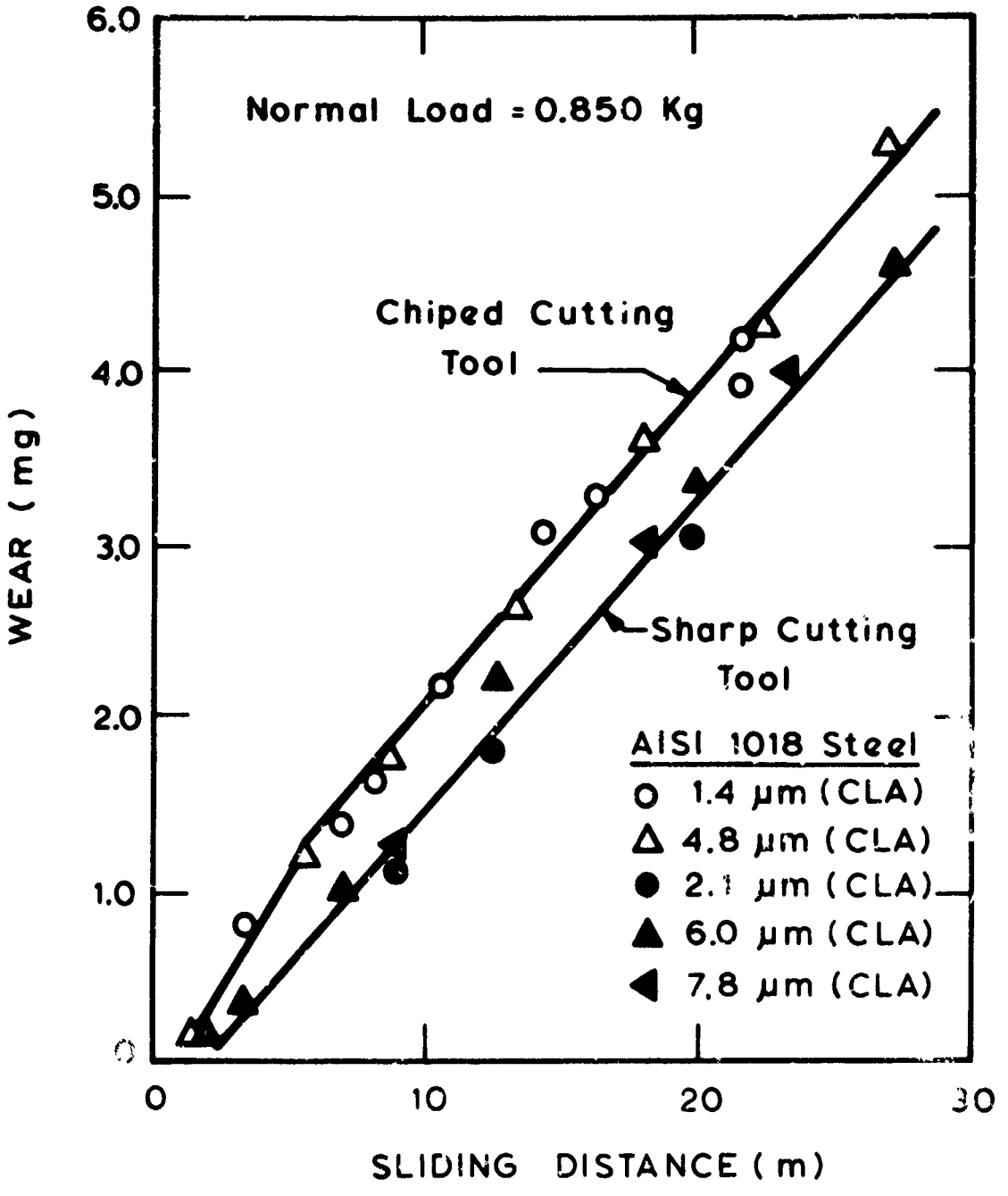

Figure 7.8

The effect of subsurface machining damage on wear of 1018 steel.

200 μ

(a)

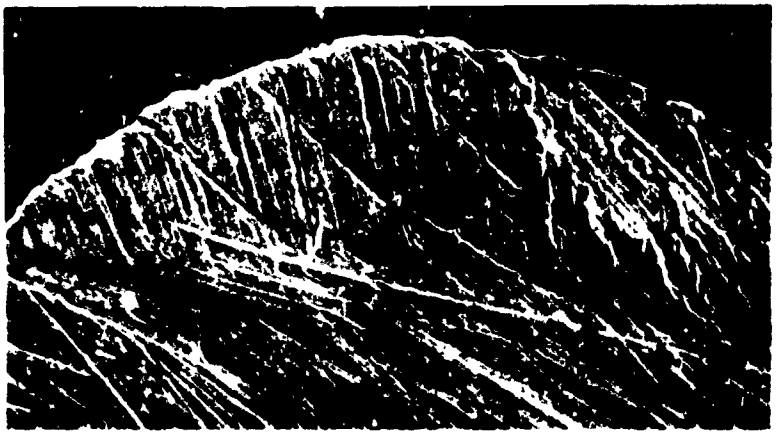

(b)

Figure 7.9

SEM micrographs of the rake face of: (a) chipped cutting tool; (b) sharp cutting tool.

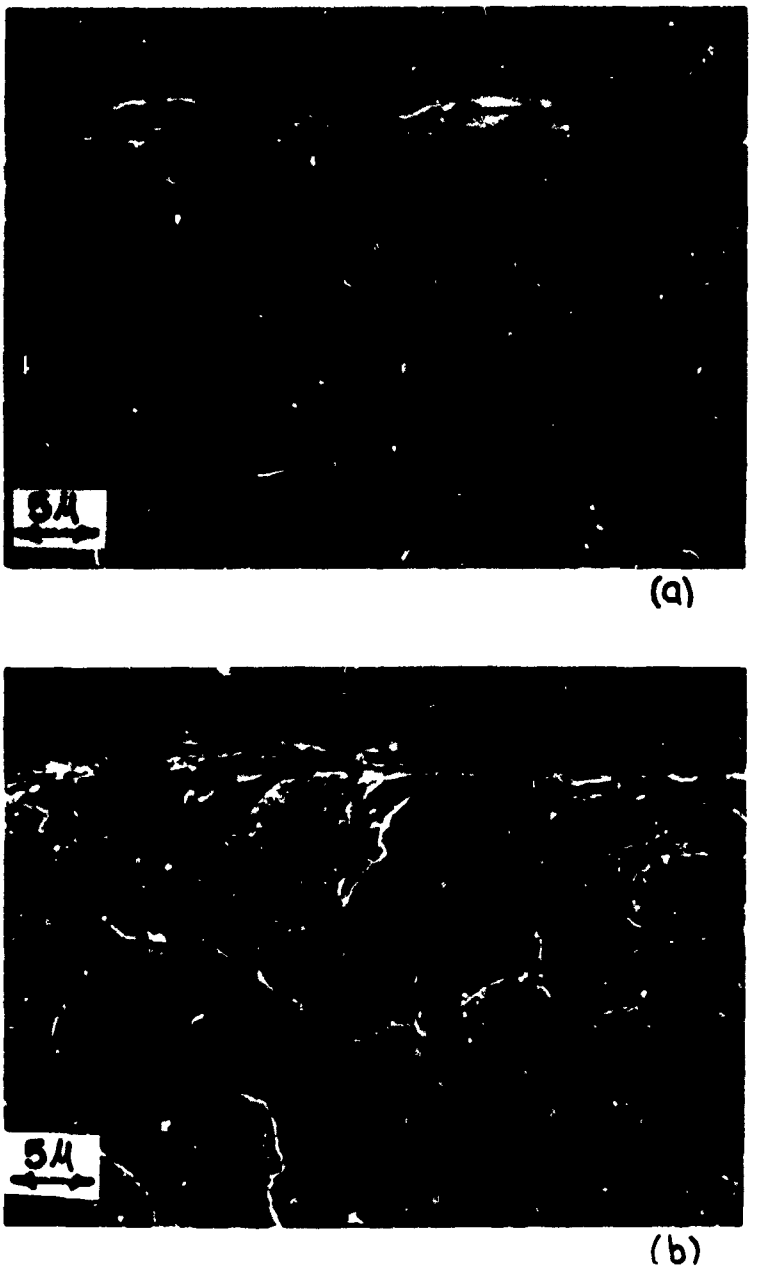

Figure 7.10

Sections perpendicular to the surface, showing typical subsurface damage of 1018 steel: (a) machined with a chipped tool 4.8 μm (CLA; (b) machined with a sharp tool 6.0 μm (CLA).

Figure 7.11

Wear sheets on the machined surface of an 3.3 μm (CLA) surface finish, prepared with chipped cutting tool.

The degree of subsurface damage associated with machining depends on the cutting rake angle and the depth of cut.[66,67] Turley has shown that the depth and the degree of deformation in 70/30 brass increases as the rake angle becomes more positive or negative. At large negative rake angles the tool does not cut any more and it slides over the surface causing plowing and subsurface deformation. The depth of deformation also increases with the depth of cut and the cutting radius.

Fig. 7.12 shows the wear of steel specimens prepared with three different tools (40^{o} rake, 8^{o} rake and 1.3 mm honed radius, 40^{o} rake). The figure shows that all specimens have the same wear. This is possible since all the tools had positive rake angle and since steel is much harder than brass and therefore the damage caused by machining with different cutting tools might have not been sufficient to affect the wear behavior.

Therefore, 70/30 brass specimens were prepared by orthogonal turning with $+25^{o}$, $+5^{o}$, and -15^{o} rake angles. The results of the wear tests on the brass indicated that there was not a large difference between the wear rates of the samples cut with positive and negative tools. Subsurface observations of the machined surfaces showed that the depth of deformation was 25 μm for the $+25^{o}$ tool and 30 μm for the -15^{o} tool. Since this difference was not large it did not lead to a substantial difference in the wear rate of the samples.

The depth of deformed layers reported by Turley [66.67] ranged from 600 μm for a $+25^{o}$ tool to 900 μm for a -15^{o} tool. In the presence of such a large difference in the deformed regions generated by the two tools, one should expect to observe a large difference in the initial wear rate. However, since the degree of machining damage in the brass samples of this work were similar, no difference in the wear behavior was observed.

The deformation depth in brass observed by Turley was much more than the deformation depth reported here, probably because of the difference in the machining operation. Turley's specimens were prepared by planing; whereas the specimen tested by us were prepared by turning. This indicates that the choice of machining operation and perhaps machine tools is an important factor in preparation of surfaces for sliding applications, since each type of machining generates a different type of damage in the finished product.

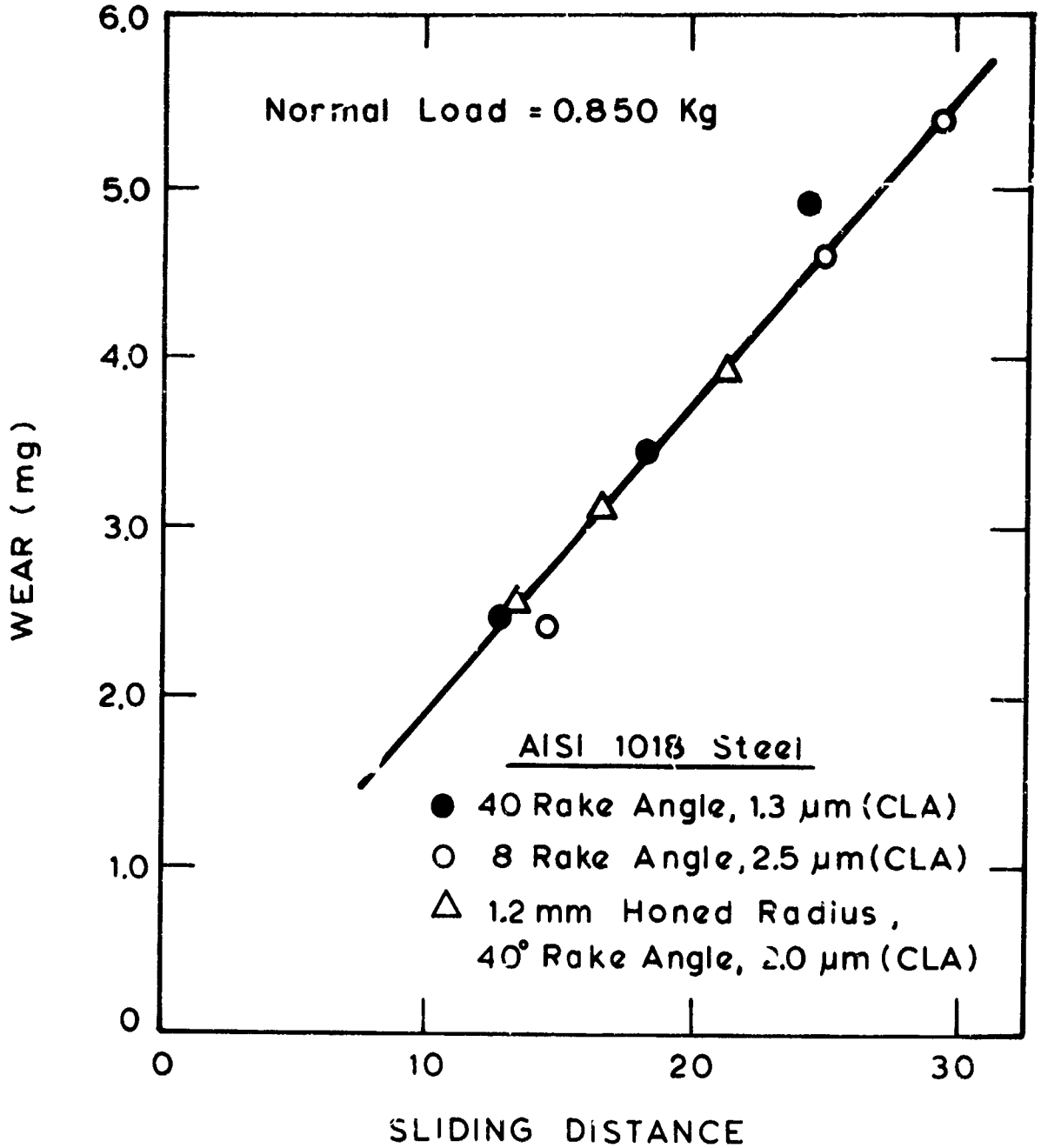

Figure 7.12

Wear of 1018 steel under a normal load of 0.85 Kg, speciments machined with three different cutting tools.

VII 6) Conclusions

1) Surface roughness influences only the initial wear behavior and not the steady state wear rate.
2) At low normal loads rough sliding surfaces have smaller wear than smoother surfaces, provided that the surfaces are free from machining damage.
3) Large subsurface damage associated with machining operations could increase the initial delamination wear rate of the sliding surfaces.
4) The choice of machining operation and variables are important factors in the preparation of surfaces for sliding applications.

Chapter VIII

SLIDING WEAR RESISTANCE OF METALLIC COATED SURFACES

VIII 1) Introduction

Earlier work[2,13,34] has shown that the delamination theory of wear may provide a theoretical basis for reducing wear through the application of soft metallic coatings to metal surfaces. The hypothesis was that if a thin layer of a softer metal is deposited on a harder substrate, heavy plastic deformation and wear of the substrate by delamination may be prevented. The critical nature of the plate thickness was explained in terms of dislocation instability very near the surface, although this has not been proved explicitly.* Plating a metal substrate with a soft metal to reduce friction and wear has been used quite extensively[68,79], but the exact nature and mechanism by which these coatings improve the tribological behavior of surfaces has not been investigated completely. Previous attempts have been made[7,79] to determine the optimum thickness of these coatings, but the results and the theoretical considerations were insufficient and inadequate.

The purpose of this chapter is to show that large wear reduction is possible by plating a soft metal on a hard surface if the deposited material is not thicker than a critical thickness** (much less than 1 μm). It is shown that, as the plate thickness is increased, wear by delamination within the plate occurs until the thickness is reduced to a stable value. Cadmium, silver, gold and nickel coating have been used on steel and the influence of substrate surface condition prior to plating has been investigated. The role of the soft metallic coatings in wear reduction is discussed both in terms of dislocation mechanics and the mechanics of delamination.

VIII 2) Review of Earlier Work on Coated Metal Surfaces

Electroplating with precious metals to increase the life of ball bearings[74-77] and gears[77,78] operated in vacuum has been reported in the literature. However, the components still exhibited a high degree of wear. The coatings were 30 to 75 μm thick, well above the probable optimum values, which may explain the high wear rates.

Other investigators[69-71] have noted the reduction in the sliding

---

*The existence of the soft layer is and has been a controversial subject. Definitive work has not been done to date.

**Patent pending.

wear rate of steel when plated with soft materials such as lead, gold, gold alloys, silver, copper and nickel. For the most part the wear was reduced only by a factor of 2 to 3. These results were obtained in tests which were run with an unplated slider rubbing against a plated specimen, leading to the possibility of transfer of the soft plating material from the specimen to the slider and also abrasive wear caused by loose wear particles.

Kuczkowski and Buckley[72] coated nickel and AISI 440 C stainless steel with 25 μm of various binary and ternary alloys of gallium and indium. A ternary alloy of gallium, indium and tin reduced the wear rate of the stainless steel by four orders of magnitude when tested in a vacuum of 10^{-11} mm Hg. Similar results were found for nickel with a coating of a binary alloy of gallium and indium. No mention was made however of the possible influence of plating thickness on the wear rate.

In previous papers by the authors[13,34] it was shown that a thin coating of cadmium (0.1 μm) on AISI 1020 steel can reduce the wear rate of steel by a factor of 5000 under an inert atmosphere. The thickness of the coating was found to be critical, since delamination within the cadmium plate occurred for thicknesses greater than 0.1 μm. It was also shown that the subsurface deformation of the parent metal below the coated wear track was much less than the corresponding deformation beneath an uncoated track. The thin plated layer retarded substrate delamination because of the reduced deformation due to the lower friction coefficient of the thin cadmium plated steel. The critical thickness of the soft plating could be predicted by utilizing the delamination theory of wear. This prediction was based on the fact that dislocations near the surface are not stable and some of them can be pulled out of the free surface by the action of the image forces acting on these dislocations. Consequently, the thickness of the "low dislocation density" layer is controlled by the magnitude of the image forces which depend on such material properties as shear modulus and friction stress. Therefore, if the plated layer is made thin enough such that most of the dislocations can be eliminated, the plate deforms continuously without appreciable strain-hardening and subsequent fracture. This thin plated layer reduces the friction coefficient because of its non-strain-hardening

properties, thus resulting in less substrate deformation and wear. However, if the plate is thicker than this critical thickness, dislocation accumulation and strain hardening can take place in the plated layer, leading to wear by delamination within the plating itself.

An alternate explanation may be provided in terms of the stress distribution. It was shown in Chapter III that the normal tensile stress component perpendicular to the surface over which an asperity has just moved becomes a maximum at a finite depth below the surface. Therefore, it can be argued that delamination cannot occur in a critically thin plated layer, since the magnitude of the tensile stress is very small in that layer.

VIII 3) Experimental Procedure

Wear tests were carried out with a cylinder-on-cylinder geometry. The specimens were 0.63 cm in diameter by 7.6 cm long with a 0.4 μm (CLA) ground finish prior to plating. In one case the surface was metallographically polished with a 0.25 μm diamond paste. The specimens were rotated at a surface speed of 1.8 m/min and the stationary pins were pushed against the specimens by a normal load of 2.25 kg. All tests were carried out dry in a chamber surrounding the mating surfaces under argon flowing at a rate of 10 ℓ/min.

The substrate materials used had a variety of hardnesses: AISI 1018 (84 kg/mm^2), AISI 1095 (170 kg/mm^2) and AISI 4140 (270,370,460 kg/mm^2 - obtained by different heat treatments). In all cases the sliders were made of the same material as the specimen, heat treated and plated in the same fashion. The plating thickness varied from .05 to 10 μm. The platings tested were gold, gold over a nickel flash, cadmium, nickel, and silver. Some of the gold plated specimens were plated with a flash of gold first and were then heated at 500°C for 2 hours in vacuum to obtain a diffused bonding between the plate and the substrate. Then the required thickness of gold was plated on the samples.

VIII 4) The Effect of Plate Thickness

The effectiveness of plating in wear reduction is dramatically shown in Fig. 8.1 for 1 μm nickel plated AISI 4140 steel. The large difference in the size of the wear tracks between the unplated (Fig. 8.1a) and the plated sample (Fig. 8.1b) should be noted. The unplated sample was tested for 30 minutes, whereas the plated sample was tested for 2 hours. Since

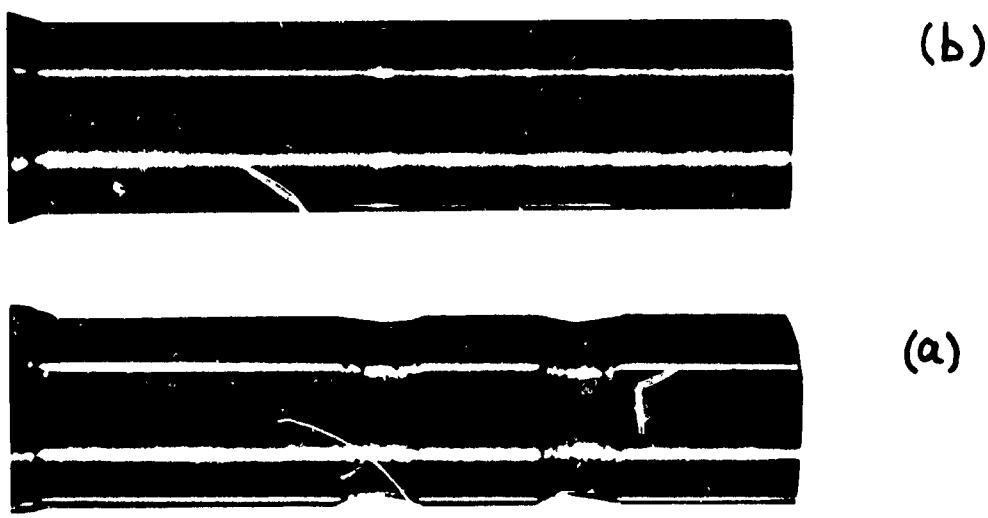

Figure 8.1

Comparison between wear tracks of AISI 4140 steel, tested in argon, 2.25 Kg normal load: (a) unplated against unplated (after 30 min of testing); (b) 1.0 μm Ni plated against 1.0 μm Ni plated (after 2 hours of testing).

no further wear could be detected on the plated specimen after 2 hours (216 m of sliding), the test was terminated.

The important effect of the nickel plate thickness on the wear rate of AISI 4140 steel is observed in Fig. 8.2. Wear reduction by three orders of magnitude is observed for the initial nickel thickness of 1 μm. This minimum thickness of the plate also decreased the coefficient of friction from 0.63 to 0.45. Fig. 8.2 shows that the wear rate increases with the nickel plate thickness. This increase in wear rate for thick plates is caused by dislocation accumulation leading to strain hardening and delamination within the plate. The cracking and delamination within a thick (25 μm) plate of gold on AISI 1018 steel is shown in Fig. 8.3. The thick layers wear off by delamination until the thickness of the layer is reduced to the optimum thickness in which the dislocations are presumably not stable. Afterwards, the wear rate is very low, similar to the case of thin platings. The transient behavior of thick coatings is shown in Fig. 8.4 for an initial 10 μm nickel plate on AISI 4140 steel. Under some sliding situations where the wear particles cannot be removed from the contact, they may act as abrasive particles and accelerate the wear process.

VIII 5) The Effect of Surface Roughness and Bond Strength

The steel samples which were plated with a thin layer of gold without any special treatments failed immediately at the beginning of sliding. This failure was found to have been caused by the lack of adhesive bonding, which was accentuated by the roughness of the substrate surface at the time of plating. In these tests, since the optimum plate thickness is very small, the substrate surface roughness may play a major role in the life of the coatings. The bond strength between electrodeposited gold and steel has been reported to be very low and to become even weaker with increasing substrate surface roughness.[80] Under sliding conditions, the roughness could cause further deterioration of the bond strength by the deformation and final fracture (Fig. 5) of the original substrate asperities. Therefore, the gold plated steel samples were specially treated to achieve a good bond strength. By thermal diffusion of a very thin layer of gold or by plating a flash of nickel over the substrate before gold plating, it was possible to increase the life of the thin gold plates from immediate failure to more than 108 m of sliding (60 min).

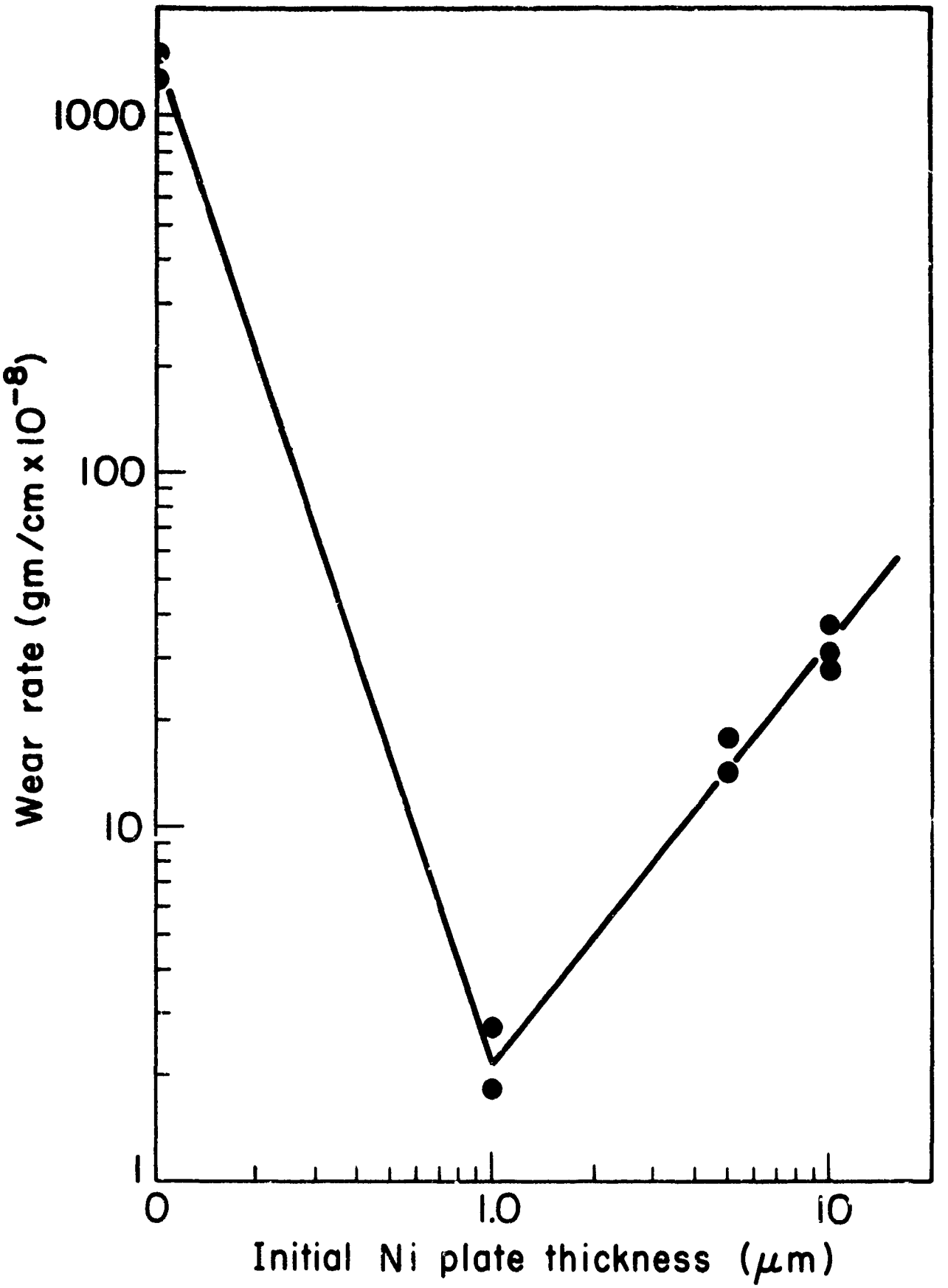

Figure 8.2

The effect of the initial Ni plate thickness on wear rate of AISI 4140 steel in argon, for 30 min tests.

Figure 8.3

Crack formation in a thick Au plate (25 μm initial thickness) after wear testing; AISI 1020 steel substrate.

Figure 8.5

The deformation of substrate asperities due to the sliding action on a thick plate of Au on AISI 1020 steel substrate.

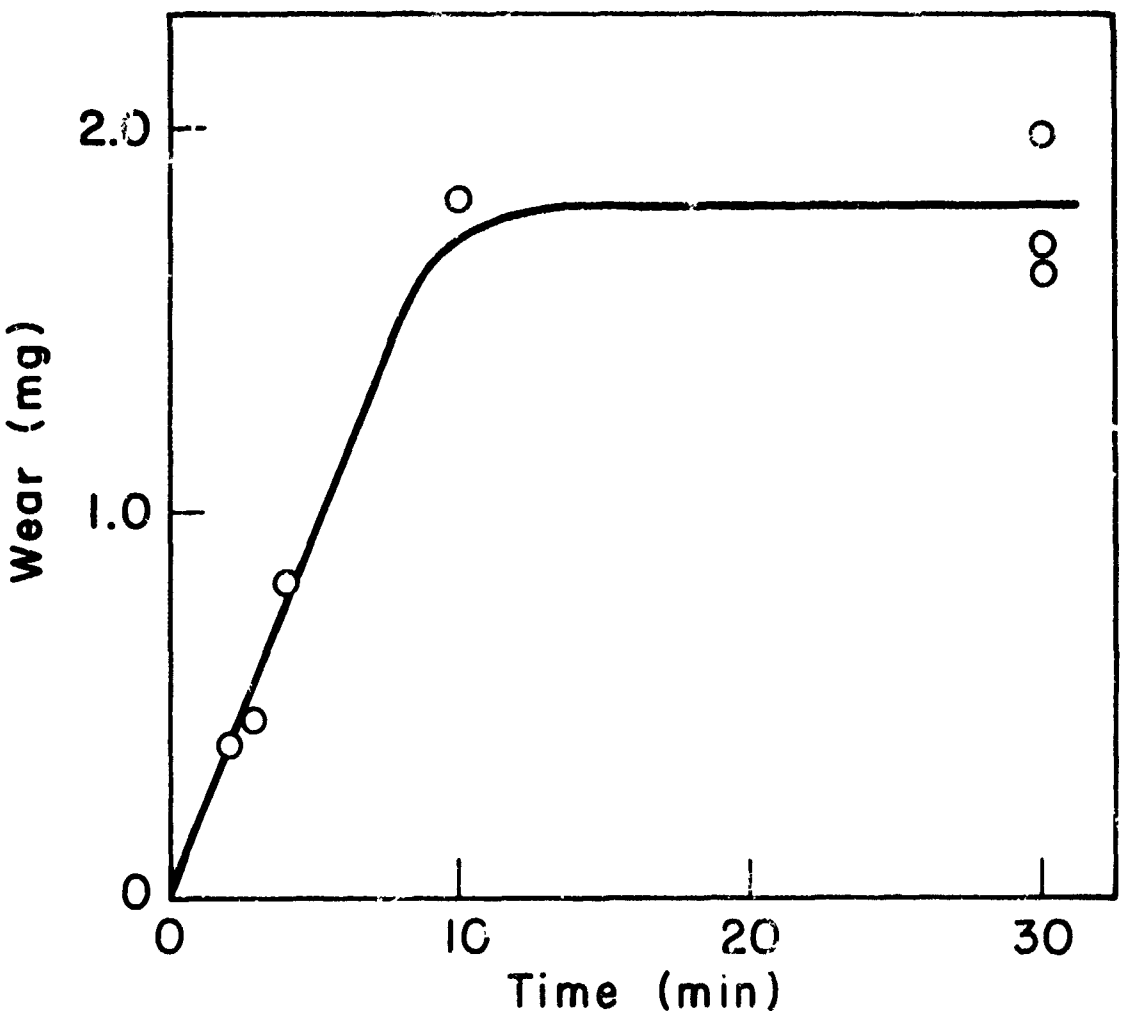

Figure 8.4

Wear of a thick Ni plate (initial thickness of 10 μm) vs. time.

The influence of the substrate surface finish on cadmium plated specimens was checked with a 0.05 μm cadmium coating on AISI 1018 steel with both a fine ground finish and a metallographically polished finish. The surface roughness had only a moderate effect on the life of the cadmium plates, and polishing increased the life of the coatings only from 25 m to 31 m of sliding. Since steel-cadmium adhesion strength is much greater than the adhesion of steel-gold,[80] this result suggests that moderate changes of surface roughness may influence only plating-substrate combinations which have low adhesive strength.

VIII 6) Hardness Matching Between the Substrate and the Coating

The wear data for all coating materials and steel substrates with various hardnesses for the tests in argon is summarized in Table 8.1. The 1 μm plate of gold (with special treatments) was also effective in air. (Nickel, silver and cadmium were not, because they oxidized and were removed early in the tests.) Wear tests were continued on the coatings which did not fail immediately. After 60 min (108 m) those coatings had remained on the surface and were still effective in reducing wear.

According to the delamination theory the plated material must be softer than the substrate to minimize the wear rate. This is supported by the results for nickel and cadmium platings presented in Table 8.1. For the substrates softer than 460 kg/mm^2 failure of the nickel plate was immediately. However, for substrate hardness of 460 kg/mm^2 nickel plating had a very low wear rate. Cadmium plate with a hardness of 30-50 Kg/mm^2[80], was successful on all substrates.

VIII 7) Discussion

The results presented in this chapter further substantiate the predictions made by the delamination theory of wear on the wear resistance of soft metal coatings. For best wear resistance the plated material must be softer than the substrate, thinner than a critical thickness, and bonded strongly to the substrate. The condition of the surface of the substrate is an important factor since it was shown that smoother plated surfaces last longer. It was shown in Chapter VII that subsurface damage caused by machining operation influences the initial wear behavior greatly. Therefore, these materials must be prepared carefully so as to minimize the damage to the substrate during machining. Otherwise, the damaged substrate may cause premature failure and offset the beneficial effects of plating. If the delaminated particles are not removed from the contact, they may oxidize and serve as abrasive particles,

Table 8.1 Experimental results on the wear resistance of 1μm plates on steel. Wear tested in argon, 2.25Kg normal load, 54m sliding distance.

Coating	Substrate and Hardness (Kg/mm^2)	Wear Rate ($mg/cm \times 10^{-8}$)	Coefficient of Friction
Cd	AISI 1018 (84)	3.6	0.35
Cd	1095 (170)	1.8	0.25
Cd	4140 (270)	3.6	0.35
Cd	4140 (370)	3.6	0.25
Ag	AISI 1095 (170)	1.8	0.33
Au (diffused)	AISI 1095 (170)	1.8	0.85
Au (Ni underlayer)	1095 (170)	-1.8	0.9
Ni	AISI 1019 (84)	immediate failure	-
Ni	1095 (170)	"	-
Ni	4140 (270)	"	-
Ni	4140 (370)	"	-
Ni	4140 (460)	1.8	0.45

thus degrading the coating and enhancing delamination.

Soft metals have been used for wear resistance previously by others[69-79]. Some of these investigators assume that the soft metal layer melts during sliding and acts as a lubricant. This explanation can only be correct when the sliding speeds and the normal loads are high enough to cause a large flash temperature at the contact. The present work has shown that even nickel can be effective in wear reduction under low speed sliding wear and that the thickness of the plate has a pronounced influence. These findings are contradictory to the previous assumptions on the mechanism of wear reduction of soft metal layers. It was shown in this chapter that it is not the absolute softness which is important; it is the relative hardness between the substrate and the coating which is the determining factor.

The experimental results presented in this chapter are not direct and explicit proof of the assumed dislocation instability caused by the image force, but they are in accordance with the original predictions made by the delamination theory of wear. It appears however, that the original postulates predicting the effects of thickness and hardness of the metallic coatings are justified by this indirect evidence. However, other explanations may be given for the low wear rates observed with these coatings.

The central questions are why the thin layer retards delamination and why it does not delaminate itself while the thicker layer does. It was shown in Chapter III that the normal tensile stress component perpendicular to the surface over which an asperity has just passed is a maximum at a finite depth below the surface. This depth of maximum tensile stress may be responsible for subsurface crack propagation and final delamination. Therefore, it can be argued that delamination cannot occur within thin layers if the layer's thickness is smaller than the depth of the maximum tensile stress. When the thickness of the plate is increased and/or maximum tensile stress is developed in the plate, the plate will delaminate. Secondly, since the plated layer reduces the frictional force, the substrate experiences a lower maximum tensile stress and less plastic deformation. Consequently, the substrate delamination is retarded and large reduction in wear is possible. The difficulty with the alternate explanation is that it cannot explain how a thin surface coating undergoes such a large plastic deformation without work

hardening, as evidenced by the low coefficient of friction which does not change during testing. Sub-grain formation and annihilation of dislocations are plausible explanations, but then the question is "why doesn't a similar phenomenon occur at the sub-surface?" Therefore, we have to come back to the postulate that there is a unique phenomenon which occurs at the surface. We think this may be associated with dislocation instability at the surface.

VIII 8) Conclusions

1. The delamination theory of wear provides the theoretical basis for reducing wear through the development of a coated metal surface.
2. For major wear reduction the coating material must be softer than the substrate material.
3. There exists an optimum thickness of soft coating for wear resistance. This thickness is in general less than 1 μm for steel plated with Cd, Ag, Au, or Ni.
4. Cd, Ag and Ni plates are effective only in inert atmosphere, but Au was effective in air or in inert atmosphere.
5. The surface roughness of the substrate and the coating/substrate bond strength are two important factors for wear reductions by a composite metal surface.

Chapter IX

SUMMARY AND CONCLUSIONS

The purpose of the MIT Wear Research Program is to control friction and wear of materials through proper design of sliding surfaces and proper selection of materials. We are approaching this goal by first analysing the friction and wear behavior of materials in terms of both mechanical and microstructural aspects, and secondly by applying the understanding to the design of sliding surfaces.

The hypotheses of the delamination theory have been examined and experimentally justified. Predictions based on these hypotheses have been used to reduce wear by many orders of magnitude. Advances have been made in understanding the mechanics of surface deformation and the effect of microstructure on the wear behavior. It has been shown that the material below the surface experiences a tension-compression cyclic state of loading, and the magnitude and the position of the maximum tension perpendicular to the surface is related to the friction coefficient and the normal load. It was indicated that a relationship between friction coefficient and wear rate could be formulated if subsurface crack propagation occurs at the position of maximum tensile stress perpendicular to the surface. Wear and friction coefficients were also shown to be related through consideration of energy conservation. Even though this analysis is very approximate, the theoretical predictions are surprisingly close to the experimental results. These types of energy and mechanics of delamination analyses will be refined during the next phase of this project since they are necessary for an understanding of wear behavior.

Studies have been carried out on microstructural effects in sliding wear, concentrating on separating and understanding the effects of hardness and hard-particle crack nucleation sites. The results substantiated the predictions of the delamination theory that the wear rate is controlled by both the hardness and the number of void nucleation and crack propagation sites. It was shown that the wear rate is decreased by increasing the hardness and decreasing the number of void nucleation and crack propagation sites.

Preliminary investigations in other modes of wear showed that the delamination process may occur under any condition where both normal and tangential forces exist at the contact. Evidence of delamination was found in fretting, abrasive and erosive wear. Indications were that the early stages of fretting wear are controlled by delamination. It was proposed that the measures which can be taken to reduce sliding wear can also be used to reduce fretting and catastrophic failure by fretting fatigue.

Studies on the effect of surface roughness on wear indicated that the original surface roughness of machined parts controls the initial wear behavior and not the steady state delamination wear rate. The influence of surface roughness on wear was shown to depend on the normal load. Under low contact loads, the delamination of rough surfaces was delayed, which resulted in low wear of rough surfaces as compared to smoother ones. However, at higher contact loads, all surfaces delaminated at the beginning of sliding and the wear of rough surfaces was larger than smooth ones because of the larger volume of the original machining asperities of rough surfaces. It was shown that the quality and the degree of subsurface damage has detrimental effects on the initial wear rate. This preliminary result indicates a strong need for quality control measures for surfaces machined for sliding applications.

The delamination theory of wear was used to develop wear resistant metallic surfaces by application of a thin soft metallic plate. The wear rate of the combination can be reduced by three orders of magnitude if the coating is softer than the substrate, has an optimum thickness ($\approx$0.1um), and is bonded strongly to the substrate. This phenomenon was demonstrated experimentally for cadmium, silver, gold and nickel plated steel specimens.

Based on the investigations reported here, the following conclusions may be made in regard to wear reduction:

1) Wear rate can be decreased by increasing the hardness and decreasing the inclusion and second-phase particle density.
2) Wear of surfaces sliding under low contact loads can be decreased by preparing rough surfaces which do not have any subsurface damage.
3) The wear rate can be decreased by plating a softer metal on a harder substrate.

4) In order to insure that these procedures or other similar ones are effective in wear reduction, surface quality control methods must be devised.

In regard to further investigation, the following courses of action are recommended:

1) Further investigation of the mechanics of crack nucleation and propagation in order to be able to predict and control these processes.
2) Extension of the delamination theory to high speed sliding wear, wear of lubricated surfaces, and other types of wear.
3) Application of the already developed wear reduction methods to practical situations.
4) Development of manufacturing and quality control criteria for the production of low-wear surfaces.
5) Investigation on the possible interaction between lubricants and worn surfaces and the influence of this interaction on wear.

REFERENCES

1. H.P. Jost, "Economic Impact of Tribology," Mechanical Engineering, 97 (1975), 26-33.

2. N.P. Suh, S. Jahanmir and E.P. Abrahamson, "The Delamination Theory of Wear," Progress Report to ARPA, Contract No. N00014-67-A-0204-0080, Sept. 1974.

3. N.P. Suh, "The Delamination Theory of Wear," Wear, 25 (1973), 111-124.

4. J.F. Archard, "Contact and Rubbing of Flat Surfaces," J. Appl. Phys., 24 (1953), 981-993.

5. A.P. Green, "Friction Between Unlubricated Metals: A Theoretical Analysis of the Junction Model," Proc. Roy. Soc. (London), A 228 (1955), 191-204.

6. E. Rabinowicz, "Influence of Surface Energy on Friction and Wear Phenomenon," J. Appl. Phys., 32 (1961), 1440-1444.

7. F.P. Bowden and D. Tabor, Friction and Lubrication of Solids, Clarendon Press, Oxford, 1954.

8. H. Koba and N.H. Cook, "Wear Particle Formation Mechanisms," Progress Report to ONR, Contract No. N00014-67-A-0204-0054, May 1974.

9. J.A. Kirk and T.D. Swanson, "Subsurface Effects During Sliding Wear," Wear, 35 (1975), 63-67.

10. K.B. Savitskii, cited in V,I, Kragelskii, Friction and Wear, Butterworth, Washington, 1965.

11. J.T. Fourie, "Plastic Deformation of Thin Copper Single Crystals," Canadian J. Phys., 45 (1967), 777-786.

12. D.J. Whitehouse, "Some Ultimate Limits on the Measurement of Surface Using Stylus Techniques," Proc. Int. Corf. on Prod. Eng., Tokyo, Part II (1974), 39-44.

13. S. Jahanmir, N.P. Suh and E.P. Abrahamson, "The Delamination Theory of Wear and Wear of a Composite Metal Surface," Wear, 32 (1975), 33-49.

14. S. Jahanmir, E.P. Abrahamson and N.P. Suh, "Wear Resistance of Thin Metallic Coatings," Wear, (1976), Submitted for publication.

15. D.H. Buckley, "Effect of Various Material Properties on the Adhesive Stage of Fretting," Proc 39th Meeting of the Structures and Materials Panel, NATO Report, AGARD-CP-161 (1974), 13.1-13.15.

16. A.P. Green, "The Plastic Yielding of Metal Junctions Due to Combined Shear and Pressure," J. Mech. Phys. Solids, 2 (1954), 197-211.

17. P.K. Gupta and N.H. Cook, "Junction Deformation Model for Asperities in Sliding Interaction," Wear, 20 (1972), 73-87.

18. J. Fleming, "On the Mechanics of Delamination," S.M. Thesis, Department of Mechanical Engineering, MIT (In Progress), 1976.

19. K.J. Bathe, "ADINA-A Finite Element Program for Automatic Dynamic Incremental Nonlinear Analysis," Report No. 82448-1, Acoustics and Vibration Laboratory, Department of Mechanical Engineering, MIT, 1975.

20. G. Agustsson, "Strain Field Near the Surface Due to Surface Traction," S.M. Thesis, Department of Mechanical Engineering, MIT, 1974.

21. D.R. Wheeler and D.H. Buckley, "Texturing in Metals as a Result of Sliding," Wear, 33 (1975), 65-74.

22. V.D. Scott and H. Wilman, "Surface Re-Orientation Caused on Metals Caused by Abrasion - Its Nature, Origin and Relation to Friction and Wear," Proc. Roy. Soc. (London) A247 (1958), 353-368.

23. J. Goddard, H.J. Harker, and H. Wilman, "The Surface Re-Orientation Caused by Unidirectional Abrasion on FCC Metals," Proc. Phys. Soc., 80 (1962), 771-782.

24. W.J. Huppman and M.A. Clogg, "The Tribological Behavior of Polycrystalline Cobalt and Relation to Crystallographic Texture and Structure," Presented at ASLE-ASME, Int. Lub, Conf., New York, Oct. 1972.

25. N.P. Suh, S. Jahanmir, E.P. Abrahamson and A.P.L. Turner, "Further Investigation on the Delamination Theory of Wear," J. Lub. Tech., Trans. ASME, 96 (1974), 631-637.

26. S. Jahanmir, N.P. Suh and E.P. Abrahamson, "Microscopic Observation of the Wear Sheet Formation by Delamination," Wear, 28 (1974), 235-249.

27. A.R. Rosenfield, "Criteria for Ductile Fracture of Two Phase Alloys," Met. Rev., 13 (1968), 29-42.

28 A.S. Argon, J. Im and R. Safoglu, "Cavity Formation from Inclusions in Ductile Fracture," Met. Trans. 6A(1975), 825-837.

29. A.S. Argon and J. Im, "Separation of Second Phase Particles in Spheroidized 1045 steel, Cu-0.6 Pct. Cr Alloy, and Maraging Steel in Plastic Straining," Met. Trans., 6A (1975), 839-851.

30. M.F. Ashby, "Work Hardening of Dispersion-Hardened Crystals," Phil. Mag., 14 (1966), 1157-1178.

31. N.P. Suh, "Microstructural Effects in Sliding Wear of Metals," Proc. Battelle Materials Science Colloquium, Fundamental Aspects of Structural Alloy Design to be published, Plenum Press, 1976.

32. E. Rabinowicz, "Friction, Wear and Lubrication," Center for Advanced Engineering Study, MIT, (1974).

33. N.P. Suh, S. Jahanmir, D.A. Colling and E.P. Abrahamson, "The Delamination Theory for Wear of Metals Sliding at Low Speeds," Proc. 2nd North American Metal Working Research Conf., (1974), 117-127.

34. E.P. Abrahamson, S. Jahanmir, N.P. Suh and D.A. Colling, "Application of the Delamination Theory of Wear to a Composite Metal Surface," Proc. Int. Conf. on Production, Tokyo, Japan (1974), 408-413.

35. E.P. Abrahamson, S. Jahanmir, D.A. Colling and N.P. Suh, "Failure by Delamination During Wear," Proc. Scanning Electron Microscopy Conf. Part IV (1974), 889-894.

36. J.H. Dautzenberg and J.H. Zaat, "Quantitative Determination of Deformation by Sliding Wear," Wear, 23 (1973), 9-20.

37. J.E. Merwin and K.L. Johnson, "An Analysis of Plastic Deformation in Rolling Contact," Proc. Instn. Mech. Engrs., 177 (1973), 676-690.

38. B.I. Sandor, Fundamentals of Cyclic Stress and Strain, The University of Wisconsin Press, (1972).

39. M.C. Shaw and G.J. DeSalvo, "A New Approach to Plasticity and its Application to Blunt Two Dimensional Indenters," J. Eng. Industry, Trans. ASME, 92 (1970), 469-495.

40. J. Morrow, "Low Cycle Fatigue Behavior of Quenched and Tempered SAE 1045 Steel," Report No. 277, Department of Theoretical and Applied Mechanics, University of Illinois, Urbana, Ill., April (1965).

41. R. Fleisher, "Substitutional Solution Hardening," Acta Met., 11 (1963) 203-209.

42. R. Fleisher, "Solution Hardening," Acta Met., 9 (1961), 996-1000.

43. B.I. Edelson and W.M. Baldwin, Jr., "The Effect of Second Phases on the Mechanical Properties of Alloys," Trans. ASM, 55 (1962), 230-250.

44. C.T. Liu and J. Gurland, "The Fracture Behavior of Spheroidized Carbon Steels," Trans. ASM, 61 (1968)156-167.

45. D.C. Lemmon and O.D. Sherby, "Effect of Microstructure on the Ductility of Steel in Torsion," J. Materials, 4 (1969) 444-456.

46. A.R. Rosenfield, G.T. Hahn and J.D. Embury, "Fracture of Steels Containing Pearlite," Met. Trans., 3 (1972) 2797-2804.

47. P.W. Bridgman, Studies in Large Plastic Flow and Fracture, Harvard Press, Cambridge, Mass., 1964.

48. T.J. Walker and M.C. Shaw, "On Deformation at Large Strains," in Advances in Machine Tool Design and Research, (1969) 241-252.

49. A.R. Austen and B. Avitzur, "Influence of Hydrostatic Pressure on Void Formation at Hard Particles," J. Eng. for Ind., Trans. ASME, 96 (1974) 1192-1196.

50. R.B. Waterhouse and D.E. Taylor, "Fretting Debris and the Delamination Theory of Wear," Wear, 29 (1974) 337-344.

51. R.B. Waterhouse, "Physics and Metallurgy of Fretting," Proc. 39th Meeting of the Structures and Materials Panel, NATO Report, AGARD-CP-161 (1974) 8.1-8.8.

52. I.F. Stowers, "The Mechanism of Fretting Wear," Ph.D. Thesis, Department of Mechanical Engineering, MIT (1974).

53. N. Ohmae, T. Nakai and T. Tsukizoe, "Prevention of Fretting by Ion Plated Film," Wear, 30 (1974) 299-309.

54. H.P. Van Loeuwen, "Discussion on Suh's Delamination Theory of Fretting Wear and the Possible Role of Hydrogen," Proc 39th Meeting of the Structures and Materials Panel, NATO Report, AGARD-CP-161 (1974) 13.19.

55. I. Finnie, "The Mechanism of Erosion of Ductile Materials," Proc. 3rd. U.S. Nat. Cong. Appl. Mech., (1958) 527-538.

56. J. G.A. Bitter, "A Study of Erosion Phenomena, Parts I and II," Wear, 6 (1963) 5-21, 169-190.

57. C.J. Sherman, "Wear of Metallic Surfaces By Particle Impingement," S.M. Thesis, Department of Mechanical Engineering, MIT (1971).

58. M.D. Speidel and G. Keser," Resistance to Rain Erosion, Stress Corosion Cracking, and Corosion Fatigue in a 12% Chromium Steel," Presented at 4th International Conference on Rain Erosion and Associated Phenomena, Meersburg, Germany (1974).

59. T. Sasada, H. Ohmura and S. Nororse, "The Wear and Mutual Transfer in Cu/Fe Rubbing," Proc. 15th Japan Cong. on Mat. Research, (1972) 1-6.

60. T. Sasada, S. Nororse and K. Sugimoto, "The Mutual Metalic Transfer at Friction Surfaces in Lubricating Oil," Proc. 17th Japan Cong. on Mat. Research, (1974) 32-35.

61. C.A. Queener, T.C. Smith and W.L. Mitchel, "Transient Wear of Machine Parts," Wear, 8 (1965) 391-400.

62. D. Landheer and J.H. Zaat, "The Mechanism of Metal Transfer in Sliding Friction," Wear, 27 (1974) 129-145.

63. E.P. Abrahamson, S. Jahanmir and N.P. Suh, "The Effect of Surface Finish on the Wear of Sliding Surfaces," CIRP Annals, 24 (1975) 513-514.

64. N.H. Cook, Manufacturing Analysis, Addison-Wesley, Reading, Mass. (1966).

65. R. Rajasekariah and S. Vaidynathan, "Increasing the Wear Resistance of Steel Components by Ball Burnishing," Wear, 34 (1975) 183-188.

66. D.M. Turley, "Deformed Layers Produced by Machining 70/30 Brass," J. of the Inst. of Metals, 96 (1968) 82-86.

67. D.M. Turley, "Dislocation Substructures and Strain Distributions Beneath Machined Surfaces of 70/30 Brass," J. of the Inst. of Metals, 99 (1971) 271-276.

68. Y. Tsuya and R. Takagi, "Lubricating Properties of Lead Films on Copper," Wear, 7 (1964) 131-143.

69. R. Takagi and T. Liu, "The Lubrication of Steel by Electroplated Gold," ASLE Trans., 10 (1967) 115-123.

70. R. Takagi and T. Liu, "Lubrication of Bearing Steels With Electroplated Gold Under Heavy Loads," ASLE Trans., 11 (1968) 64-71.

71. A.J. Solomon and M. Antler, "Wear Mechanisms of Gold Electrodeposits," Plating, Aug (1970) 812-816.

72. T.J. Kuczkowski and D.H. Buckley, "Friction and Wear of Low Melting Binary and Ternary Gallium Alloy Films in Argon and in Vacuum," NASA TN D-2721 (1965).

73. H.E. Evans and T.W. Flatley, "Bearings for vacuum Operations, Retainer Material and Design," NASA TN D-1339 (1962).

74. H.E. Evans and T.W. Flatley, "High Speed Vacuum Performance of Gold Plated Miniature Ball Bearings with Various Retainer Materials and Configurations," NASA TN D-2101 (1963).

75. T.W. Flatley, "High Speed Vacuum Performance of Miniature Ball Bearings Lubricated with Combination of Barium, Gold and Silver Films," NASA TN D-2304 (1964).

76. P.E. Brown, "Bearing Retainer Material for Modern Jet Engines," ASLE Trans., 13 (1970) 225-239.

77. T.L. Ridings, "Operational Evaluation of Dry Thin Film Lubricated Bearings and Gears for Use in Aerospace Environmental Chambers," AEDC-TR-65-1 (1965).

78. R.D. Lee, Jr., "Lubrication of Heavily Loaded, Low Velocity Bearings and Gears Operating in Aerospace Environmental Facilities," AEDC-TR-65-19 (1965).

79. E. Rabinowicz, "Variation of Friction and Wear of Solid Lubricant Films with the Film Thickness," ASLE Trans., 10 (1967) 1-9.

80. W.H. Safranck, The Properties of Electrodeposited Metals and Alloys, Elsevier, New York (1974).

81. K.E. Easterling, H.F. Fishmeister and E. Navara, "The Particle to Matrix Bond in Dispersion Hardened Austenitic and Ferritic Iron Alloys," Powder Met., 16 (1973) 128-145.

82. M.F. Ashby, "Work Hardening of Dispersion-Hardened Crystals," Phil. Mag., 14 (1966) 1157-1178.

83. J. Gurland, "The Fracture Strength of Sintered Tungsten Carbide-Cobalt Alloys in Relation to Composition and Particle Spacing," Trans. Met. Soc. AIME, 227 (1963) 1146-1150.

84. B.A. Wilcox and A.H. Clauer, "Creep of Thoriated Nickel Above and Below 0.5 T_m," Trans. Met. Soc. AIME, 236 (1966)570-580.

85. A.M. Turkalo and J.R. Low, Jr., "The Effect of Carbide Dispersion on the Strength of Tempered Martensite," Trans.Met . Soc. AIME, 212 (1958) 750-758.

86. F.A. McClintock, "On the Mechanics of Fracture From Inclusions," in Ductility, American Society of Metals, (1968) 255-277.

87. S.P. Timoshenko and J.N. Goddier, Theory of Elasticity, 3rd ed., McGraw-Hill, 1970.

Appendix A

THE FINITE ELEMENT METHOD

A 1) Introduction

The finite element method is a procedure for numerical solution of partial differential equations, such as those that arise in continuum mechanics. The basic formulation of the finite element method has been known for over fifty years[1]*; however, application of the method was not practical for complex problems until the development of high-speed digital computers. The advantages of finite element over finite difference methods (at least for elliptic partial differential equations) include the ease of handling complicated boundary conditions and the relative ease of writing generalized programs to solve any well-posed problem.

This appendix consists of three sections. First is a derivation of the basic equations of the displacement based finite element method in elasticity. Second is a discussion of how nonlinearities such as plasticity are included. The final section discusses the particular program and models being used in the ongoing analysis of the wear process.

A 2) Derivation of the Finite Element Method

The equations of the finite element method may be derived in several ways. The most elegant, physically meaningful, and theoretically useful derivation is obtained by applying the principles of variational calculus[2]. Since the variational calculus method is long and complicated, the following derivation follows the simpler weighted residual method for a displacement based two dimensional elasticity problem to arrive at the same result.

Consider an arbitrarily shaped two-dimensional elastic body. On some region or regions of the boundary, S_f, the applied force $\underline{F}$ is proscribed. On the remainder of the boundary, S_u, the displacement $\underline{U}$ is prescribed. The equations of elasticity may be nondimensionalized into Poisson's equation in the displacement $\underline{\phi}$ and the body force $\underline{\rho}$:

$$\nabla^2 \phi - \rho = 0 \qquad \phi = U \text{ on } S_u$$

$$\frac{\partial \phi}{\partial n} = -F \text{ on } S_f \; . \qquad \text{(A.1)}$$

---

* The numbers in parenthesis designate the references at the end of this appendix.

Then let ϕ_a be some approximate solution which satisfies the displacement boundary condition $\phi_a = U$ on S_u. In general, ϕ_a will not satisfy the differential equation or the force boundary condition at all points. Let the total error E_t be defined as the sum of the integrals of the error at each point times some arbitrary weighting function w:

$$E_t \equiv \int_A (\nabla^2 \phi_a - \rho)\, w dA + \int_{S_f} \left(- \frac{\partial \phi_a}{\partial n} - F \right) w dS. \tag{A.2}$$

Note that there are many equally "good" ways to define E_t; this particular choice is taken to obtain the same final result as the variational formulation.

To obtain a more convenient form, apply Gauss's theorem to the first of the integrals in Eq. A.2 to yield:

$$\int_A (\nabla^2 \phi_a - \rho)\, w dA = \int_{S_f + S_u} \frac{\partial \phi_a}{\partial n} w dS - \int_A \left(\frac{\partial \phi_a}{\partial x} \frac{\partial w}{\partial x} + \frac{\partial \phi_a}{\partial y} \frac{\partial w}{\partial y} \right) dA - \int_A \rho w dA \,. \tag{A.3}$$

Since w is still arbitrary, and by definition ϕ_a satisfies the boundary condition on S_u, let $w = 0$ on S_u. Substituting into Eq. A.2,

$$E_t = - \int_A \left(\frac{\partial \phi_a}{\partial x} \frac{\partial w}{\partial x} + \frac{\partial \phi_a}{\partial y} \frac{\partial w}{\partial y} \right) dA - \int_A \rho w dA - \int_{S_f} F w dS \,. \tag{A.4}$$

It would be extremely difficult to find a function ϕ_a which reasonably satisfies the differential equation and boundary conditions over the whole body. However, we may reasonably try to approximate ϕ in small areas first, and then "paste together" the approximations to obtain a good overall approximation.

Consider the body broken up into small "finite" elements, generally triangles and quadrilaterals. Then, within the n^{th} element, ϕ is approximated by ϕ_{an}. Any portion of S_f that coincides with the boundary of the element is denoted by S_{fn}. Then

$$E_t = \sum_{n=1}^{N} E_n \,,$$

$$E_n \equiv - \int_{A_n} \left(\frac{\partial \phi_{an}}{\partial x} \frac{\partial w_n}{\partial x} + \frac{\partial \phi_{an}}{\partial y} \frac{\partial w_n}{\partial y} \right) dA - \int_{A_n} \rho w_n dA - \int_{S_{fn}} F w_n dS \,. \tag{A.5}$$

Now the approximating functions ϕ_{an} and the weighting functions w_n must

be defined. Consider the three to eight node isoparametric quadrilateral element illustrated in Figure A.1. Assume that the value of ϕ_{an} at node i is denoted by ϕ_i. Then assume that ϕ_{an} at any point in the element is given by a linear combination of ϕ_i:

$$\phi_{an}(x,y) = \sum_{i=1}^{8} h_i \phi_i \quad . \tag{A.6}$$

The functions h_i are called interpolation functions or shape functions since their order and type determine the way in which displacement may vary within the element. For the element of Fig. A.1, the h_i are polynomials of order one or two. This assumption, together with the fact that $h_i = 1$ at node i and $h_i = 0$ at all other nodes, determines the interpolation functions completely. To actually evaluate the interpolation functions, the element is mapped onto the "natural" (r,s) plane as shown in Figure A.2.

This type of element is called isoparametric because the interpolation functions and the mapping functions are of the same type and order; indeed, the mapping functions are inverses of the interpolation functions, i.e.

$$x = \sum_{i=1}^{8} h_i(r,s) x_i$$

$$y = \sum_{i=1}^{8} h_i(r,s) y_i \quad . \tag{A.7}$$

We have a form for ϕ_{an} in Eq. A.6, but the weighting functions must still be chosen. Since there are as many unknowns (ϕ_i) as there are nodes, we may choose as many weighting functions as there are nodes. From experience and certain theoretical considerations, choose $w_i = h_i$

Now if we define

$$K_{ij}^{n} = \int_{A_n} \left(\frac{\partial h_j}{\partial x} \frac{\partial h_i}{\partial x} + \frac{\partial h_j}{\partial y} \frac{\partial h_i}{\partial y} \right) dA \quad , \tag{A.8}$$

then, using Eq. A.6

$$\int_{A_n} \left(\frac{\partial \phi_{an}}{\partial x} \frac{\partial w_n}{\partial x} + \frac{\partial \phi_{an}}{\partial y} \frac{\partial w_n}{\partial y} \right) dA = \sum_{j=1}^{8} K_{ij}^{n} \phi_j \quad , \tag{A.9}$$

where K_{ij}^{n} depends only on the element geometry and material properties. Physically, K_{ij}^{n} is the force at node i per unit displacement at node j. The eight by eight symmetric matrix $[K]^n$ made up from K_{ij}^{n} is called the element stiffness matrix.

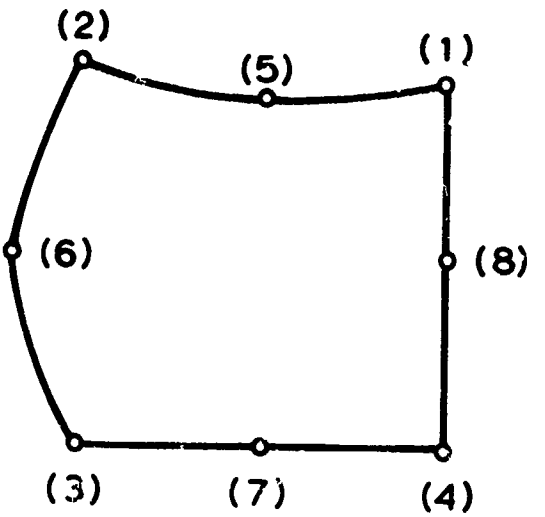

(1) = Local Node Number
(Adina Convention)

Figure A.1

Three to eight node isoparametric quadrilateral finite element.

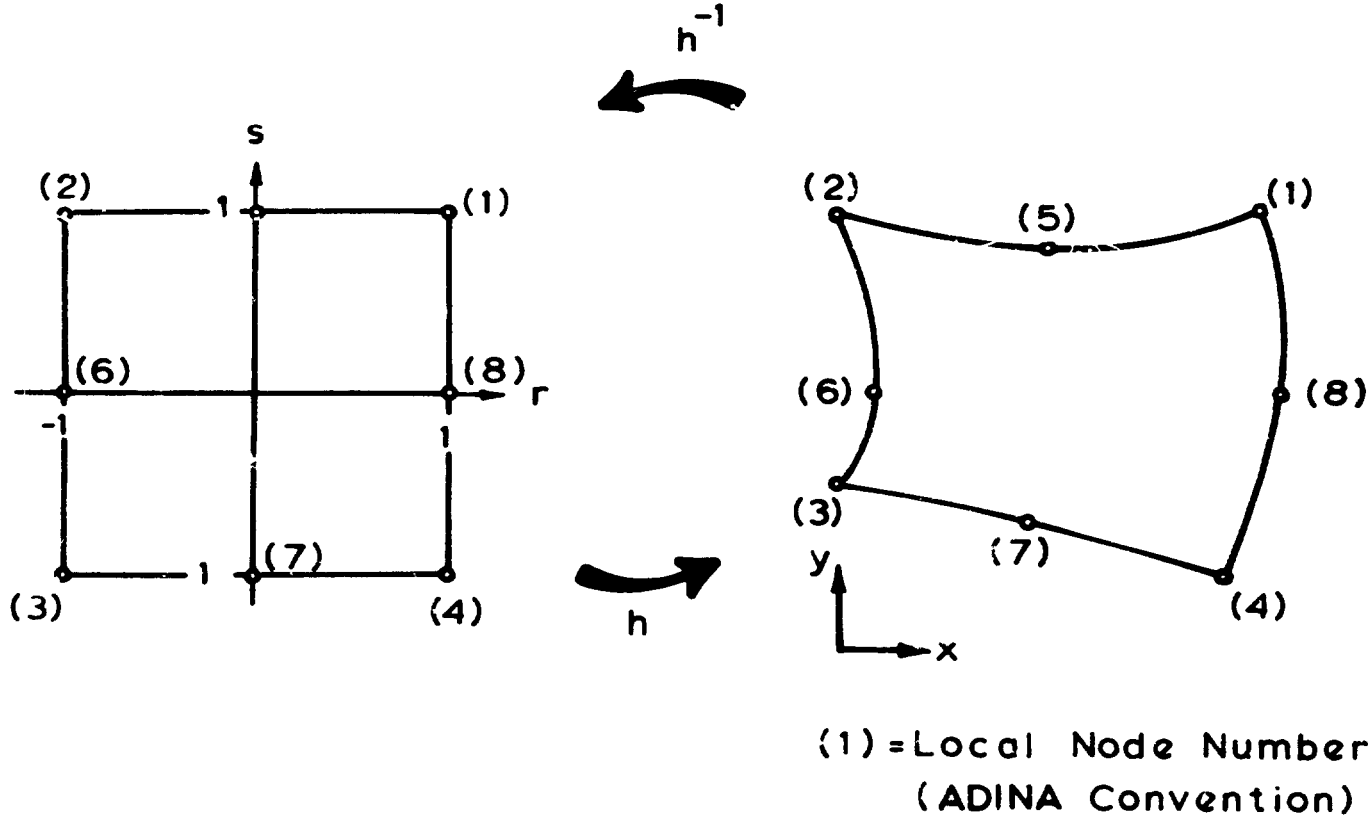

Figure A.2

Mapping between (x, y) plane and (r, s) plane.

		TERMS TO INCLUDE ONLY IF NODE i IS DEFINED		
	i = 5	i = 6	i = 7	i = 8
$h_1 = \frac{1}{4}(1+r)(1+s)$	$-\frac{1}{4}(1-r^2)(1+s)$			$-\frac{1}{4}(1-s^2)(1+r)$
$h_2 = \frac{1}{4}(1-r)(1+s)$	$-\frac{1}{4}(1-r^2)(1+s)$	$-\frac{1}{4}(1-s^2)(1-r)$		
$h_3 = \frac{1}{4}(1-r)(1-s)$		$-\frac{1}{4}(1-s^2)(1-r)$	$-\frac{1}{4}(1-r^2)(1-s)$	
$h_4 = \frac{1}{4}(1+r)(1-s)$			$-\frac{1}{4}(1-r^2)(1-s)$	$-\frac{1}{4}(1-s^2)(1+r)$
$h_5 = 0$	$+\frac{1}{2}(1-r^2)(1+s)$			
$h_6 = 0$		$+\frac{1}{2}(1-s^2)(1-r)$		
$h_7 = 0$			$+\frac{1}{2}(1-r^2)(1-s)$	
$h_8 = 0$				$+\frac{1}{2}(1-s^2)(1+r)$

TABLE A.1 Interpolation Functions for Three to Eight Node Isoparametric Quadrilateral Element

Defining

$$\int_{A_n} \rho h_i \, dA_n \equiv F_{bi} \, ,$$

$$- \int_{S_{fn}} F h_i \, ds \equiv F_{si} \, , \qquad \text{(A.10)}$$

the consistent element nodal force vector $[F_b + F_s]^n$ may be assembled. Eqs. A.10 are merely a method for splitting up the forces into statically equivalent point forces at the nodes.

If we number each node in the total assemblage of elements with a unique global node number, and define the connectivity matrix $[C]$ such that C_{ij} = the global node number of local node j of element i, the global stiffness matrix $[K]$ and the global displacement and force vectors $[\Phi]$ and $[F_b + F_s]$ may be defined. Substituting into Eqs. A.5 results in a complete set of linear equations for the nodal displacements:

$$[K] [\Phi] = [F_b + F_s] \, . \qquad \text{(A.11)}$$

Here, K_{ij} is the force at global node j per unit displacement at global node i. $[K]$ is symmetric, positive definite, and banded ($K_{ij} = 0$ unless nodes i and j are in the same element). Φ_i is the displacement of global node i, and $F_{b_i} + F_{s_i}$ is the applied force at global node i.

After solving the system of equations given above, strains may be found by differentiating Eqs. A.6, and stresses found by using Hooke's law or any other appropriate stress-strain relationship.

A 3) Nonlinearities in the Finite Element Method

The preceding derivation covered a linear problem. Nonlinearities that may be introduced in static structural mechanics problems include plasticity and creep (material nonlinearity) and finite strain (geometrical nonlinearity). The methods of implementing these nonlinearities are many, and are too complicated to discuss in detail here. However, it may be said that all methods of handling nonlinearities reduce to linearizing the governing equations in some manner and carrying out the analysis in small time or load steps.

The process of linearization automatically introduces errors. In plasticity, the error is a failure to satisfy equilibrium. For any nonlinearity, the solution procedure must be iterated without any increase in load or time to reduce the error. The incremental nature of nonlinear analysis and the necessity of iterating for equilibrium or its analogue are the major factors in the expense of nonlinear analysis.

A 4) The Finite Element Program and Models Used in Studying Wear

The program used in the analyses has been ADINA, developed by Bathe[3]. The program is designed to carry out static or dynamic, linear or nonlinear (geometrically or materially) structural analyses. Thus far, only static linear and static materially nonlinear (elastic - plastic) analyses have been used in our study of wear. Two programs have been developed at the Materials Processing Laboratory: CNFCALC (Consistent Nodal Force CALCulator), which numerically integrates the second of Eqs. A.10 for any two-dimensional grid under any loading[4], and CALPLOT (CALcomp PLOTter), which produces the stress and displacement field plots shown elsewhere in this report.[5]

The models used here have been intended to investigate several processes of delamination wear: strain accumulation, crack nucleation and crack propagation. The crack nucleation studies have concentrated on calculating stress fields around inclusions. Since the boundary conditions for the loading of inclusions under asperities during plastic deformation are as yet unknown, these studies have been essentially preliminary, designed to verify other's results and to learn the use of the program.

The majority of the analyses have been intended to study possible mechanics of crack propagation, strain accumulation, and to calculate boundary conditions for use in studying crack nucleation. The problem considered has been that of an infinite half-plane two dimensional solid in plane strain, loaded by a stationary, rigid, straight sided asperity as shown in Figure A.3. The asperity is straight sided to avoid the necessity of considering an increase in the area of contact (geometric nonlinearity).

Since the finite element method deals only with finite bodies, the body analysed must be a cutout of the infinite half-plane. The grid of Fig. A.4 represents a cutout along the lines $\overline{AB}$, $\overline{BC}$, $\overline{CD}$ in Fig. A.3.

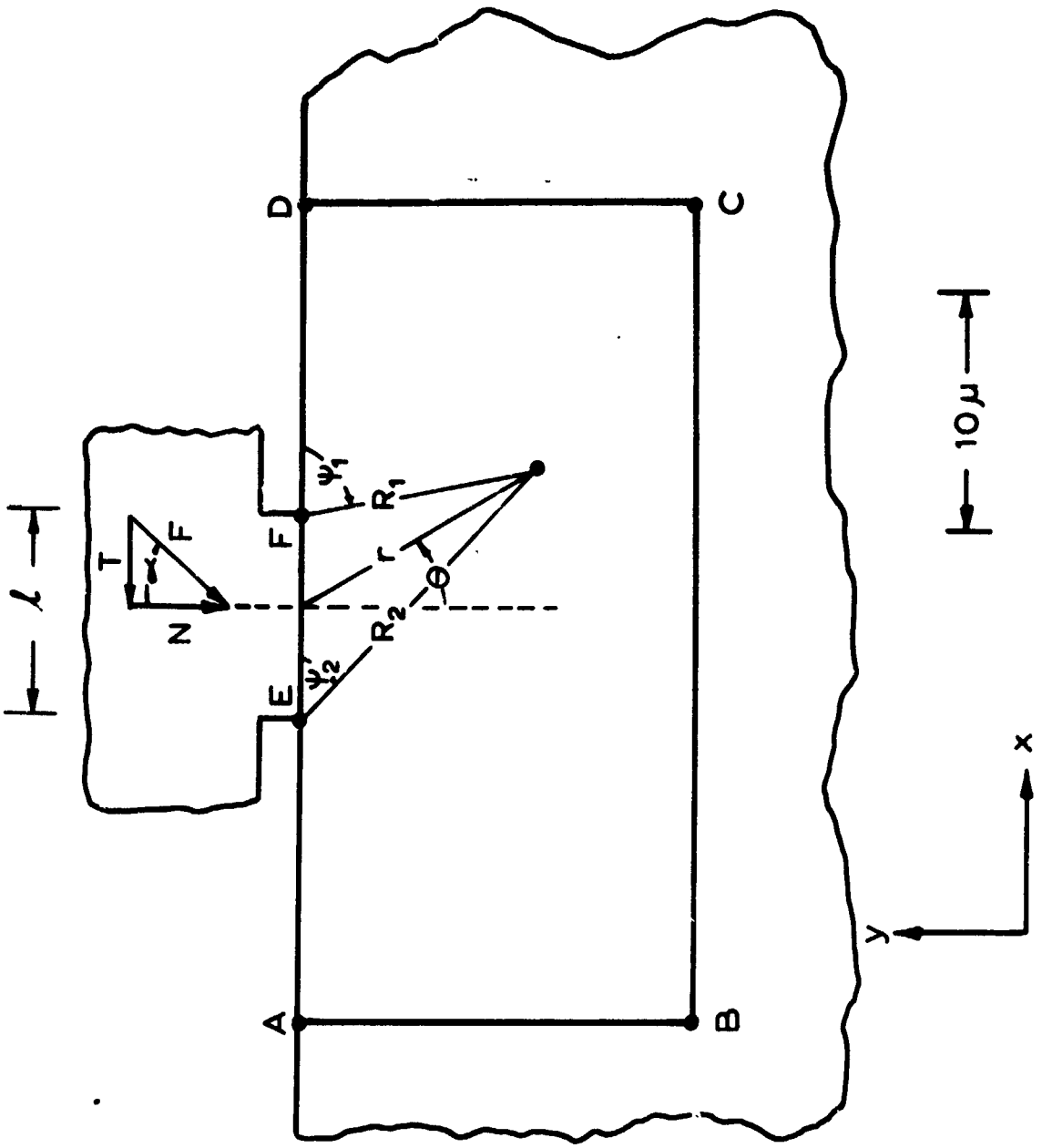

Figure A.3

The contact model used for subsurface stress and strain distribution by the finite element method.

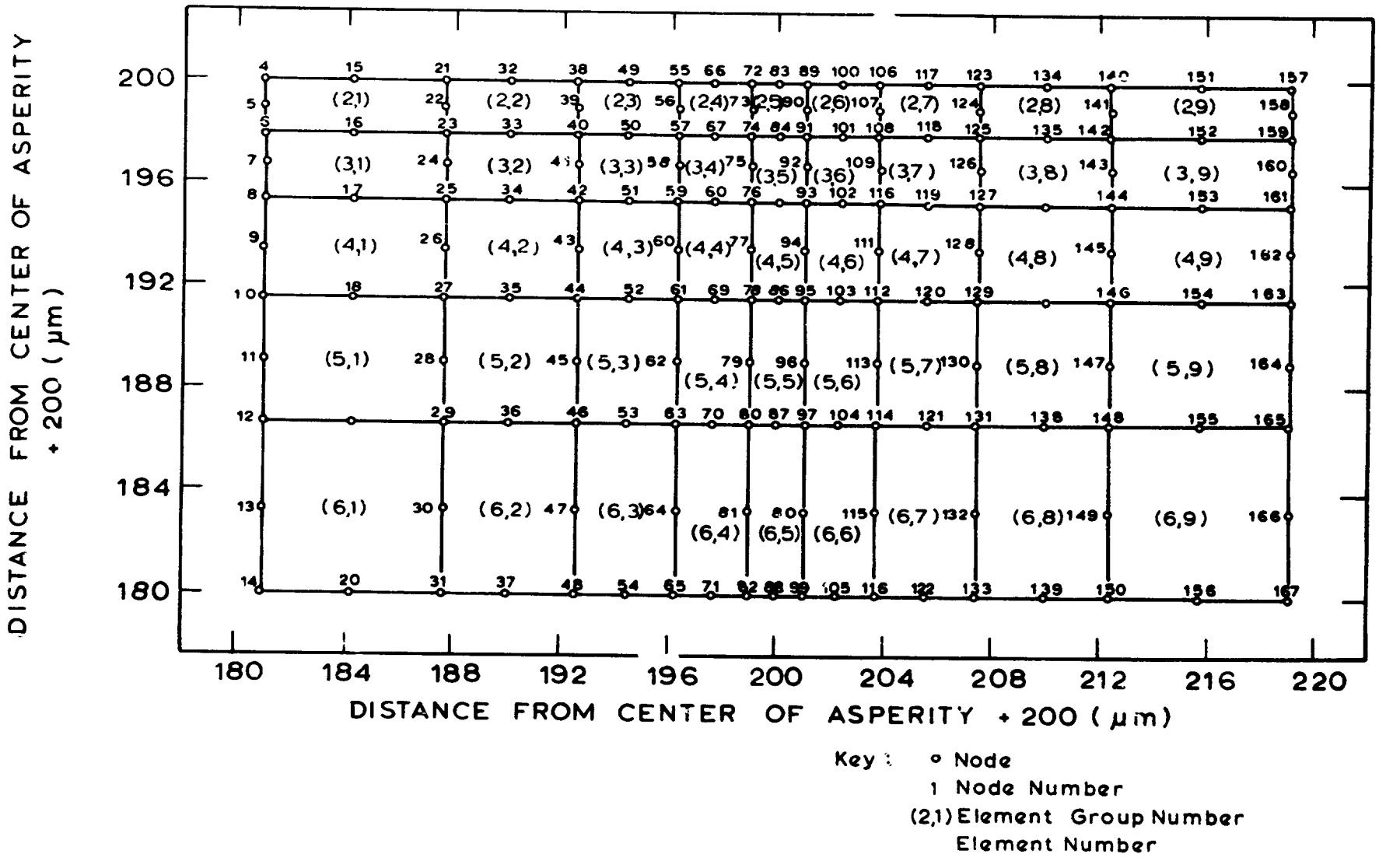

Figure A.4

Typical finite element grid: Cutout of an infinite half-plane (truss elements used to apply displacements omitted for clarity).

Since the asperity is considered rigid, the loading on the top surface consists of a step function of load from E to F in Fig. A.3. The loading along $\overline{AB}$, $\overline{BC}$, and $\overline{CD}$ in Fig. A.3 must be derived from an elastic stress solution (valid as long as the boundaries remain elastic). With the notation defined in Fig. A.3, the elastic solution is given by Green and Zerna[6] as:

$$\frac{\sigma_{xx} + \sigma_{yy}}{2} = \frac{2N}{\pi l}(\Psi_1 - \Psi_2) - \frac{2T}{\pi l}\ln\left(\frac{R_1}{R_2}\right)$$

$$\frac{\sigma_{xx} + \sigma_{yy}}{2} + i\sigma_{xy} = \frac{(T-iN)}{\pi l}\left[e^{2i\Psi_1} - e^{2i\Psi_2}\right] - \frac{2T}{\pi l}\left[\ln\left(\frac{R_1}{R_2}\right) + i(\Psi_2 - \Psi_1)\right] . \qquad (A.12)$$

This solution was substituted into Eqs. A.10, which were numerically integrated by CNFCALC, to obtain the force boundary conditions along the cutout.

For a plane problem, at least three non-colinear displacements must be specified in order to "pin down" rigid body translation and rotation. In view of the difficulty of integrating the strains derived from Eqs. A.12, an approximation was introduced. If the distance from the asperity is large enough that the asperity may be modeled by a line load (into the paper in Fig.A.3), the stress solution is given by Timoshenko and Goodier[7] in notation defined in Fig. A.4 as

$$\sigma_{rr} = -\frac{2F}{\pi r}\cos(\alpha + \theta)$$

$$\sigma_{\theta\theta} = \sigma_{r\theta} = 0 . \qquad (A.13)$$

Finding strains subject to the plane strain condition, and integrating the strain displacement equations subject to the boundary conditions $u_\theta = 0$ along the line $\theta = -\alpha$ and $u_r = 0$ at $\theta = -\alpha$ and $r = d$ (d being arbitrary: d was chosen as 100 microns) yields equations for displacements in terms of Poisson's ratio ν and Young's modulus E:

$$u_r = -\frac{2F}{E\pi}(1 - \upsilon^2)\cos(\alpha + \theta)\ln\left(\frac{d}{r}\right) + \frac{F}{E\pi}(2\upsilon^2 + \upsilon - 1)(\alpha + \theta)\sin(\alpha + \theta)$$

$$u_\theta = \frac{2F}{E\pi}(\upsilon + \upsilon^2)\sin(\alpha + \theta) + \frac{2F}{E\pi}(1 - \upsilon^2)\sin(\alpha + \theta)\ln\left(\frac{r}{d}\right) \qquad (A.14)$$
$$+ \frac{F}{E\pi}(2\upsilon^2 + \upsilon - 1)\left[(\alpha + \theta)\cos(\alpha + \theta) - \sin(\alpha + \theta)\right] .$$

Eqs. A.14 were used to specify displacements at points A and C in Fig. A.3.

The analysis of asperity loading has been carried out for a stationary asperity, taking the coefficient of friction μ as 1/2, 3/4, and 1. E was taken as 1195 $x10^{-5}$ $Kg/\mu m^2$, υ was 1/3, and the linear hardening plastic modulus (the slope of the plastic portion of the stress-strain curve) was 0.4.5 $x10^{-5}$ $Kg/\mu m^2$. This material corresponds to an elastic-almost perfectly plastic approximation of copper.

To date, the analysis has consisted of loading the model to investigate the plastic stress field and calculate boundary conditions for loading on an inclusion. The small tolerance (0.1%) used in iterating for equilibrium and the good agreement of the elastic parts of the stress field with Eqs. A.13 indicate good accuracy in the results.

Plans for future analysis include a study of the effect of inclusions, unloading of the model to study residual stress and strain distributions, and experimental development of a constitutive equation for cyclic softening in order to determine the effects of repeated asperity contact.

References

1. G.B. Maney, "Studies in Engineering No. 1," University of Minnesota, Minneapolis, Minn., 1915.

2. K.J. Bathe and E.L. Wilson, Numerical Methods in Finite Element Analysis, Prentice-Hall, In Press.

3. K.S. Bathe, "ADINA-A Finite Element Program for Automatic Dynamic Incremental Nonlinear Analysis," Report No. 82448-1, Acoustics and Vibration Laboratory, Department of Mechanical Engineering, MIT, 1975.

4. J. Fleming, "CALPLOT: A Plotting Routine for Tensors, Vectors, Symbols, and Surfaces," Research Memorandum 1, Materials Processing Laboratory, Department of Mechanical Engineering, MIT, 1975.

5. J. Fleming, "CNFCALC: A Consistent Nodal Force Calculator for 2-D Finite Elements," Research Memorandum 2, Materials Processing Laboratory, Department of Mechanical Engineering, MIT, 1975.

6. A.E. Green and W. Zerna, Theoretical Elasticity, 2nd ed., Oxford, Clarendon Press, 1968.

7. S.P. Timoshenko and J.N. Goodier, Theory of Elasticity, 3rd ed., McGraw-Hill, 1970.

Appendix B

PREPARATION OF COPPER-TIN SOLID SOLUTIONS

B 1) Introduction

Interest in the study of wear properties of FCC solid solutions arose from the fact that alloying in the solid solution range without introducing second phase particles as crack nucleation sites could increase the wear resistance of alloys. Clean solid solutions without inclusions or unwanted impurities were prepared by melting the alloys in dry and purified argon gas. Details of the equipment, alloy production and specimen preparation are described in this appendix.

B 2) Alloy Preparation

The induction unit which was used to melt the alloys had an output of 7.5 KW at a frequency of 900 kHz. The water cooled induction coil, 67 mm in diameter and 180 mm long, was made with 6 mm O.D. copper tubing. The main body of the furnace was a 64 mm O.D. vycor tube held in vertical position. Flanges at both ends of the tube provided a good seal and had the necessary vacuum and gas fittings (see Fig. B.1). Graphite was used both as susceptor and as mold.

Initially the system was evacuated by means of a mechanical pump with a capacity of 425 ℓ/min (free air displacement). The pressure in the chamber was measured with a thermocouple vacuum gauge. In the vaccum line there is a vaccum trap containing drierite (anhydrous calcium sulphate) to dehumidify the gas. There is also a bubbler system to indicate the gas flow.

Different amounts of copper and tin were melted in the graphite mold. The temperature in the mold was monitored by means of an optical pyrometer to an accuracy of $\pm$ 5°C. After reaching a temperature of 1200°C , about 100°C higher than the melting point of copper (1083°C), the temperature was maintained for an hour to allow good mixing of the two components of the alloy. The cooling was very slow until the solvus temperature was reached and then it was increased to avoid any precipitation.

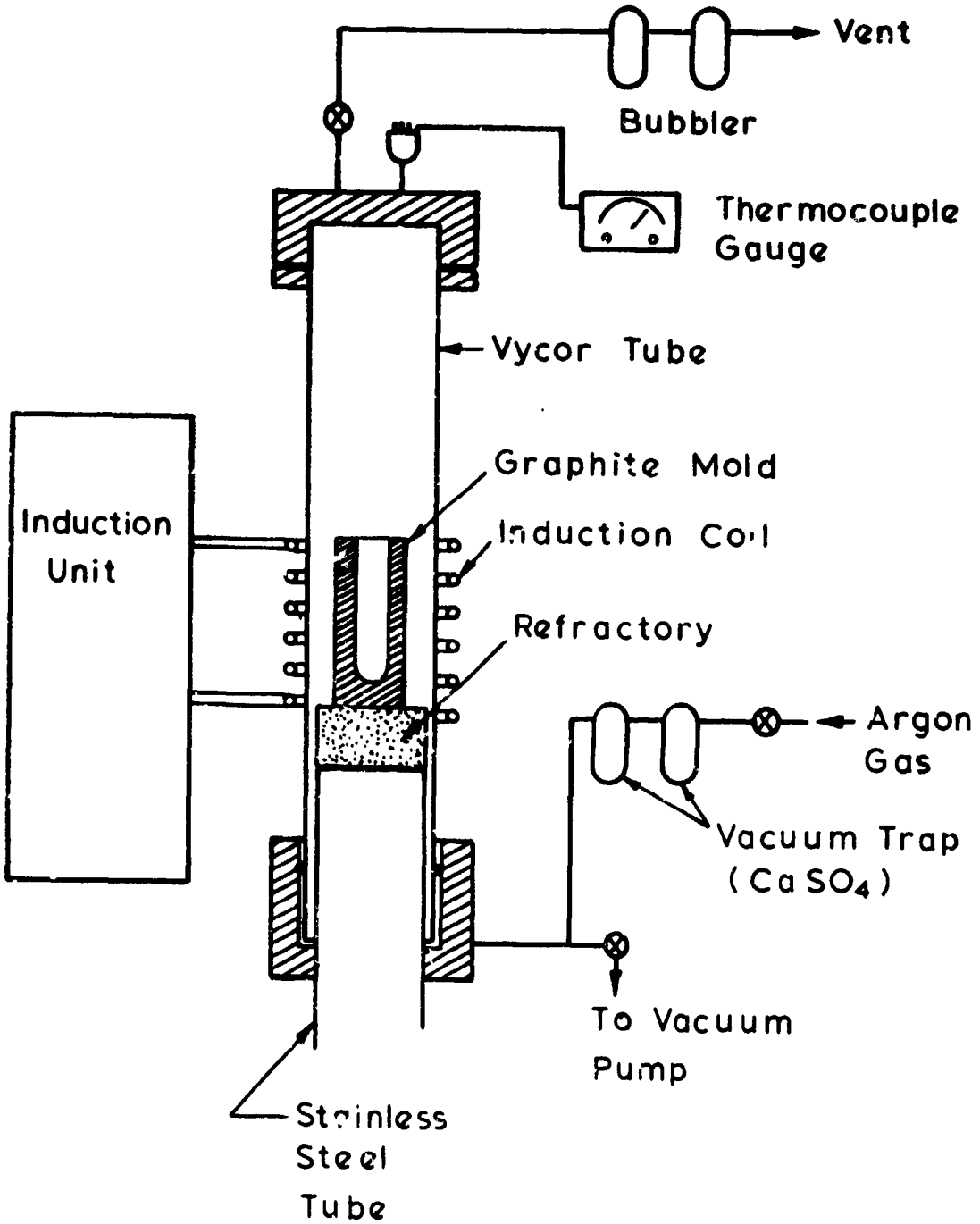

Figure B.1

Schematic of the vacuum melting equipment used for preparation of copper solid solutions.

B 3) Specimen Preparation

The cast rods which had a diameter of 17 mm were then encapsulated in vycor tubes under vacuum, and homogenized at 800°C for 50 hours. The temperature was controlled within ± 3°C. After homogenization, the rods were swaged down to a diameter of approximately 7 mm and then machined to a diameter of 6.3 mm in two passes at a spindle speed of 214 r.p.m. and feed of 0.06 mm with a sharp tool. The machined rods were vacuum sealed again and recrystallized. Details of this treatment are given in Table B.1. After recrystallization, the specimens were polished with No. 4/0 emery paper for wear tests.

B 4) Metallography

For measuring the grain size and other metallographic observations the specimens were sectioned and polished by the usual methods. The final polishing, however, was carried out in a vibratory polisher with a slurry of 0.05 μm alumina powder. The etchant used was potassium dichromate. Fig. B.2 shows the microstructure of Cu 1.5 at % Sn alloy. It is observed that the material does not contain any inclusions or second phase particles.

Table B.1 Copper-Tin Solid Solutions: Metallurgical Variables

Material	% of Cold Work in Reduction of Area	Recrystalization		Grain Size (μm)	Hardness ($Kg\ mm^{-2}$)
		Temp	Time		
OFHC Cu	83%	360°C	4 hr	18	31
Cu-1.4 at % Sn	57%	790°C	2 hr	35	42
Cu-3.4 at % Sn	57%	790°C	1 hr	40	54
Cu-5.7 at % Sn	57%	790°C	½ hr	25	70

Figure B.2

The microstructure of a Cu-1.5 at % Tin specimen.

Appendix C

INTERNAL OXIDATION OF Cu-Si AND Cu-Cr ALLOYS

C 1) Introduction

Oxide dispersion strengthened alloys are gaining recognition as high temperature creep resistant materials.[1]* Such unique properties of the oxide particles as insolubility, fineness, uniformity and stability to coarsening make these alloys very strong compared to their solid solution or precipitation hardened counterparts. High strength in these alloys is further achieved by thermomechanical treatments. Some alloys, such as Cu-BeO, are also used at room temperatures where both strength and electrical conductivity are important. The reasons for choosing these alloys for wear tests were already given in the text. The chief reason being to investigate the effect of the number of void nucleation sites on delamination wear.

A number of methods of producing oxide dispersoids in metallic matrices are available.[2] They include: internal oxidation, thermal decomposition, mechanical blending, co-precipitation etc. Almost all commercial alloys are produced chiefly by powder metallurgy methods. In the laboratory, internal oxidation is the most convenient method of incorporating the oxide particles in the metal matrices. This appendix describes the procedure used to prepare the specimens for wear tests.

All alloy systems are not susceptible to internal oxidation. Certain thermodynamic and kinetic conditions are to be satisfied. Rhines[3] proposed the following conditions as the necessary criteria for internal oxidation to take place: (a) the alloy must have solubility for oxygen at the temperature of oxidation, (b) oxygen should diffuse faster than the alloying element, (c) the standard-free energy of formation of the solute metal oxide must be more negative than the free energy of formation of the lowest oxide of the base metal, and (d) the oxide should be insoluble in the metal. Rapp[4] added another condition to the above. He proposed that the solute content of the bulk must always be lower than that required for the transition from internal to external oxidation.

---

*The numbers in paranthesis designate the references at the end of this appendix.

A variety of methods exist for controlling the right partial pressure of oxygen for internal oxidation process to take place. By controlling the flow rates of H_2-H_2O and CO-CO_2 in gas flow systems, right partial pressure of oxygen can be maintained. A second method is to vaccum seal the alloy to be oxidized with a mixture of powders of the solvent metal and its oxide in a vycor tube and heat to the temperature required for diffusion. For copper alloys the mixture, called Rhines Pack, consists of equal parts by weight of Cu and Cu_2O. Some times Al_2O_3 is also mixed with the Rhines Pack to avoid sintering of the powder to the specimen.(5)

In the present work, a slight variation of that procedure is used. Instead of using vacuum sealed capsules of the specimen and Rhines Pack, the specimens were placed in the pack and purified argon was allowed to pass over the pack while oxidizing. By this method large quantities of glass in the form of capsules need not be used. Further, the danger of capsule explosion during treatment can be avoided. Enough quantities of Cu and Cu_2O were used so that the right partial pressure of oxygen was maintained even while the argon was flowing in small quantities.

C 2) Apparatus and Procedures

The copper silicon (Cu-0.5 Si, Cu-1.0 Si) and copper-chromium alloys (Cu-0.18 Cr) used in this work were in the form of solid solutions before internal oxidation. Copper-silicon alloys were melted in an induction furnace in dried argon atmosphere. Alloy preparation and solutionization procedures for these alloys were given in Appendix B. Cu-Cr alloy was supplied by American Metal Climax Company. This alloy in the form of 1.3 cm dia. 7.5 cm long specimens, was solutionized at 900°C for 50 hours in vacuum sealed vycor capsules, and water quenched after solution treatment. The water quenched samples were then swaged to 0.6 cm diameter rods in steps at room temperature without intermittent annealing. Specimens of 0.6 cm x 7.5 cm were cut from the swaged rods and were polished with No. 3/0 emery paper and cleaned with trichloroethylene for internal oxidation.

Internal oxidation was carried out in the apparatus shown in Fig. C.1. The specimens were packed in Rhines Pack (equal parts of Cu, Cu_2O and Al_2O_3) in an alundum boat. The boats were kept in a vycor tube which has

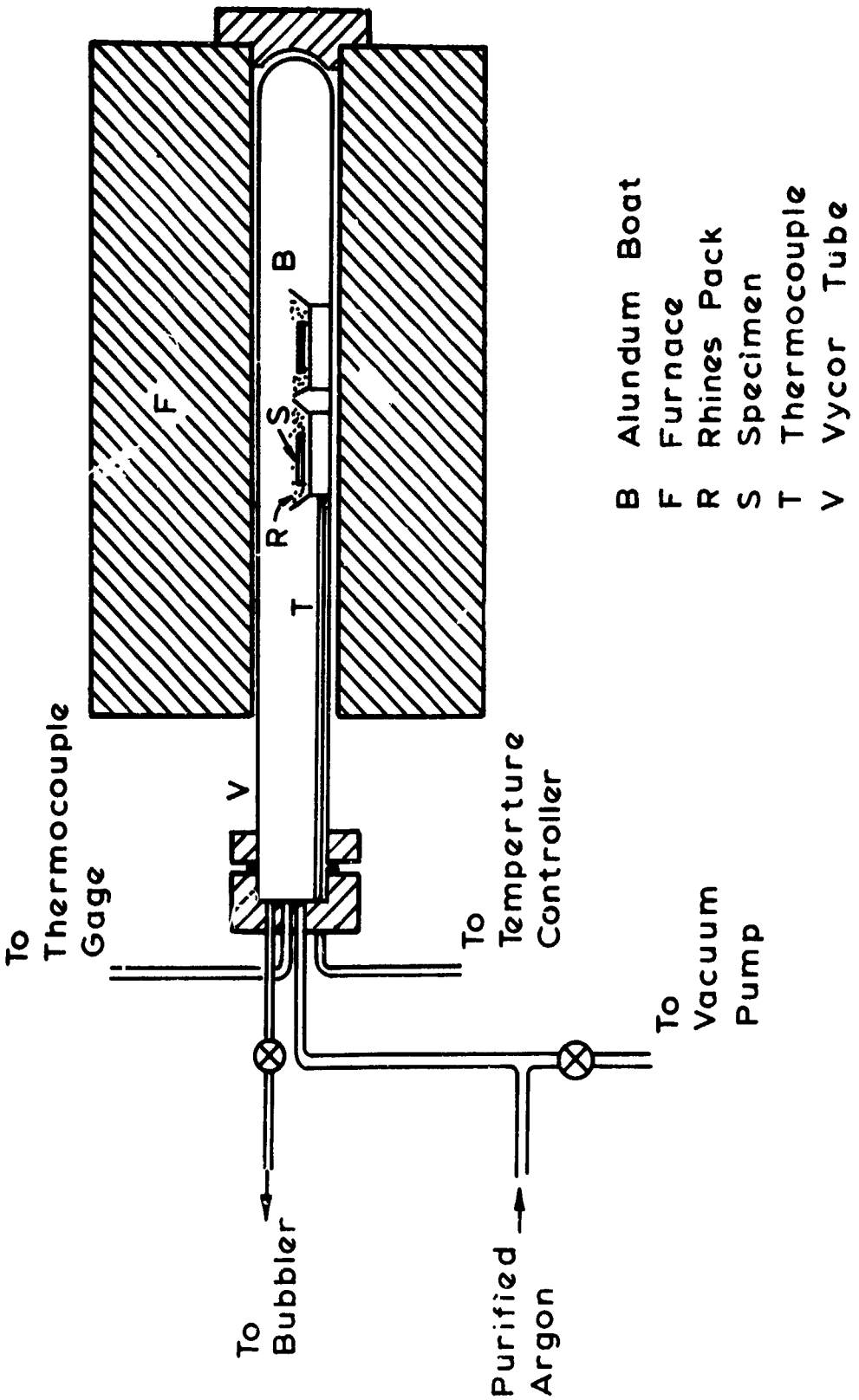

Figure C.1

Schematic of the internal oxidation equipment.

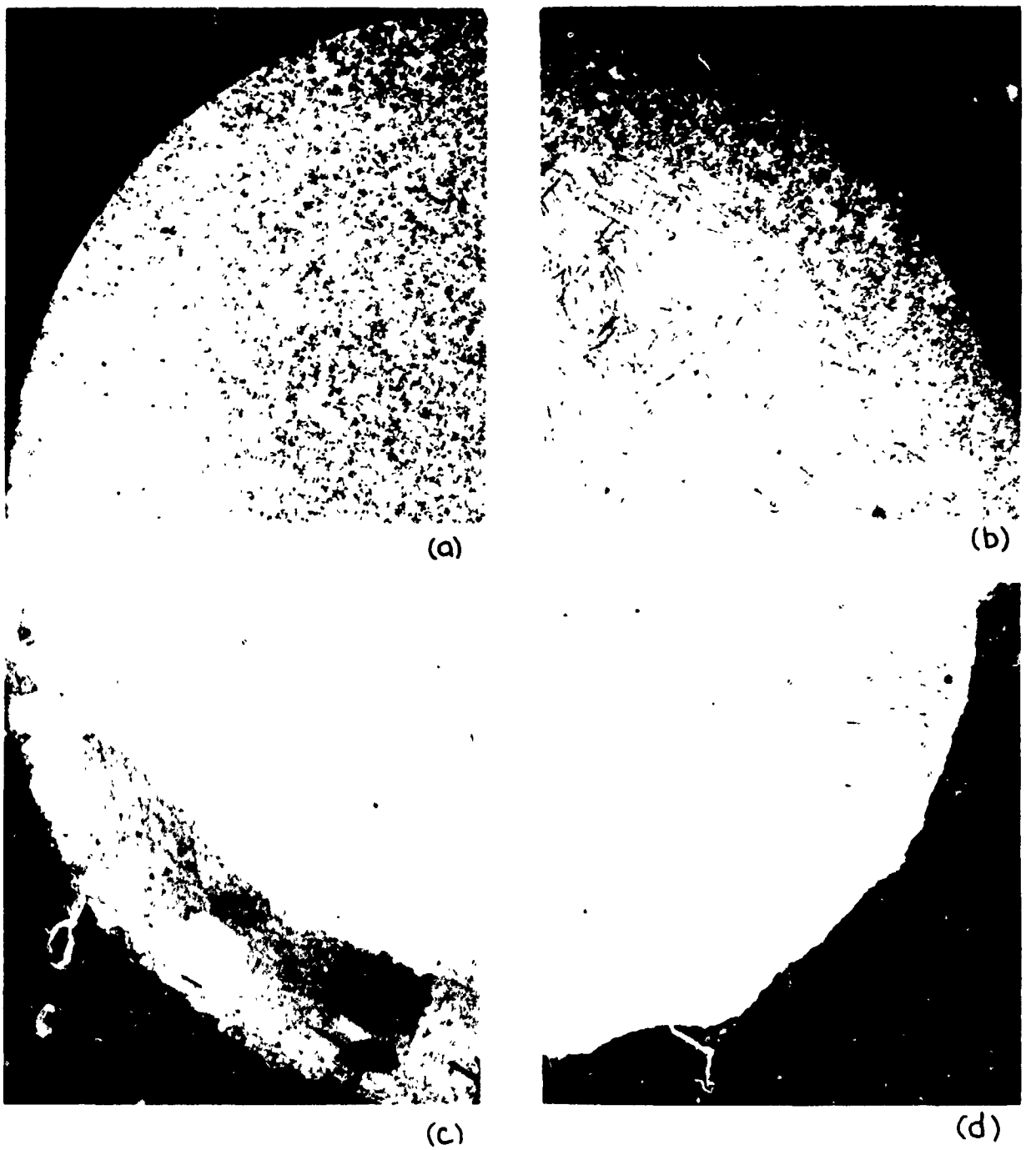

Figure C.2

Microstructures of (a) OFHC copper, (b) internally oxidized Cu-0.18 Cr, (c) Cu-0.5 Si, and (d) Cu-1.0 Si.

Table C.1 Internally Oxidized Copper Alloys: Metallurgical Variables

Material	Hardness Kg/mm^2	Volume Fraction of Oxide Particles
OFHC	31	0.00
Cu-0.18 Cr	36	0.004
Cu-0.5 Si	44	0.036
Cu-1.0 Si	34	0.073

vacuum fittings at one end and closed at the other end. The vycor tube was then placed in a horizontal tube furnace. The system was evacuated by means of a mechanical pump and then it was purged with argon. The flow rate of argon was kept very small (about a bubble every two seconds). The argon was dried and purified by allowing it to pass through drierite and copper turnings kept at 700°C. About 2 hours duration was necessary for the furnace to reach the oxidation temperature. All alloys were oxidized at 1000°C for 100 hours. Four samples were oxidized in a single run. After internal oxidation, the specimens were furnace cooled. No surface oxidation was noticed after internal oxidation although some sintering of the powder to the specimen was unavoidable. Following the internal oxidation process the specimens were cleaned with No. 3/0 emery paper and washed in trichloroethylene.

C 3) Metallography

Usual procedures of sectioning, polishing and etching were used in the metallographic preparation of the oxidized alloys. The etchant was equal volumes of NH_4OH and 3 per cent H_2O_2 at room temperature. Thickness of the oxidized layers was measured on the optical micrographs at 25 x (see Fig.C.2). It can be seen from Fig.C.2 that the oxidation was not complete in that the oxidation front did not penetrate to the center of the specimen. Though this is a problem when the specimens are tested in tension, it is however immaterial for wear tests since only a thin surface layer is subjected to wear.

References

(1) G.S. Ansell, "The Mechanism of Dispersion Strengthening - A Review," Oxide Dispersion Strengthening, G.S. Ansell et al, ed., Gordon Breach Science Publishers (1968) 61-142.

(2) M.J. Grant, "Dispersed Phase Strengthening," The Strengthening of Metals, Reinhold Publishing Corporation (1064) 163-199.

(3) F.N. Rhines, "A Metallographic Study of Internal Oxidation in the Alpha Solid Solutions of Copper," Trans. Met. Soc. AIME 137 (1940) 246-290.

(4) R.A. Rapp, "Kinetics, Microstructures and Mechanism of Internal Oxidation - Its Effect and Prevention in High Temperature Alloy Oxidation," Corrosion, 21 (1965) 382-401.

(5) M.F. Ashby and G.C. Smith, "Structures in Internally Oxidized Copper Alloys," J. Inst. Metals, 91 (1962-63) 182-187.

Appendix D

WEAR TESTING EQUIPMENTS AND PREPARATION OF THE SPECIMENS FOR SEM OBSERVATION

D 1) Wear Testing Equipments

A cylinder on cylinder sliding geometry, Fig. D.1b, was used in all wear tests. The specimens were rotated by the spindle of a lathe. The stationary slider pin was placed in a special holder and was connected to a lathe tool dynamometer. The dynamometer was attached to the carriage of the lathe. The normal contacting force was applied by the transverse motion of the carriage of the lathe. The friction force was measured by the bending stress in the pin-holder bar. The normal and frictional forces were monitored through the dynamometer and recorded on a Sanborn 321 Recorder.

The sliding surfaces were enclosed in a plexiglass chamber. Argon gas entered the chamber at a flow rate of 10 ℓ/min. For the tests on copper solid solution specimens (Chapter V) the chamber was redesigned such that it could be evacuated and purified argon could enter the chamber, Fig. D.2. Purification procedure similar to the one already discussed in Appendix B (Section B.2) was used.

D 2) Specimen Preparation After Wear Tests

After the wear tests, the specimens were gently brushed to remove the loose wear debris. Then, they were degreased in trichloroethylene, dried and weighed to an accuracy of 0.1 mg.

a) Wear Track Observations

The specimens were placed in a scanning electron microscope to examine the wear tracks. The cylindrical specimens were positioned so that the cylindrical axis was parallel with the electron beam. Then by tilting the specimen, the wear track on the cylindrical surface was observed. Tilting was very important to discern the shape and dimension of the wear sheets.

b) Sectioning and Observations

After observing the wear track, the specimen was cut by a hack saw approximately 1/8" away from the wear track, parallel to the sliding direction and perpendicular to the worn surface. Then it was placed in a special holder and abraded on grade 2 and 1 emery papers. The specimen

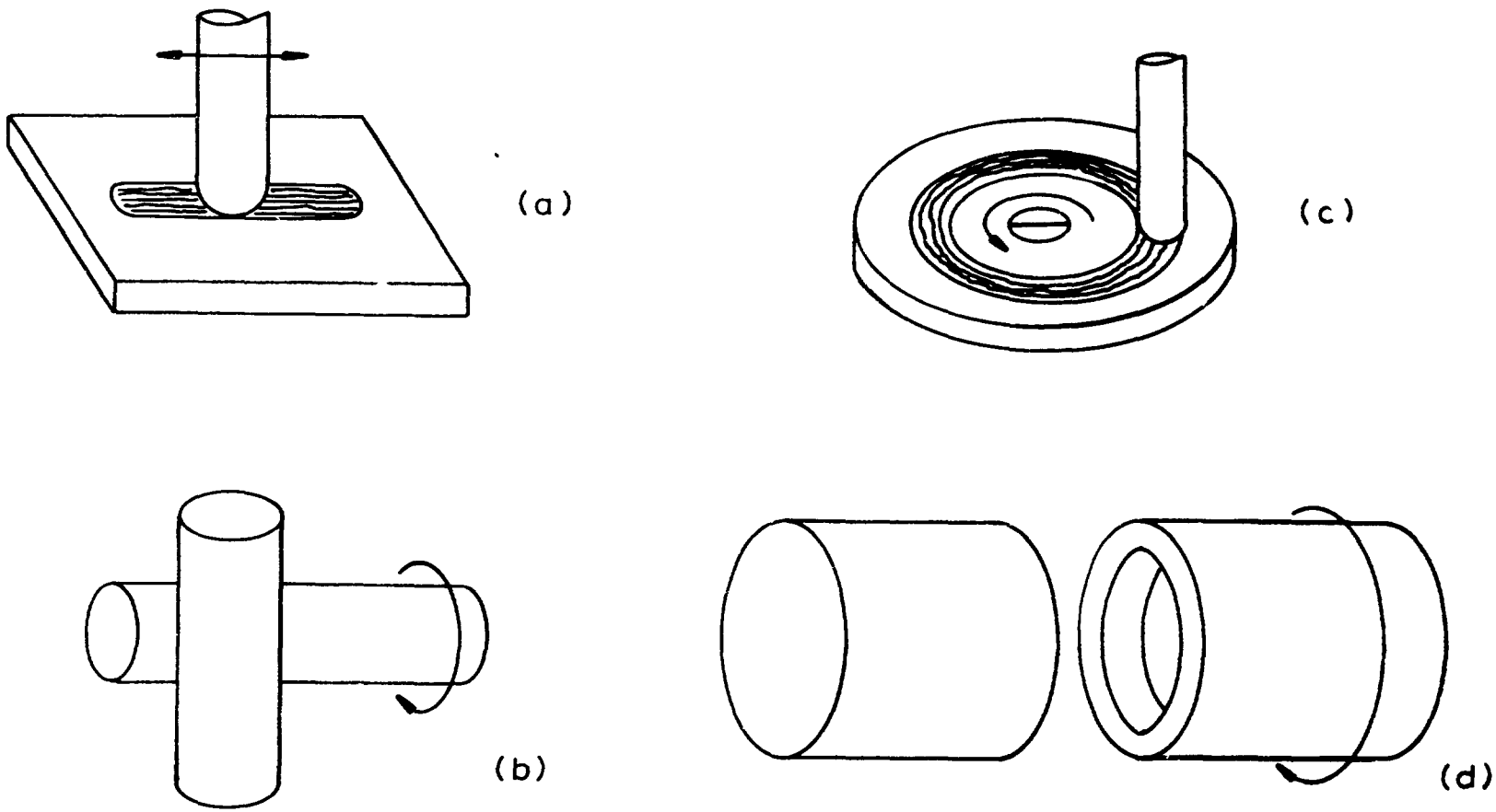

Figure D.1

Cylinder-on-cylinder wear testing geometry (b).

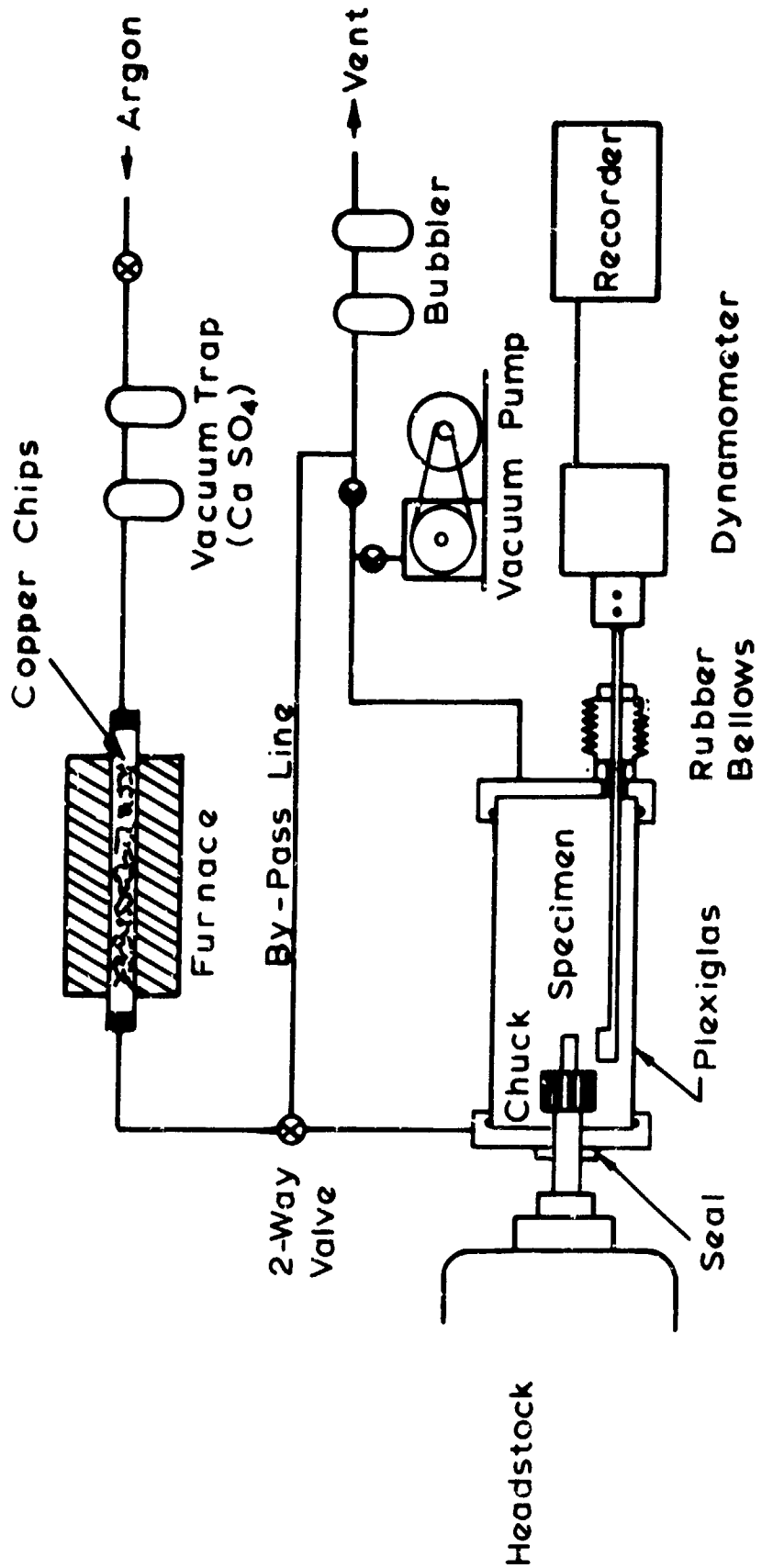

Figure D.2

Schematic of atmosphere controlled wear testing equipment.

holder was used to protect the edges during polishing. When a desired location in the wear track was reached, the section was metallographically polished.

After polishing, the specimens were etched to reveal the microstructure. The effectiveness of the etching procedure was checked by an optical microscope. The scanning electron microscope was then used to observe the microstructure and the subsurface damage due to wear.

Wear Particle Collection

The wear particles were collected in the plexiglass chamber which enclosed the sliding surfaces. After the wear tests, the particles were collected on a polished aluminum disk. The particles were then observed by the SEM.

Appendix E

PAPERS PUBLISHED AND PRESENTED ON THE DELAMINATION THEORY OF WEAR

1. N.P. Suh, "The Delamination Theory of Wear", Wear, 25 (1973) 111-124.

2. N.P. Suh, S. Jahanmir, E.P. Abrahamson, II and A.P.L. Turner, "Further Investigation of the Delamination Theory of Wear", J.Lub. Tech., Trans. ASME, 96 (1974) 631-637.

3. S. Jahanmir, N.P. Suh and E.P. Abrahamson, II, "Microscopic Observations of the Wear Sheet Formation by Delamination", Wear, 28 (1974) 235-249.

4. E.P. Abrahamson, II, S. Jahanmir, D.A. Colling and N.P. Suh, "Failure by Delamination During Wear", Proc. Scanning Electron Microscopy Conf., (1974) part IV, 889-894.

5. N.P. Suh, S. Jahanmir, D.A. Colling and E.P. Abrahamson, II, "The Delamination Theory for Wear of Metals Sliding at Low Speeds", Proc. 2nd North American Metalworking Research Conf., (1974) 117-127.

6. E.P. Abrahamson, II, S. Jahanmir, N.P. Suh and D.A. Colling," Application of the Delamination Theory of Wear to a Composite Metal Surface", Proc. Int. Conf. on Production, Tokyo, Japan, (1974) 408-413.

7. S. Jahanmir, N.P. Suh and E.P. Abrahamson, II, "The Delamination Theory of Wear and the Wear of a Composite Metal Surface", Wear, 32 (1975) 33-49.

8. N.P. Suh, E.P. Abrahamson, II and S. Jahanmir, "Wear Resistance of Soft Metal Coatings", U.S. Patent application, filled October 1, 1974.

9. N.P. Suh, "Microstructural Effects in Metals", Proc. Battelle Materials Science Colloquium, on "Fundamental Aspects of Structural Alloy Design", To be published by Plenum Press, 1976.

10. N.P. Suh and P. Sridharan, "Relationship between the Coefficient of Friction and the Wear Rate of Metals", Wear, 34 (1975) 291-299.

11. S. Jahanmir, E.P. Abrahamson, II and N.P. Suh, "The Effect of Second Phase Particles on Wear", Proceedings Third North American Metalworking Research Conference, Carnegie Press, (1975) 854-864.

12. E.P. Abrahamson, II, S. Jahanmir and N.P. Suh, "The Effect of Surface Finish on the Wear of Sliding Surfaces", CIRP Annals, 24 (1975) 513-514.

13. N.P. Suh, "The Delamination Theory of Wear - Its Present Status and Future Prospects", ONR Tribology Workshop, October 14, 1975.

14. S. Jahanmir, N.P. Suh and E.P. Abrahamson, II, "The Effect of Surface Roughness and Integrity on Wear", Wear, submitted for publication.

15. S. Jahanmir, E. Abrahamson, II and N.P. Suh, "Wear Resistance of Thin Metal Coatings", Wear, submitted for publication.

16. S. Jahanmir and N.P. Suh, "Metallic Coatings for the Reduction of Wear Utilizing the Delamination Theory", N.B.S. Conference on The Role of Coatings in the Prevention of Mechanical Failures, Gaithersburgh, Maryland, October 1975.